Ministry of Higher Education and Scientific Research

University of Babylon / College of Science

Department of Physics

Evaluation of the Solar Radiation and Skin Cancer Infection in Babylon Province Using Remote Sensing Techniques

A Thesis

Submitted to the Department of Physics – College of Science – University of Babylon

In partial fulfillment of the requirement for the degree of Doctorate of Philosophy in physics

Submitted By

Ghazwan Abdulelah Dahash Azeez

B. Sc. in physics\ 2005

M. Sc. in physics\ 2017

Supervisors

Prof.

Dr. Ameerah Ab. Al-Sadooni

Prof.

Dr. Ebtesam F.Khanjer Idris

2023 A.D. **1445 A.H.**

(هوَ الَّذي جعلَ الشّمْسَ ضِياءً والقمرَ نوراً وقدّرهُ مَنازِلَ لِتَعْلموا عدد السِنينِ والحِسابْ وما خَلق الله ذلِكَ الاّ بالحَقّ يفصّلُ الآياتِ لقومٍ يعلمونْ۞)

صدق الله العلي العظيم
سورة يونس (٥)

Supervisor Certification

We certify that this thesis is titled (**Evaluation of the Solar Radiation and Skin Cancer Infection in Babylon Province Using Remote Sensing Techniques)** was prepared by the student (**Ghazwan Abdulelah Dahash Azeez**) under our supervision at partial fulfillment of the requirements for practical degree of Physics Doctorate of Philosophy in physics.

.

Signature:

Supervisor: Dr. Ameerah Ab. Al-Sadooni

Title: Prof.

Address: Department of Physics

College of science – University of Babylon.

Data: / / 2023

Signature:

Supervisor: Dr. Ebtesam F.Khanjer

Title: Prof.

Address: Department of Remote Sensing and GIS

College of science – University of Baghdad.

Data: / / 2023

Certification of the Head of the Department

In view of the available recommendation, we forward this thesis for debate by the examination committee.

Signature:

Name: Dr. Samira Adnan Mahdi (Head of Physics Department)

Title: Assistant Professor

Address: Head of Department of Physics – College of science –University of Babylon.

Data: / / 2023

Dedications

To my mother, may Alah rest her soul in heaven, my first love and source of my success.

To my father, my first source of strength, may Alah prolong his life

To my beloved wife, you are the gift that Alah has given me, for your support and help, and by your side I challenge all difficulties in this world. May the creator please you all the time.

The piece of my heart, the hope of tomorrow, the source of my happiness, the reason for my joy, and the light of my life, my children.

My dear brothers, my support in life and childhood companions, my source of pride and strength

To everyone who contributed to the completion of this modest thesis, hoping that it will be an outlet for science and knowledge.

Ghazwan

Thanks and appreciation

All thanks to "Alah" who helped me and gave me patience and strength in preparing this work and helped me in this stage of my life. I extend my appreciation, gratitude and thanks to the honorable professors. Prof. Dr. "Ameera Ab. Al-Saadouni" and Prof. Dr. "Ibtisam F. Khanjar" without their assistance,I will not be able to complete this work. They act as a guide and teacher during the thesis preparation period. I learned a lot from them and took a lot of their time. I hope I achieved my goal and I hope you are proud of where we are after all the hard work we have done together. I ask God Almighty to make their efforts blessed.

Thanks are extended to the Department of Physics in the College of Science, represented by the head of the department and members of the faculty, as well as the Deanship of the College at the University of Babylon for their great assistance and support.

I would like to thank my friends and brothers for their help and encouragement during this time of my studies and the preparation of my dissertation. I am grateful to my family for their endless love and support, and for your understanding and encouragement throughout this work.

Ghazwan 2023

Abstract

This thesis includes studying the distribution of the solar radiation intensity in Babylon province. Five different months (January, March, July, August and October) were chosen to cover the four seasons of 2021, where the months of July and August were selected to represent the summer season due to the high intensity of solar radiation and the extremely rise in temperatures, which appear in both months. To achieve this study, the ALOSPALSAR satellite data were adopted, as it has a wide range, high-resolution, multi-spectral image capability and provides images with a resolution of 10 m. Five DEM digital elevation images were downloaded to cover the province of Babylon (5119 km^2) for each month from the geographical survey site the American.

The second stage was a merger of the images using the Mosaic program. Then the geometric and radiometric corrections were done, and the province of Babylon was extracted by adopting the Arc GIS technology. During the daytime, the solar radiation was calculated every 30 minutes. The results show that the highest rates of solar radiation are in July and August, which represent the summer season, reaching (4056383 – 3820022) W H m^{-2}, as the solar radiation energy was calculated for four periods depending on the number of hours in the daytime. The rest of the months display typical solar radiation (1764067, 3076873 and 2635710) W H m^{-2}. In January, March and October, the solar radiation was calculated in three periods, and the areas of high radiation were concentrated in barren areas and less in urban and agricultural areas. It was observed that the rate of radiation is associated with a direct relationship with the air temperature and an inverse relationship with the relative humidity. The increase in the amount of solar radiation includes height in the air

temperature and a lowering in the relative humidity. The increase in the relative humidity is accompanied by a decrease in the amount of radiation in all seasons.

The land surface temperature was studied based on both remote sensing technology (RS) and geographic information systems (GIS), and the thermal and near-red bands of the Landsat 8 satellite were adopted. The spatial distribution of the surface temperature of Babylon province was drawn for five months for the year 2021 to cover the four seasons of the study year, as the results showed clear disparity in the land surface temperatures of the four seasons, and their highest values were in the months of July and August (summer season), to reach high levels that touched 60 Cº, and this constitutes a threat to human life. The LST was 25 Cº in the winter on a sunny day and reached 40 Cº in the spring and autumn seasons. The thesis also dealt with the study of the intensity of solar radiation and its impact on human health through the emergence of cases of skin cancer in the province, and based on the data of the number of injuries, that obtained from the Health Department of Babylon and the Department of Health of Najaf for the study area. The results were distributed to all regions and districts of Babylon province. The highest concentration of injuries is in the city of Hilla, the center of Babylon province, compared with the rest of the regions, followed by the Abu Gharak region, and then the regions of Al-Musayyib and Al-Mahaweel, then the rest of the regions. It is likely that the reasons for the distribution of injuries are not only the high intensity of solar radiation and high temperatures, but also population density, environmental pollution, buildings, factories and other reasons.

contents

List of Tables

List of Figures

Abbreviations

Abbreviation	Meaning
RS	Remote Sensing
GIS	Geographical Information System
LST	Land Surface Temperature
TIR	Thermal Infrared Region
MIR	Mid-wave Infrared Region
SR	Solar Radiation
UV	Ultraviolet Rays
UCAR	University Corporation Atmospheric Research
LULC	Land Use Land Cover
NDVI	Normalized Difference Vegetation Index
RMSE	Root Mean Square Error
ANN	Artificial Neural Networks
SVR	Support Vector Regression
MLR	Multiple Linear Regression
SRTM- DEM	Shuttle Radar Topography Mission- Digital Elevation Model
GPS	Global Positioning System
CCT	Tapes Compatible with Computers
IFOV	Instantaneous Field Of View
DEM	Digital Elevation Model
UTM	Universal Transverse Mercator
SAR	Synthetic Aperture Radar

GDEM	Global DEM
NASA	National Aeronautics And Space Administration
USGS	United States Geological Survey
OLI	Operational Land Image
VIS	Visible
TIRS	Thermal Infrared Region Sensor
JAXA	Japan Aerospace Exploration Agency
PRISM	Panchromatic Remote Sensing Instrument for Stereo Mapping
AVNIR	Advanced Visible And Near Infrared Radiometer
PALSAR	Phased Array type L- band Synthetic Aperture Radar
ECMWF	European Center for Medium- range Weather Forecasts
DN	Digital Number
TOA	Top Of Atmosphere
BT	Brightness Temperature
PV	Proportion of Vegetation
LSE	Land Surface Emissivity
TOVS	Tiros Operational Vertical Sounder
NOAA	National Oceanic Atmospheric Administration

CHAPTER ONE

General Introduction and Literature Review

1.1 Introduction

The sun is a star that is considered the most important source of energy for our planet. The scientist Hermann von Helmholtz put forward the idea of gravitational contraction as the source of the sun's heat. The scientist Ernest Rutherford also concluded that the radioactive materials have the ability to produce large and huge amounts of energy, which can add this energy heat to the surface of the earth. The scientist Radium explained that the energies emanating from sun is not due to the energies of radioactive decay, but rather it is from the interactions of the nuclei in the hot nuclei dense [1].

The sun is the most important member of the solar system, without which life cannot exist on Earth. Although the sun is considered the most important celestial star for the continuity of life on Earth, Figure (1-1), but it is considered an ordinary star. The cosmic importance of this star is limited to considering it the central target of the planet system in which we live.

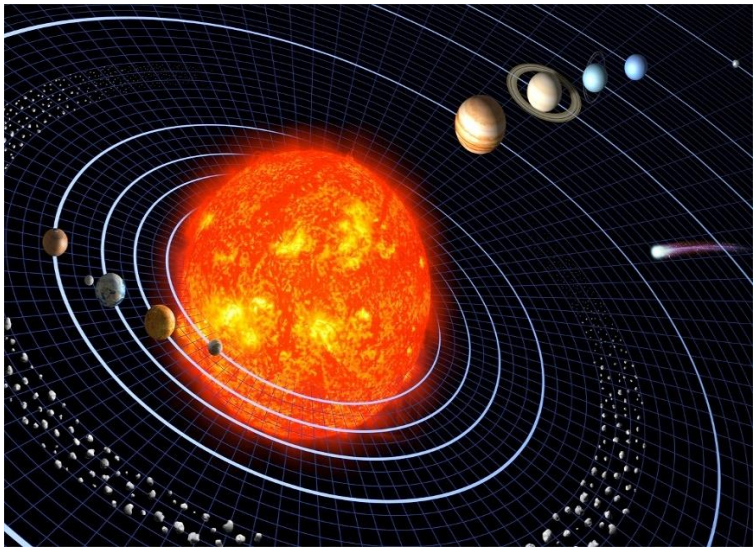

Figure (1-1): The solar system [2].

Studies have found that there are many stars larger and brighter than the sun. The sun has a very large mass estimated at about 1.99 $x10^{30}$ kg, and this is about 333,000 times the mass of the Earth, while the average density of this star is 21.41 g/cm^3 and is considered the same as the density of Jupiter. This is one of the many similarities that we will see between the sun and some planets in the solar systems [2].

The average distance between Earth and the Sun is about $1.50x10^8$ km. About 400 years ago, the scientist Galilo used the telescope for the first time to see the sun, and he noticed the presence of dark spots moving on its surface, in the Figure (1-2a) and (1-2b). Through the movement of these spots, the scientist Galilo was able to conclude that the sun rotates for more than a month, and since the movement of the sun is a differential rotation, the sun rotates 35 days at the poles and about 25 days at the equator [3].

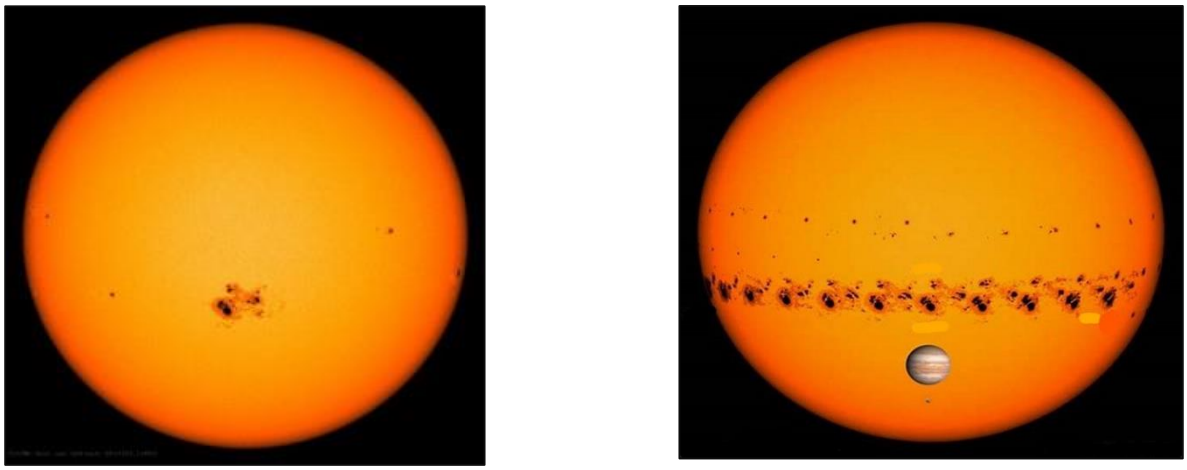

(a) (b)

Figure (1-2): (a) Sunspots appear as dark spots on the sun surface. **(b)** The same sunspots appear many times as the sun rotate around its axis [3].

The emitted energy from the sun is in all parts of the electromagnetic spectrum, and this energy is measured with high accuracy through satellites above the atmosphere. The solar energy hits the earth atmosphere at an average of about 1370 watts/m^2. This is shown by international measurements. This value was used to show the luminosity of the sun (which is the amount of energy that the sun radiates into space during one second). It measures to be approximately $3.85x10^{26}$ W.

This is a very large amount of energy. If we assume the solar energy that reaches the Earth it can be collected and harnessed with high efficiency, then it will be sufficient to cover the world's population of energy 10,000 times. All estimates and measurements indicate that alteration in the sun's brightness by 1% causes a change in the planet's temperature by 1 or 2 C^o. The subsoil cannot be examined directly, but scientists have learned a lot about its interior through computer modeling. Then confirm all the observations based on the surface of the sun, and the ability to know the behavior of matter about the necessary temperature and pressure necessary to maintain the fusion reaction. At high temperatures, such as the sun, matter is in the form of a gas and not as a solid or liquid. Where the temperature on the sun is estimated to be 5800 K, but in its interior, it is approximately $\approx 15 x10^6$ K, and here most of the electrons are stripped from their nuclei [4].

1.2 Solar Radiation and Wind

The sun is un active star with several different type of emissions frome X-rays, ultraviolet rays, plasma particles, magnetic fields, and large rays sent with a large magnetic effect in space. It is within the scope of the sun called the solar field, that includes the solar wind and all the magnetic cover of the solar system. The solar wind is defined as a stream of charged particles emanating from the top of the solar atmosphere, called the halo or plasma. It often consists of several elements,

electrons, protons, and alpha particles with kinetic energy (0.5-10) KeV. It also consists of a mixture of materials (tiny amounts) of ions. Heavy and atomic nuclei are there such as C, N, O, Ne, Mg, Si, S, Fe.

In additions, there are some nuclei and isotopes such as P, Ti, Cr, Fe^{54}, Fe^{56}, Ni ^{58}, Ni ^{60}. The winds of the sun differ among themselves in terms of speed, temperature and density. These particles are not affected by solar gravity across solar latitudes and longitudes and over long periods of time, due to the high energy that results from the high temperatures of the solar corona generated by the coronal magnetic field. [5].

The speed of the solar wind is faster than sound, as its speed is estimated at (250-750) km/s, thus, its movement is faster than the speed of magnetic waves. The radiation, emissions and solar winds that reach the earth have a relationship and influence on the climate. There are two types of emissions from the sun:

1.2.1 The First Type

It represents the X-rays, radio rays, infrared rays, visible rays, and ultraviolet rays. These radiations are called electromagnetic radiations, and they have characteristics, including [6]:

1- Traveling at the speed of light and in straight lines.
2- The part that reaches the surface of the earth will have a clear effect on the hemisphere facing the sun, as it runs in straight lines, as this indicates the total eclipse of the sun, when it occurs, its access to the globe stops at the moment of interruption and the arrival of visible radiation is blocked.
3- The corona layer is a source of X-rays and short wavelengths, rays with hundreds of thousands of degrees of heat.

4- There are areas called solar disturbances that emit ultraviolet radiation and are the main factor in the formation of the ionized layer surrounding the Earth's atmosphere. Therefore, we will notice a period of increased solar activity. These radiations will cause disturbances in the ionizing zone and cause a malfunction in wireless communications.

5- Radio radiation always has wide windows between millimeter waves and meter waves, and during the solar irritation phase it is emitted in three types:

- Intense radio emissions that last a few minutes and in many wavelengths, resulting from the plasma ejected from the regions surrounded by sunspots.
- The second type is called turbulent storms, and they are continuous for periods ranging from several hours to days, and during wavelengths estimated (1-2) m, resulting from the collision of magnetic particles and the movement of plasma waves.
- The third type is within the centimeter waves and is called radio emissions and it lasts for a few weeks, it is related to the activities of sunspots in most of the bright areas surrounding the sun.

1.2.2 The Second Type

These emissions are in the form of thin clouds and gases and consist of electrically charged particles with several properties, including [7]:

1- They are relatively slow, with an arrival time to the surface of the earth ranges from 20 to 30 hours.

2- These electrical particles are not affected by the earthly part facing the sun, due to their deviation from their straight path. The Earth's magnetic field can significantly affect it, this explains the reason for its continuous access to the Earth's surface during the occurrence of a total solar eclipse.

3- Has a short and little effect on the Earth’s atmosphere, as it occurs only when it is emitted from special and specific locations on the disk of the sun, this is in accordance with the appropriate position of the Earth. We notice in the spring and autumn equinoxes the intensification of the Earth’s magnetic storms, because the latitude of the center of the solar disk is at its maximum.
4- The solar aurora phenomenon (Aurora) occurs because of these rays. The aurora borealis is a bright and changing phenomenon that always occurs near the earth's poles, and the reason for its occurrence is that when electrons and particles are emitted from the sun to the earth, their direction is towards the magnetic centers of the north and south poles by virtue of the earth's magnetic field. During that, it will collide with all the orbits of the elements in the upper atmosphere, such as oxygen and hydrogen.

1.3 The Four Seasons

The year is divided into four seasons; each season includes several months that differ between them in weather and the amount of sunlight that reaches the Earth, as well as the timing of night and day. Each of these seasons is a period of time and has special climatic conditions and characteristics [8], shown in Figure (1-3).

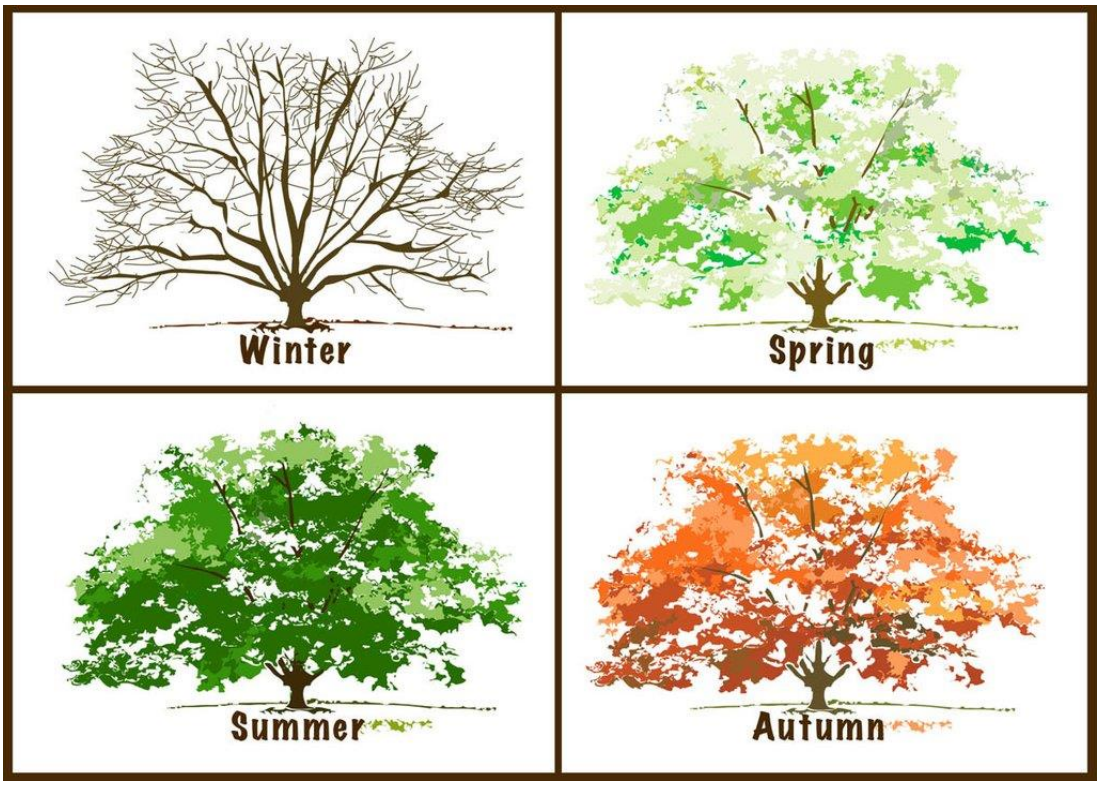

Figure (1-3): The four seasons [9].

The Earth revolves in certain orbits around the sun, and at the same time the planet rotates around itself in an axial rotation, and this movement includes all planets of the solar system.

The movement of the planet around its axis is from the west towards the east, and this movement is completed in a period of approximately 24 hours, forming the sequence of night and day. As for its movement around the Sun, it is in an elliptical orbit (ellipse) around the parent star (the Sun), it completes every solar year exactly, the rotation period is 365.25 days and a speed of approximately 108000 km/h. This movement results in the succession of the four astronomical seasons. These seasons (winter, summer, spring, and fall) are a result of the Earth's rotation around the Sun, approximately one revolution every year, in addition to that the angle at which the Earth's axis is inclined around the Sun is 23.5º [10].

There are many factors that are considered a major reason for the four seasons of the year and the change of climate from one season to another, including the Earth's rotation around the Sun, the inclination of the earth’s axis during rotation, and the shape of the oval planet. Figure (1-4), shows the position of the Earth in four seasons.

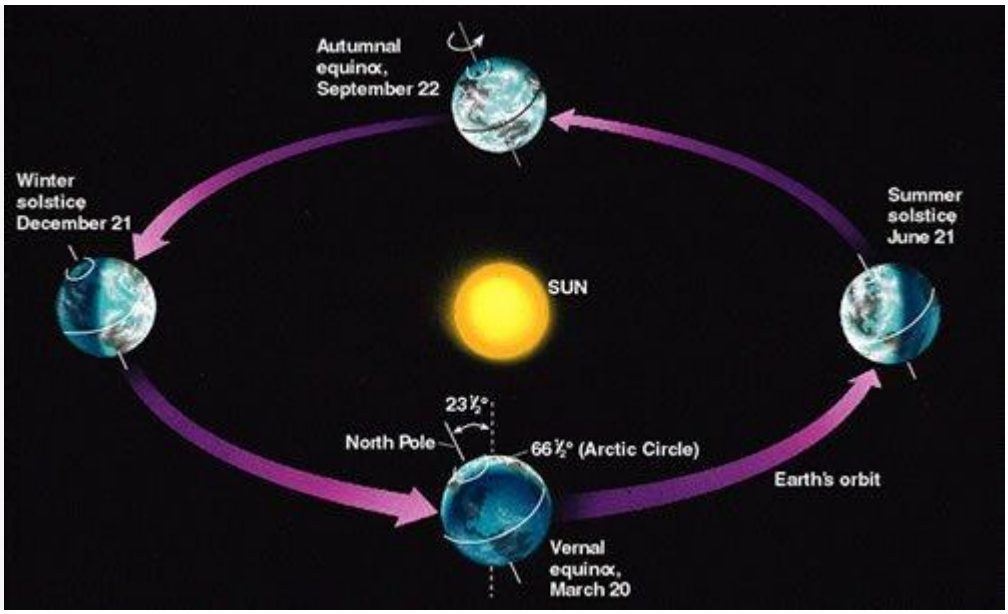

Figure (1-4) Earth's rotation around the sun and the four seasons [11].

In order for the relationship to be more accurate and clear between the movement of the planet around the sun and the succession of the four seasons of the year, some important points must be known:

_ Objects with a large mass attract objects with a smaller mass according to the principle and laws of gravity, and thus the Earth is attracted towards the sun and revolves around it, given that the mass of the sun is greater than the mass of the Earth, as it is 300,000 times the mass of the Earth.

the Earth revolves around the Sun in an elliptical orbit at a speed of 108,000 km /h , and the tilt of the imaginary Earth's axis at an acute angle ranges between (22.1-24.5)º.

_ The change in the intensity of the seasons is related to the change in the angle of inclination of the earth's axis, so the seasons become moderate when the inclination of the imaginary axis of the earth decreases during its movement around the sun and the intensity increases, i.e. the summer is hotter and the winter is colder when the inclination of the earth’s axis increases.

_ The direction of the Earth's rotation around the sun is from the western side to the eastern side, and this cycle takes about 365.25 days.

The four seasons have specific times of the year, but it is worth noting that there are areas on the surface of the globe that do not reach the full four seasons of the year, as there are many countries that have one climate or only two climates throughout the year, but most regions of the globe pass through four climate seasons are variable and varied in seasons and have many cosmic benefits as each of these seasons has many characteristics and features related to it.

The change of the four seasons is the result of the inclination of some areas towards the sun or away from it during the rotation of the earth around the sun, and this leads to the emergence of opposite seasons, it is located in the northern hemisphere on the one hand and the southern hemisphere on the other.

And because the earth orbits around the sun in elliptical orbits, the distance from the sun is constantly changing. Earth is very close to the sun at certain times and far from it at other times. These two locations are called perihelion and apogee.

Perihelion: is the closest distance the earth reaches from the sun during the period of rotation, and it is estimated at approximately 147,090,000 km.

Apogee: is the farthest distance the earth reaches from the sun during its orbit around the sun, which is approximately 152,100,000 km [12].

1.4 The Earth

Earth is the third planet in the arrangement of the solar system, it is the only place in which life and habitation exist. Although the Earth does not have large quantities of water in the solar system, it contains only surface water, which amounts to approximately 70.8% of the total area of the Earth. One of the most water-retaining regions of the globe are the polar regions, where there are ice layers that cover the oceans and the land, and this is the main reason for dwarfing the land [13].

The land part of the earth is represented by continents and islands, which extend to approximately 29.2%. The vegetation cover is widespread. The layer or material under the earth's surface is called the earth's crust, and this crust consists of several tectonic plates that move very slowly, and these plates interact to form mountains, volcanic eruptions and earthquakes. The magnetic field is generated by the Earth's liquid outer core. which in turn forms the planet's magnetosphere. This causes deflection of the destructive solar wind and cosmic radiation significantly, Figure (1-5):

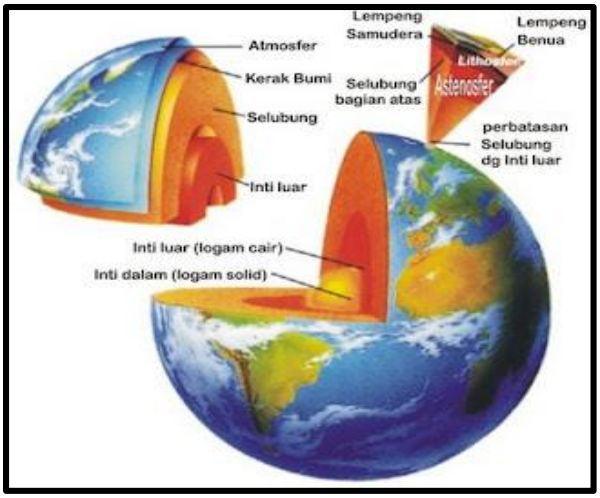

Figure (1-5): The atmosphere and the outer and inner layers of the Earth [14].

There is a covering around the earth called the atmosphere, which is of great importance in protecting the planet from meteorites and harmful ultraviolet radiation, this cover consists of two basic elements, nitrogen and oxygen. Global warming present in the atmosphere such as carbon dioxide. Energy reaches different levels of the earth due to the geometric shape of the earth (for example, the equatorial region of the planet receives the largest amount of light compared to the polar regions), which causes currents in the atmosphere and oceans [15].

This generates a global climate system in different regions, as well as generates a group of weather phenomena such as precipitation and others. The Earth's circumference is approximately 4,000 km, and it is elliptical in shape. It is considered one of the planets with a high density in the solar system. It is the largest of the four rocky planets. The average distance between the Earth and the Sun is about eight light minutes and it revolves around it. The rotation period is one year, 365.25 days. Earth planet also revolves around itself in less than a day by 23.56 hours.

The Earth's axis of rotation is inclined to the orbital plane of the Sun. This will be the four seasons of the year. There is a moon that orbits the Earth permanently at a distance of about 384,400 km, which is equivalent to (1.28 light seconds). About 4.5 billion years ago, the Earth was created, so are most other things in the solar system. The ocean was created and life developed during the first billion years, then life spread throughout the world and worked to influence the earth's atmosphere, which led to the occurrence of the Big Bang two billion years ago. 300,000 years ago, humans began to negatively affect the planet's environment [16].

1.4.1 The Land Surface Temperature (LST)

The different Earth surface temperatures are important and fundamental observables that are closely related to climate and weather patterns. They also have a clear impact on human health. They are of great importance in managing all water resources and agricultural resources. There is a relationship for each of the surface air, seas, lakes, land and ice masses in formation of the degrees of the Earth's surface. These temperatures are usually monitored and recorded continuously using several complementary methods, and vary in several ranges according to time and place, and they have interrelated and essential roles for the atmosphere surrounding the Earth's surface (atmosphere) [16].

As for the Earth's surface temperature, it is considered a major and essential factor that enters into determining the radiation energy of the Earth's surface. It is also widely used in defining and monitoring areas of moisture and areas of drought and the processes of evaporation and transpiration, as it works to push away the long-wave rays coming out and the flow of temperatures from the surface of the Earth, that is one of the most important reasons changes in climate and the scale of time periods is surface temperatures. It is responsible for controlling the division of energy into potential thermal quantities and impulses, it also acts as a clear indicator of surface temperature trends due to climate changes. There is a common rule in physics called Planck's rule, which states that the total energy emitted from the Earth's surface increases significantly and clearly with the increase in temperature.

Thus, the relationship between temperature and LST is positive, and this is the basis of the theoretical principle of remote sensing of the Earth's surface temperature. This principle is opposite to the air temperature near the surface of the earth, which is measured in meteorological stations and displayed on a daily basis in weather

reports. Sometimes the LST is called the skin temperature or is called the radiant temperature. Therefore, the LST is an accurate description of the hotness or the coldness of the Earth's surface upon contact. More precisely, the LST is the temperature of the layers near the surface of the exposed soil, which are estimated at very few micrometres. It is also the temperature of the dense and canopy plant leaves and the lower part, such as the tips and branches. The LST is most often recovered by evaluating and estimating the amount of radiation emitted from the surface. Earth, which is taken from the atmospheric correction of remote sensors. After this, the Planck theory can be inverted, taking into account the signs of the emission fluctuation. The maximum of all radiative emissions of Earth's surface temperatures except for fires and lava occurs in two spectral regions of the infrared, the first region is in the mid-infrared (3.5-5) m, and the second is the thermal infrared region (TIR) (8-13) m. These are less affected by the spread and absorption of the atmosphere. The variation and difference in water vapor in the atmosphere has a small effect on the absorption of wave regions, so the total is the reflected solar radiation and is subtracted from the signal before obtaining the LST readings. The TIR region is considered the applicable wavelength range. In order to retrieve the LST mainly, this leads to the creation of a small band of O3 whose dimensions are from (9.6-10) m, but sensors usually ignore this region. In Planck's theory, the black body radiation describes the electromagnetic radiation, which is called the spectral departure emitted in these Windows with specific wavelengths in meters, Figure (1-6), Planck's law explains and describes the radiant emitted energy of a specific temperature and wavelength as a specific material, element or element that absorbs all wavelengths of radiation with 100% efficiency [17].

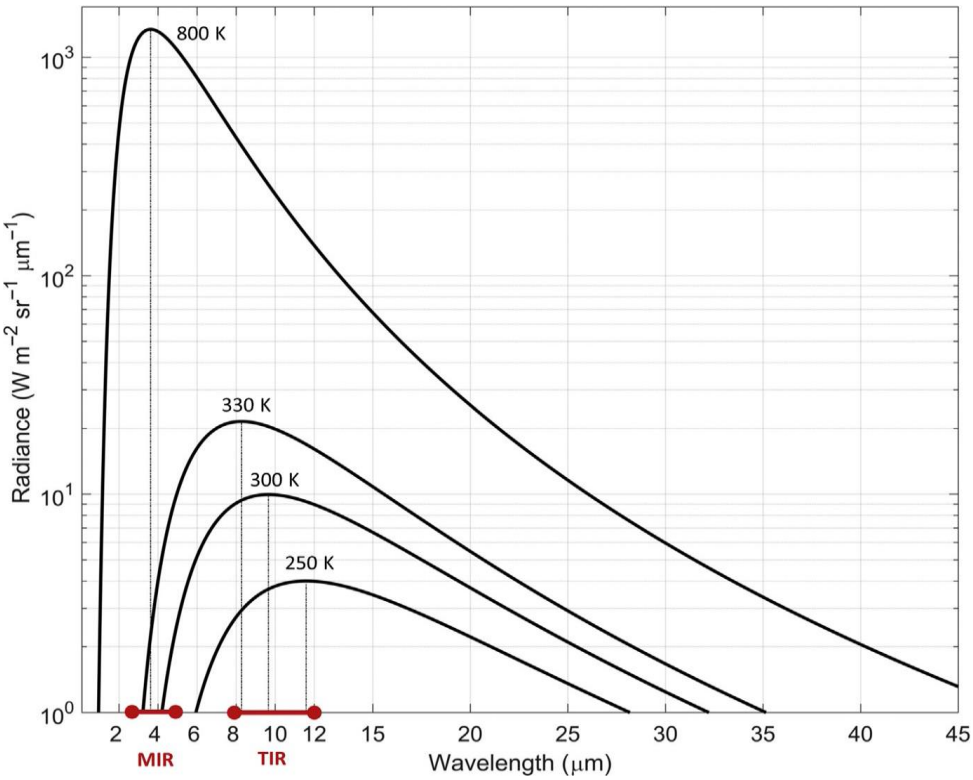

Figure (1-6): Planck blackbody radiance curves at four temperatures [17].

Four degrees of the Planck-Blackbody curves were selected and calculated from equation (1) with vertical black dashed lines to mark the positions of the max lamda (λ_{max}). It is important to note that the average temperatures recorded on Earth lie within (250-330) Kelvin (23-60) degrees Celsius and occur at wavelength emissions usually within the thermal infrared (TIR) between 8 and 12 micrometers, but greater temperatures drop to shorter wavelengths, eg the mid-wave infrared region (MIR) shown in red on Earth would peak at 3.6 μm for a typical fire at 800 K (3-5 μm). For any specific body, the thermal efficiency can be defined as the latent ability of the material to emit light by spectral emission, and it can be calculated as the ratio of the spectral radiation to the black body radiation for the same temperatures.

$$B_\lambda(T) = \frac{2hc^2}{\lambda^5\left(\frac{hc}{e^{\lambda KT-1}}\right)} \qquad (1-1)$$

Where

$B_\lambda(T)$= spectral radiance of a blackbody at temperature, ($W.m^{-2}.\mu m^{-1}.sr^{-1}$)

T= temperature, i.e., LST (K).

h= Planck's constant (6.626×10^{-34} J.s).

c= speed of light (2.99792458×10^{8} $m.s^{-1}$).

λ= wavelength (μm).

k= Boltzmann constant (1.3806×10^{-23} $J.K^{-1}$) [18].

The wavelength of maximum radiant energy emitted (λ_{max}) at a given temperature, can be found by using Wien's displacement law as follows:

$$\lambda_{max} = \frac{B}{T} \qquad (1-2)$$

Where

B=Wien's constant (2897.8 μm.K).

T= temperature (K).

λ_{max}=wavelength of maximum spectral radiance (μm)[18].

The "thermal efficiency" of an object, or a material's inherent ability to emit light, is known as spectral emissivity and is calculated as the ratio of the spectral radiance to that of a blackbody at the same temperature.

$$\varepsilon_\lambda = \frac{\mathrm{L}_\lambda(\mathrm{T})}{\mathrm{B}_\lambda(\mathrm{T})} \qquad (1-3)$$

Where for a given wavelength, λ, $L_\lambda(T)$ is the spectral radiance of the material at temperature, T, and $B_\lambda(T)$ is the blackbody radiation at the same temperature, T. Therefore the component of outgoing radiance from the surface is given by a blackbody radiance at the surface temperature, T, multiplied by the surface emissivity ε_λ. i.e., $L_\lambda = \varepsilon_\lambda B_{\lambda\,(T)}$[18].

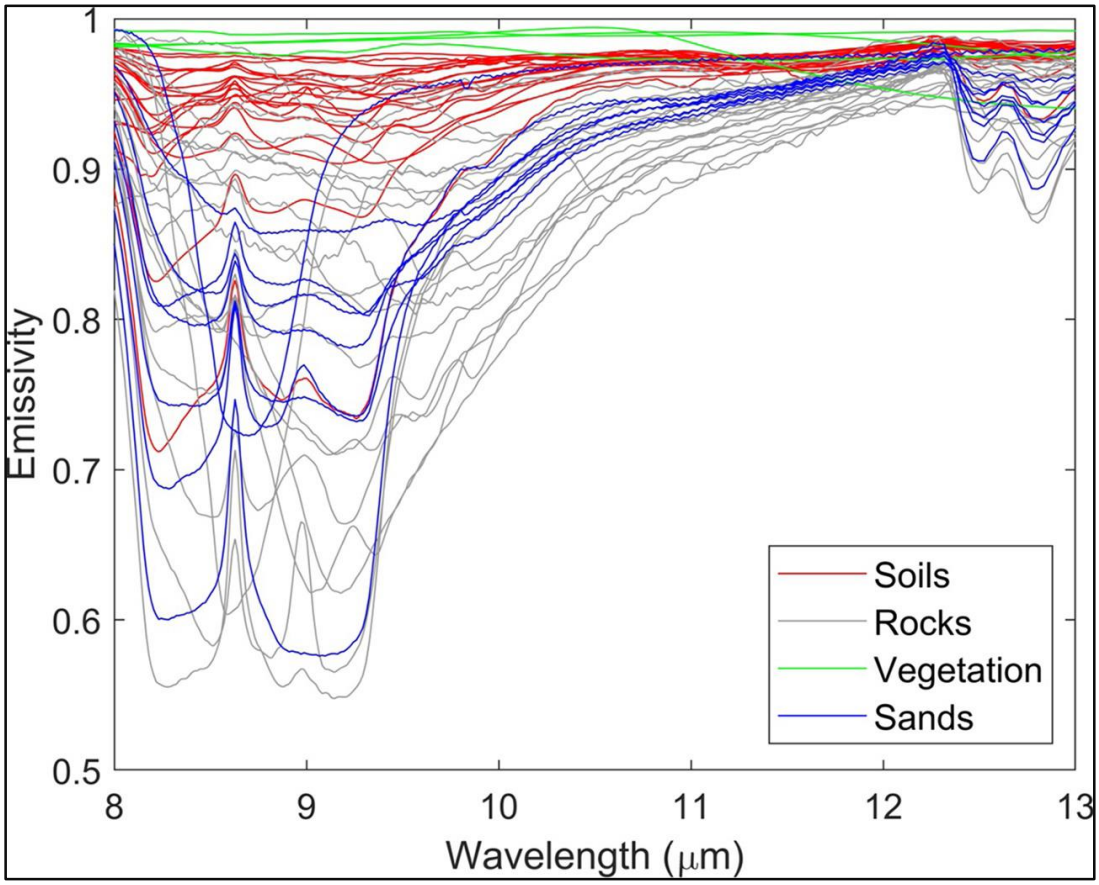

Figure (1-7): A selection of natural emissivity spectra from the ASTER spectral library consisting of soils, rocks, graybodies (water, vegetation, ice and snow) and sands in the thermal infrared (8-13) μm [18].

The use of GIS and remote sensing systems made it possible to estimate and calculate the distribution of LST on the surface of the earth and for a specificlocation.

The emissivity is an intrinsic property off any material and independent of its temperature therefore the emissivity will not change unless the underlying physical characteristics of that material changes.

1.5 The Solar Radiation

Radiation is emitted from the sun in the form of electromagnetic waves. The sun is the main source of light and heat energy for Earth planet. Electromagnetic radiation has different lengths when distributed and is called the spectrum. Figure (1-8), shows the different ranges of the electromagnetic radiation [19].

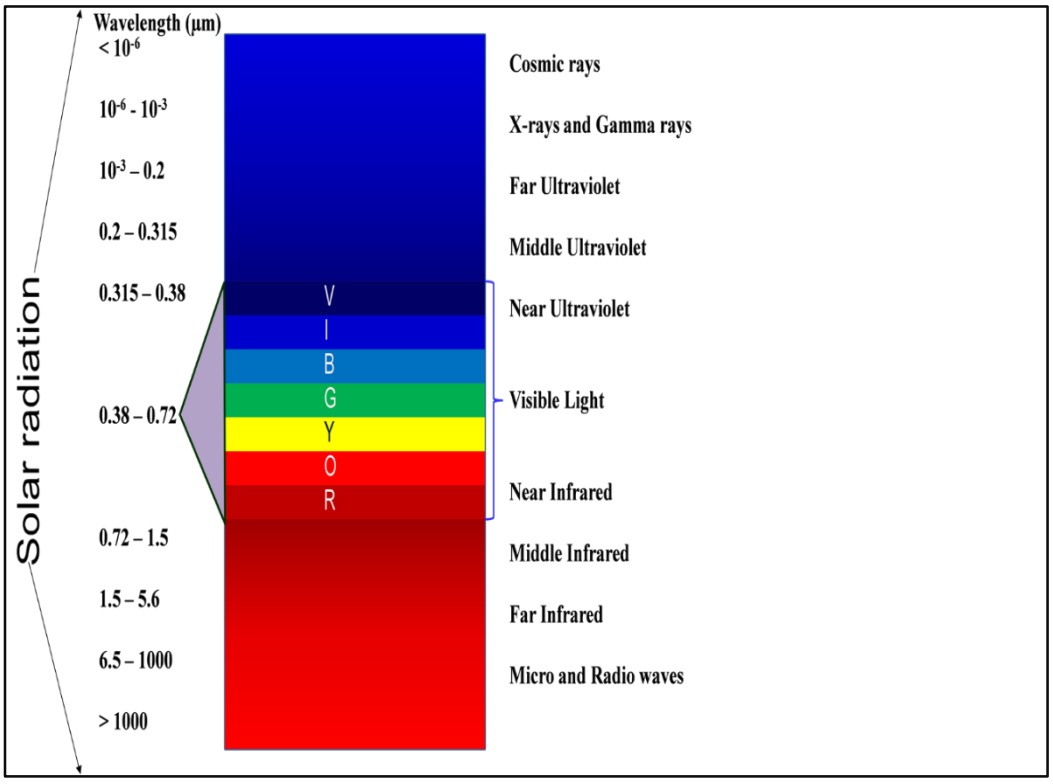

Figure (1-8): Spectral ranges of electromagnetic radiation [20].

The solar spectrum is divided into two parts. The first two parts are visible to the eye and the second part is invisible to the human eye. The visible part is also called visible light, which the human eye can see, it consists of several colors whose wavelengths range from 380 nm, which is the violet color, to 750 nm, which is the red color, as follows:

- The violet color has a wavelength between 380 nm and 450 nm, and a frequency between 789 Hz and 688 Hz respectively.

- Blue color has a wavelength between 450 nm and 495 nm Green color has a wavelength of 495 nm to 570 nm.
- Yellow color and its wavelength starts from 570 nm to 590 nm.
- Orange color and its wavelength starts from 590 nm to 620 nm.
- The red color has wavelengths between 620 nm and 750 nm and has a frequency from 400 Hz to 484 Hz.

The part that is not visible to the naked eye is also called invisible rays and is located outside the wave band:

- Gamma rays.
- X-Ray.
- UV.
- Infrared.
- Radio waves.

Not all solar radiation can reach the Earth's surface, but a small part of it reaches the earth and the largest part is subject to diffusion in space before entering the atmosphere due to the presence of obstacles as well as the lack of gravity in space. When a quantity of radiation enters the atmosphere surrounding the surface of the Earth, part of it is exposed to reflection due to the presence of clouds and plankton, and the other part is exposed to absorption by the surface of the Earth to provide the Earth with heat and light [20], as in Figure (1-9).

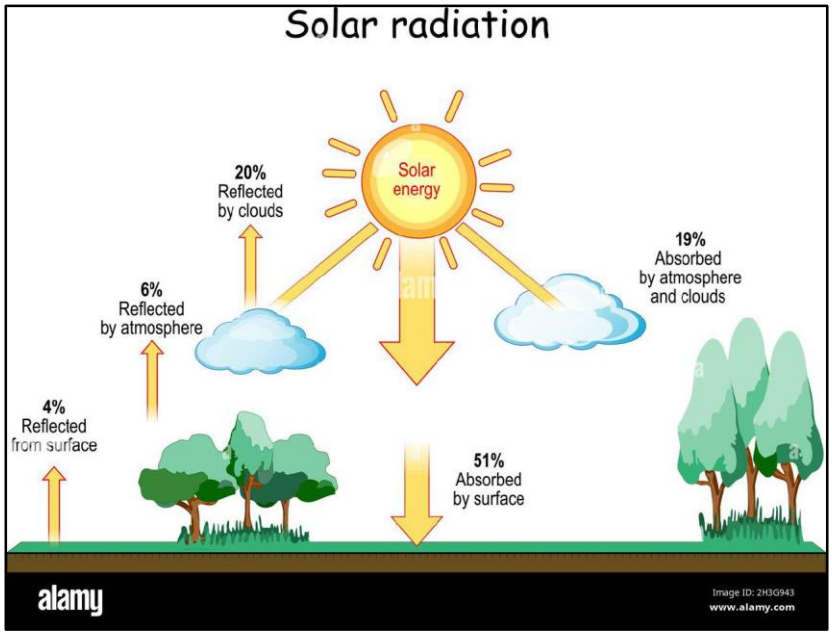

Figure (1-9): Represents the parts of solar radiation absorbed and reflected [21].

The solar radiation emitted by the sun is energy of different wavelengths, proportional to an adverse relation between the amount of energy and its wavelength as the wavelength of the incoming sun rays increases energy decreased. This means that infrared rays have low energy and ultraviolet rays have relatively high energies, and thus are harmful to human skin when exposed to them for long periods. The sun's nuclear reactions occur in its nucleus, where hydrogen atoms merge to turn into helium atoms, this leads to the production of a large amount of gamma rays. During these interactions, the sun loses about 600 million tons of its matter every second [22].

1.6 The Atmosphere

It is known as a typical intermediate phenomenon that surrounds the globe and contains the air that reaches us. There is also a great benefit to this envelope as it protects the globe from high temperatures and harmful radiation emitted from the sun. It is also considered the first responsible for heating the planet during the day and cooling it at night, and the only planet has an atmosphere that enables it to sustain life. The thickness of the atmosphere is estimated at about 480 km. For every square centimeter, the air pressure decreases by 1 kg until it reaches a height of 3 km. The air pressure reaches 0.7 kg per square centimeter, and here the oxygen gas will decrease. So, the atmosphere is defined as the space that surrounds the planet with all its components, including land, icebergs, oceans, etc., and extends from the surface of the earth to outer space. It's most important components are gases, dust, and particles suspended in the atmosphere. These particles are called aerosols [23].

The density of this envelope near the Earth's surface is more than its density in space, so the density of the envelope will be directly proportional to its approach to planet Earth. Earth's gravity plays a main role in this, as it attracts gases, dust particles, and smoke to the Earth's . It is also the main reason for Earth's retention of its outer atmosphere. Low gravity led to the loss of the atmosphere of some planets, such as Mercury. The earth's atmosphere is characterized by containing water in its three states: liquid, solid, and gaseous. The earth's atmosphere has several constituent layers, starting from the surface of the earth and extending to outer space. The most important of these layers are [24]:

1- The troposphere.
2- The stratosphere.
3- The mesosphere.

4- The thermosphere.

5- The ionosphere.

6- The exosphere.

Figure (1-10) shows the layers of the atmosphere.

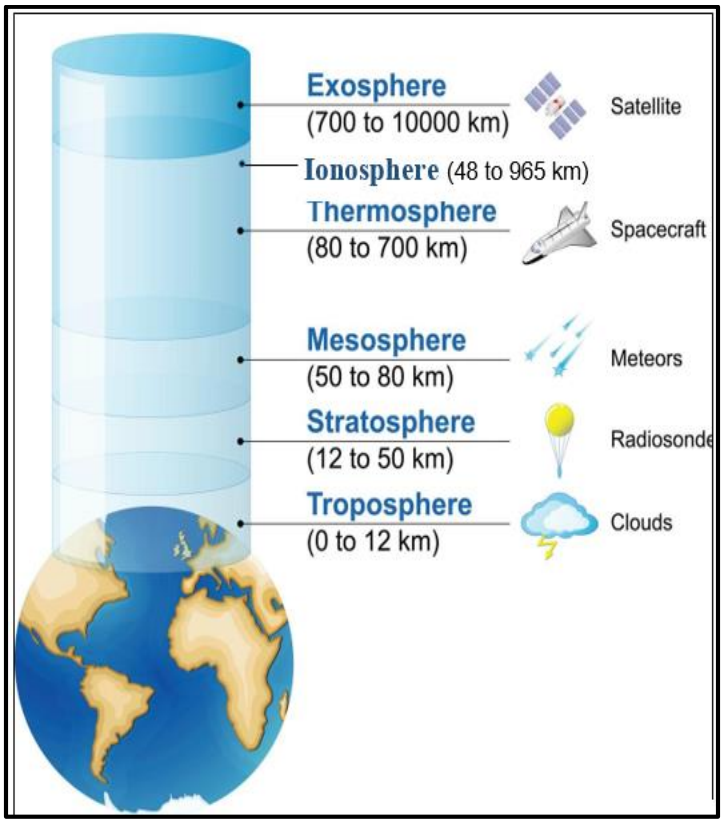

Figure (1-10): The layers of the atmosphere [25].

1.6.1- The Troposphere

Starting from the Earth's surface and going up into outer space, the troposphere is the first layer of the Earth's atmosphere because of its proximity to the Earth's surface, and it is a vertical extension from sea level for a distance of 10 km. How close to the north and south poles during the winter season, this height depends on

latitudes and seasons, as its length increases during the summer and decreases during the winter. Due to the high density of this layer of the atmosphere, it contains most of its components up to 75-80% of the overall mass of the atmosphere, and for this reason, this covering is a place for the appearance of all weather conditions and all different climate conditions, and also this layer is an incubator for most types of clouds [26].

1.6.2 The Stratosphere

According to its proximity to surface of planet Earth, this layer is considered the second in the order of layers and it is at various altitudes in the troposphere, starting at a height of about 10 km above the Earth's surface in circles and mid-latitudes., and this height varies according to latitudes and seasons. The stratosphere layer is at an abute of 20 km at the equator and begins to decrease towards the north and south poles until it reaches 7 km during the winter season, and extends in the atmosphere until it reaches a height of approximately 50 km. Below this layer there is another layer called the tropopause located below the stratosphere and the troposphere.

The temperatures in this layer are inversely proportional to the height of the layer, and this is the opposite of the troposphere, where temperatures increase in the stratosphere at altitude, and given that the air is stable in this layer, it is considered a place for jet aircraft to fly. The stratosphere contains ozone gas, where 85% to 90% of the total of this gas is present in the stratosphere. Ozone gas is formed when an oxygen molecule is exposed to UV rays emitted from the sun. Ultraviolet rays decompose the oxygen molecule into its atoms and then combine with other oxygen molecules to produce ozone gas. The stratosphere contains many gases and other compounds, in addition to ozone, such as nitrogen oxide, nitric acid, sulfuric acid, and halogen oxide, in addition to many compounds resulting from the occurrence of

volcanoes, such as hydrochloric acid and hydrofluoric acid. Flying is often at the bottom of the stratosphere, due to the lack of air turbulence.

The ozone layer is at an altitude of (15-30) km and its thickness varies according to the different seasons and latitudes. This layer is considered very important because ozone gas absorbs most of the harmful ultraviolet radiation emanating from the sun, and as a result the protection of the earth and the continuation of life in it due to the great harms caused by these rays. It is possible these rays penetrate the cells and destroy the nucleic acids in them then its death and destruction. In other words, without the ozone layer, there is no life on the earth [27].

1.6.3 The Mesosphere

It is the third layer rising from the earth's surface towards space, and it is rich in many iron atoms and many other minerals, and the reason is due to the fall of meteorites towards the earth, where this layer is a rust for it and the meteorites evaporate in it, and thus its basic materials remain stuck in this layer. Also in these are the sparkling or sparkling clouds at night, which are located in the north and south poles at high altitudes. In this layer, phenomena similar to the phenomenon of lightning occur at heights of tens of kilometers, such as thunderstorms that occur in the troposphere. One of the characteristics of this layer is that it is dry and has little moisture.

This layer has been known to be mysterious despite knowing many properties and characteristics of this layer. The reason is the difficulty of access scientific research instruments such as weather balloons and exploration aircraft for this high layer. Above this layer, satellites rotate, but it was not possible to directly identify the characteristics of this layer. The height of this layer reaches about 85 km above the surface of the planet and the height in this layer, the temperatures decrease, as the

lowest temperatures are at the top of this layer, reaching -90 Cº. The mesosphere layer is very thin, but this does not prevent it from being sufficient to burn meteorites passing through it. The upper part of this layer is called the mesopause [28].

1.6.4 The Thermosphere

The fourth layer of the atmosphere and comes after the mesosphere layer and its extension is at a height of 90 km above the earth's surface. Its height is between (500 – 1000) km, and the boundary between this layer and the next layer is called the thermopause, and what is in between is called the mesopause. This layer represents the International Space Station and some other space shuttle orbits. And the temperature is high. The temperatures in this layer are very high, reaching about 200 Cº, and it can increase during the daytime to reach 500 degrees Celsius. Usually the temperatures are different and unstable depending on their height. For example, at the high layers with a distance of (200-300) km, the temperatures It rises dramatically and sharply, after which it begins to settle. As for the upper layers of it, the temperature is between (500 – 2000) Cº, and even more than that sometimes, and the air density decreases dramatically in this layer.

The components of this layer are many different atoms and molecules, and as a result of the collision of the molecules that make up the gases with each other, they will disintegrate, due to the effect of photons of x-rays and UV rays emanating from the sun, and separates them from each other. This layer also consists of oxygen and nitrogen gas, but these components will vary and change in the upper parts of this layer. The higher the height in this layer, the proportion of molecules will decrease, and the ionization processes and levels will vary, as well as the density of the molecules and their chemical composition. This layer absorbs X-rays with high

energies as well as ultraviolet rays coming from the sun, and this is one of the reasons for the high temperatures in this layer [29].

1.6.5 The Ionosphere

It is also called the ionosphere and was given this name because of the presence of ionized and electrically charged particles of ions and electrons in high concentrations. This layer overlaps with the layer of the mesosphere, the thermosphere, the exosphere, and some of its parts overlap with the Earth's magnetosphere. The amount of solar energy reaches this layer in variable and unstable quantities, and this disparity affects the thickness of this layer, as it may increase or shrink. This layer is divided into several sub-regions called F, E, D according to the wavelengths of solar radiation. The magnetic fields generated by the Earth and the Sun affect the charged particles present in this layer, whose heights are (48-965) km from the beginning of the Earth's surface to the edge of outer space. The phenomenon of the aurora borealis occurs, which appears near the north and south poles.

Through this layer, radio signals and the International Space Station are transmitted. It is worth noting that some scientific research centers for space, such as the University Corporation Atmospheric Research (UCAR) Center it is considered that the ionosphere is not among the main layers of the atmosphere, as it is distributed and divided through multiple layers: Such as, the mesosphere and the thermosphere. Although, it has its own characteristics [30].

1.6.6 The Exosphere

This layer is the last of the layers of the outer shell and is farthest from the surface of the earth and also it is completely devoid of air molecules inside it, as one particle can pass through it into space without colliding with any other existing particle, if the force of gravity does not affect it and if it has sufficient speed It enables him to escape into outer space. The beginning of this layer is the thermopause or exopause, at a height of about (250-500) km above the earth's surface, and this height varies according to the activity of the sun, which in turn affects the atmosphere.

The upper limit of this layer has not been determined yet, but there are some scientific researches that estimate the distance at 193000 km, and this is almost half the distance to the moon. At such very large distances, the amount of radiation pressure of the sun on the hydrogen atoms there is much greater than the earth's gravitational force, and this leads to the formation of a new phenomenon called the Earth's halo. This phenomenon can be observed at an altitude of approximately 96,560 km [31].

1.7 The Ozone Layer

This layer is centered below the stratosphere and is blue in color and is considered part of the atmosphere, due to the ultraviolet rays emitted from the sun, part of the oxygen gas turns into ozone gas due to the absence of thick layers of air above it. The ozone layer is very important as it prevents the arrival of short ultraviolet waves in concentrations high to the planet Earth, so its role is very important for the sustainability of life on the Earth's surface, as it prevents the intrusion of harmful ultraviolet rays emitted by the sun. The most dangerous of these types is the last type: UVa, UVb and UVc. Ultraviolet rays are classified as It is considered very harmful to humans. Ultraviolet rays are purified by the ozone layer

at an altitude of 35 km. Ozone gas is classified as a toxic gas at low altitudes, as it causes bleeding when exposed to it.

When the skin is exposed to type 2 ultraviolet rays, it can cause burning that appears in the form of severe redness, and this severe and continuous exposure leads to a change in the genetic codes that cause skin cancer. Completely, as some of them reach the planet, unlike the first type, most of them do not pass through the ozone layer and reach the surface of the earth, but they do not harm the skin when exposed to them only, they can cause a change in the genetic codes.

The weakness and depletion of the ozone layer allows ultraviolet rays, especially the sun, to reach the surface of the earth, which leads to changes in the genetic genes of living things on the surface of the earth, and this is what happens when the ozone layer is damaged and a hole occurs in it.[32]

1.8 The Ultraviolet Rays (UV):

It is an electromagnetic wave with a wavelength shorter than visible light but longer than X-rays. It is called ultraviolet because the wavelength of violet is the shortest among the colors of the spectrum and its wavelength starts from (10-400) nm and its shot starts from (3-12.4) eV.

They are found in sunlight and are emitted by electric arc or black light. They are ionizing rays (that is, separating electrons from their atoms) and have high frequencies, followed by X-rays and gamma rays, which are of three types: UVc, UVb and UVa[33].

The first type, UVC, has the largest energy because it has the shortest wavelength

and is absorbed by ozone. The second type, UVB, has lower energy than the first type. The third type, UVA, is the least effective of the two previous types, which reaches the Earth. Figure (1-11) shows these types.

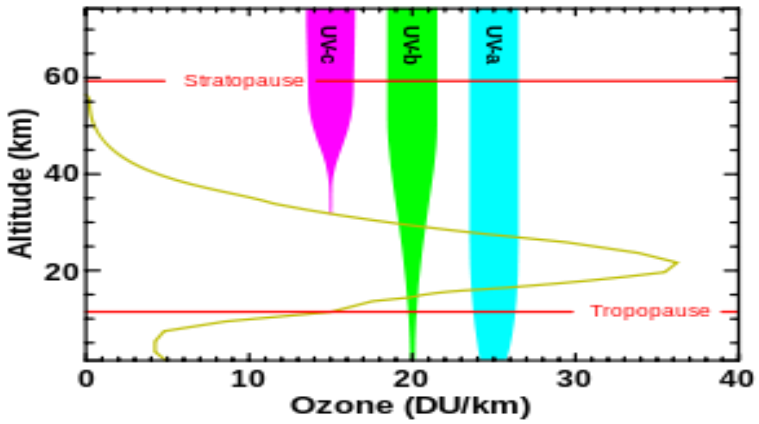

Figure (1-11): Ultraviolet radiation absorption rate of the ozone layer [34].

When we mention that the rays are visible or invisible, it depends on their wavelength, so the wavelength of ordinary light is long, while ultraviolet rays have a short wavelength, as well as X-rays are less than the wavelength of ultraviolet rays and are more harmful than that, the lower the wavelength the more X-ray damage.

The degree and intensity of ultraviolet radiation varies according to the seasons of the year and according to your location on the globe because your distance from the sun depends on your location on the earth. The main source of ultraviolet rays is the sun, so when the sun is absent, the effect of these rays end [35].

Exposure to sunlight for long periods and in a concentrated manner affects human health. It may affect the skin and cause skin cancer and also on the retina of the eye, as well as cause hardening of the arteries. The ozone layer is uneven in the atmosphere. Three oxygen atoms O_3 are aligned with each other and this layer is able to weaken, absorb or block ultraviolet rays heading to the earth. These rays are

used to purify water because of the power of high-energy photons and are able to kill microorganisms [36].

1.8.1 The Solar Radiation and Skin

Ultraviolet radiation is considered a source of energy that arrives naturally from the sun directly and mainly, and sometimes it arrives abnormally through sunbeds. Excessive exposure to ultraviolet radiation for long times can lead to damage to the deoxyribo nucleic acid DNA present in the skin cells and as a result causing skin cancer. On the other hand, exposure to the sun for long periods of time and sunburn at least once every two years leads to an increase in the probability of skin cancer three times compared to the case of not being exposed to sunburns at all. There are three types of ultraviolet radiation, which are divided according to dangerousness and the rate of its arrival to the surface of the earth [37]:

1- UVa: Which is the first type, and is called long rays, and its wavelengths range from 315 to 400 nm, and it penetrates the entire atmosphere to reach the earth, since 95% of the electromagnetic radiation that reaches the earth is long electromagnetic radiation, which is less dangerous to human health.
2- UVb: This second type of ultraviolet radiation is called medium and has wavelengths between 280 to 315 nm, and represents only 5% of the electromagnetic radiation that reaches the earth and is more dangerous than the first type and can cause burns to the skin.
3- UVc: This third type of ultraviolet radiation is called short, as its wavelengths range from 180 to 280 nm, and it is the most dangerous of all, but the ozone layer completely obscures it and prevents it from reaching the earth, as well

as the presence of oxygen molecules and water vapor in the upper layers of the atmosphere. It absorbs short wavelength radiation.

1.9 The Atmospheric Effects on the Solar Radiation

The atmosphere surrounding the globe has many effects on solar radiation and is considered positive and important for the continuity of life on the planet

- The scattering, reflection and absorption in the atmosphere are factors that lead to a decrease in the energy of solar radiation emitted from the sun.
- The increase in the absorption or scattering of wavelengths leads to a change in the spectral content of the solar radiation.
- There are diffusion elements that have an indirect effect on solar radiation, such as water vapor, clouds, and polluting elements [38].

All these effects are shown in Figure (1-12).

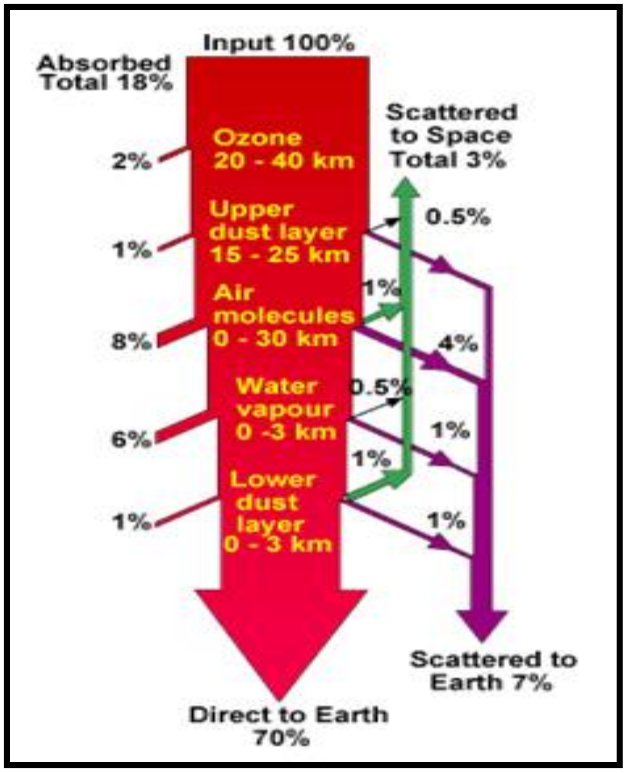

Figure (1-12): Atmospheric effects on solar radiation, typical clear sky absorption and scattering of incident sunlight [39].

1.9.1 Direct and Diffuse Radiation Due to Scattering of Incident Light

When light passes through the atmosphere, it is more susceptible to absorption and scattering. The scattering mechanism in the atmosphere is known as Rayleigh scattering, and it occurs due to particles in the atmosphere. This mechanism is effective and important for short wavelengths (blue light), as it depends on λ^{-4} . There is another scattering known as Mie scattering, it depends on aerosols and dust particles that also contribute to the scattering of light. The dispersed light is by its nature undirected, as it is considered to come from any region of the sky and is scientifically called (diffuse light), where the light is mainly blue light, and the color of the sky is black in the absence of dispersion in the atmosphere, where the sun

appears as a light source for the disc on a clear day only 10% of the incident solar radiation is transmitted [40].

1.9.2 Effect of Clouds and Other Local Variations in the Atmosphere

The factors of local differences in the atmosphere are the main and final cause of the effect of the atmosphere on the incident solar radiation, and depending on the cloud cover and its type, the radiation power is reduced severely. The update occurs on the incident solar radiation (insolation) during its passage through the atmosphere and is modified more widely[41]. Through topography and surface factors, it is intercepted on the surface of the earth as direct, diffuse and reflected components. Figure (1-13), direct radiation passes unhindered in a direct line from the sun, while diffuse radiation is spread by atmospheric components such as clouds and dust, and reflected radiation is done by the surface of the earth, all these types of direct, diffuse and reflected radiation are called total or global solar radiation. Surrounded by highly reflective objects such as areas of snow cover, the methods used to calculate radiation do not include reflected radiation in calculating the total radiation, so the total radiation is calculated from the sum of direct and diffuse radiation, direct radiation is observed from the beginning of sunrise to sunset, and global radiation is observed in twilight, that is, before sunrise or after sunset. Solar radiation is measured in W/m^2, and the total amount of radiation is measured in J/m^2 [42].

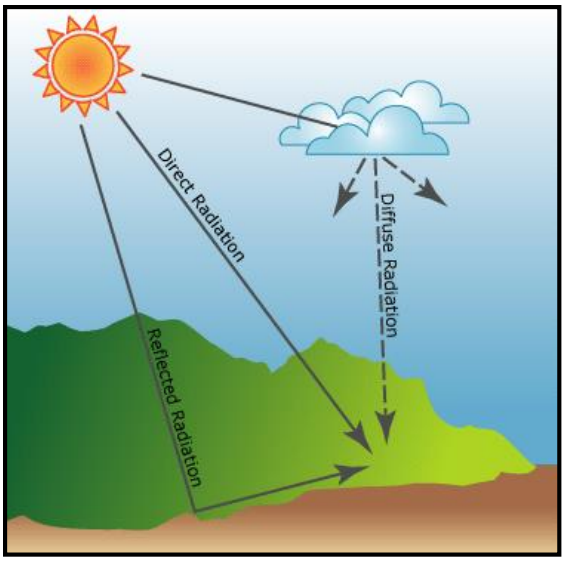

Figure (1-13): Incoming solar radiation and is intercepted at the earth's surface as direct, diffuse, and reflected components [42].

Conversion between the currently used unit (SI) and the former unit (calories) can be performed using the following formulae:

Solar irradiance: 1 kW. m^{-2} = 1.433 cal. cm^{-2} .min^{-1}

Total amount of solar radiation: 1 MJm^{-2} = 23.89 $cal.cm^{-2}$

1.9.3 The Sunshine Duration

Sunshine duration sunlight, ultraviolet rays, 120 W per sunlight in certain Earth conditions and are sometimes an average years. This description is about insolation, the latter measures the amount of insolation, the latter measures the amount of total energy produced by light for a specific time, the hourly duration of brightness during a year or the average hours during a day of the annual first measure, compared to the general brightness, compared with other regions of the

second measure, it is a brightness comparison for different seasons and times for one particular location. Brightness duration data [43].

Duration of the day when the sun is above the horizon by 50% of the time for the standard year, which consists of 8760 hours, the maximum apparent day will be 8380 hours for a specific point on the surface of the earth. There are physical and astronomical effects that change the apparent image of it. It is possible for the sun to remain visible even after it has actually set. This is due to the atmospheric refraction of the sun, and this is a major reason for the average day (away from the effects of clouds in the polar regions) to be the longest, as the visible sun is most of the time around horizon. The regions in the Arctic Circle have a total annual daylight of 4647 hours, which is the longest, and at the North Pole it is 4575 hours due to the elliptical nature of the earth, and it is 4530 in the southern hemisphere, which is not the same. The total daylight hours at the equator are 4422 hours a year [44].

Definition and measurement after clarifying the theoretical maximum duration of the day at a specific point or location, it must be noted that there is a practical measurement of the duration of the brightness for the same specific points, but when there is a sufficient amount of daylight so that we can consider it (the hour of sunshine), when the sun is bright, the hours of sunshine are the total hours of strong brightness, i.e. the strongest period of sunshine, which is unlike other hours of visible brightness only, which are at sunrise and sunset, where these hours are not strong and weak, and as a result, they are not sufficient to excite measuring and sensing devices.

There are tools called sunbeam recorders through which a practical measurement is made for the duration of the sun's brightness, including Campbell-

Stokes recorders, which contain spherical glass lenses placed on a special tape to focus the sun's rays. Burnt is proportional to the number of luminous hours.

There are radio recorders of another type called Jordan recorders, and the method of their work is electronic, which is the latest and has more sensitivity than the first type that uses paper tape. The duration of brightness is determined and calculated based on the period in which the direct solar radiation exceeds the value of 120 watts / m^2 [45].

1.10 The Skin Cancer

In general, cancers are defined as abnormally growing cells that have the ability to invade and spread to multiple parts of the human body. Skin cancer is divided into three types: the first is called basal cell carcinoma, the second is squamous cell carcinoma, and the third is called melanoma skin cancer. The first and second types are called non-melanoma, carcinoma. Basophils grow slowly and have the ability to damage the tissues surrounding the skin, but they do not spread to other parts of the body, and death rates are very low. It appears on the surface of the skin in the form of a raised, painless area, and sometimes it is shiny when vessels pass over these spots and they are also ulcerated. The second type is called carcinoma. Squamous cells are more widespread in the body or cause death. It is more capable of spreading in the body. It often appears as a solid mass, scaly on top, but it can also form ulcers. As for melanomas, they are the most aggressive of all. One of its signs is a mole (a dark area of the skin (a mole)) some of its characteristics have changed in size, color, or shape, or its edges have become irregular, or it has become more than one color, has become bleeding or causes itching [46].

The causes of injuries for more than 90% of cases are due to direct exposure of the skin to ultraviolet rays of the sun, and this exposure increases the incidence of the three types of cancers mentioned above and increases, especially after the ozone layer became thinner and lighter than before. People with fair skin are more susceptible than others in addition to people with low immunity as a result of taking medications that weaken the immune system. The use of sunscreen to block sunlight, as well as reducing exposure to ultraviolet rays, are effective ways to prevent melanomas. and squamous cell carcinomas. Non-melanomas are usually fully curable. In general, treatment is either by surgical removal, or, less commonly, by radiotherapy or by the use of topical medications. Treatment of melanomas may include more than one treatment together, including surgery, chemotherapy, radiotherapy, in addition to targeted treatment. Globally, skin cancer is generally the most common type, as it represents 40% of cancer cases in general, and it spreads in greater proportions among people with fair skin, and non-melanoma cell cancer is the most common among other types, with an estimated number of infections at an average of 2-3 million cases. incidence annually, 80% of basal cell carcinomas and 20% of squamous cell carcinomas that rarely lead to death [47] as shown in Figure (1-14).

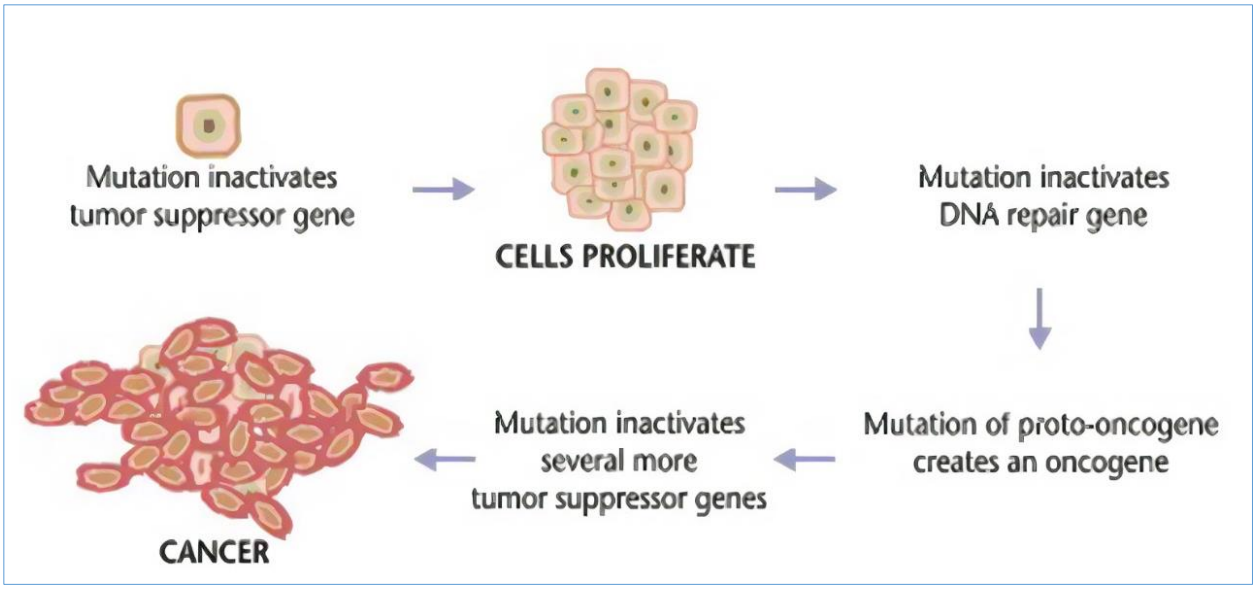

Figure (1-14): The process of transforming a healthy cell into a cancerous cell [48].

There are several types of cancer, and skin cancer is one of the most important of these types, and it is divided into three categories:

1- Basal cell carcinoma

2- squamous cell carcinoma

3- Melanoma (malignant) skin cancer

Basal skin cancer is the most common and reaches 80% of cases. In terms of growth, it is the slowest, and in terms of spread, it does not spread and remains limited to the skin only and is in the form of pigmentation or redness on the skin and its edges are uncombined Figure (1-15) although it takes specific shape and surgically treated

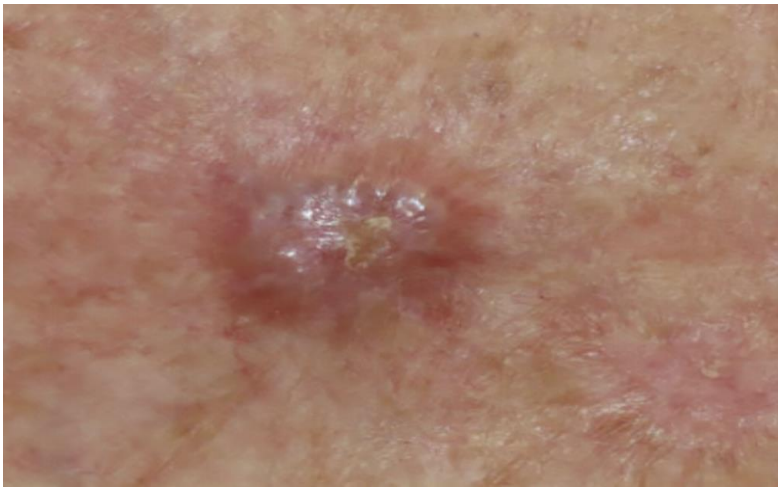

Figure(1-15): Basal cell carcinoma [49].

As for squamous skin cancer, it is more complex than the basal and is characterized by rapid growth compared to the basal. It is in the form of a pigmented mass, often in the form of ulcers on the skin and in the form of a raised mass that is not joined by the edges Figure (1-16), and it is also treated with surgical intervention, especially if it is discovered early and needs simulation to find out whether it spread or not, especially if it was discovered late[50].

Figure(1-16): Squamous cell carcinoma [50].

Melanoma cancer is considered more severe, deadly and dangerous because it is rapidly growing and multiplying and spreads to other parts of the body such as the liver, bones and kidneys, and its shape is similar to a mole and changes its color and size quickly, and it is also not joined by the edges [51], Figure (1-17).

Figure (1-17): Melanoma cancer [51].

1. 10.1 Symptoms

Skin cancer often consists of continuous exposure to sunlight (ultraviolet rays) the face, hands and scalp are more susceptible to infection and ultraviolet rays have a major role in skin cancer and symptoms are the appearance of a small mass that increases in size constantly and changes color to dark and has irregular edges and sometimes painful [52].

1. 10.2 Dangerous factors

1- Constant exposure to sunlight, especially in the afternoon, because ultraviolet rays destroy DNA, and thus skin cancers are formed.

2- People with white skin (light) are more susceptible to infection because they lack melanin, unlike people with dark skin.

3- The presence of moles in abundance, it is possible for the mole to turn into cancer, so it must be monitored (size and color).

4- Weak immunity: People with weak immunity are more likely to get skin cancer due to the presence of a disease or the use of drugs that reduce immunity.

5- Having a family history of skin cancers or having a family member.

6- Some work related to chemicals, the person is more susceptible to injury.

1.10.3 Prevention

To prevent skin cancer, you should avoid exposure to the midday sun, when the percentage of ultraviolet rays is very high than at any time of the day, by wearing hats and sunscreen, standing in the shade, and using sunscreen that protects the skin from rays [53].

1.10.4 Diagnosis

After the appearance of moles or pigmented lumps on the skin, this is an indication of infection. Therefore, the competent centers should be reviewed, and this is done through a clinical examination. After that, simulation is performed and a biopsy is taken of the area and analyzed [54].

1. 10.5 Treatment

Treatment is through surgical intervention and removal of these pigment masses or through the use of laser to freeze them. After that, chemotherapy and radiotherapy are carried out according to the doctor's direction. The period of detection of the disease is considered one of the most important factors in increasing the rates of recovery. The earlier the detection, the higher the rates of success and recovery [55].

1.11 The Study Area

The city of Babylon was chosen as a study area for the research, as the city of Babylon is located on the western side of the continent of Asia in the center of the Republic of Iraq, it is about 88 km south from the capital, Baghdad And it is considered the fifth in the country in terms of population, which is approximately 2 million people, and the fourth smallest province in Iraq in terms of area [56]:

1- Geographic position :-

The study area (Babylon) is located in the middle of Iraq: between latitude 32˚ 6` N to 33˚8` N, and longitude 43˚57` E to 45˚12` E.

2- Survey and administrative units :-

The area of the governornte of Babylon represents about 1.2% of the total area of Iraq, which is about 5307 km^2, and includes about 7 districts and 17 sub-districts, as shown in the following Table (1-1):

Table (1-1): Shows the districts and sub-districts of the city of Babylon (prepared by the researcher)

Districts	Sub-districts
Hilla district	Abi gharak , Sinjar
Al-Mahaweel district	Al-Mahaweel, Al-Imam, Al-Nil
Kotha district	Jableh, Al-Mashrou
Hashemite district	Al-Hashimiyya, Al-Qasim, Al-Talee'a
Musayyib district	Musayyib, Alexandria, Sedt Al-Hindiya, Jurf Al-Sakher
Western Hamza district	Al-Medhatiya, Al-Shomali
Al-Kifl district	Bani Muslim, Tufail, Aufi

3- Temporal boundaries :-

For the data limits for the study area of the research, and as evidenced it is for the period July and August of 2021, see Figure (1-18) and (1-19):

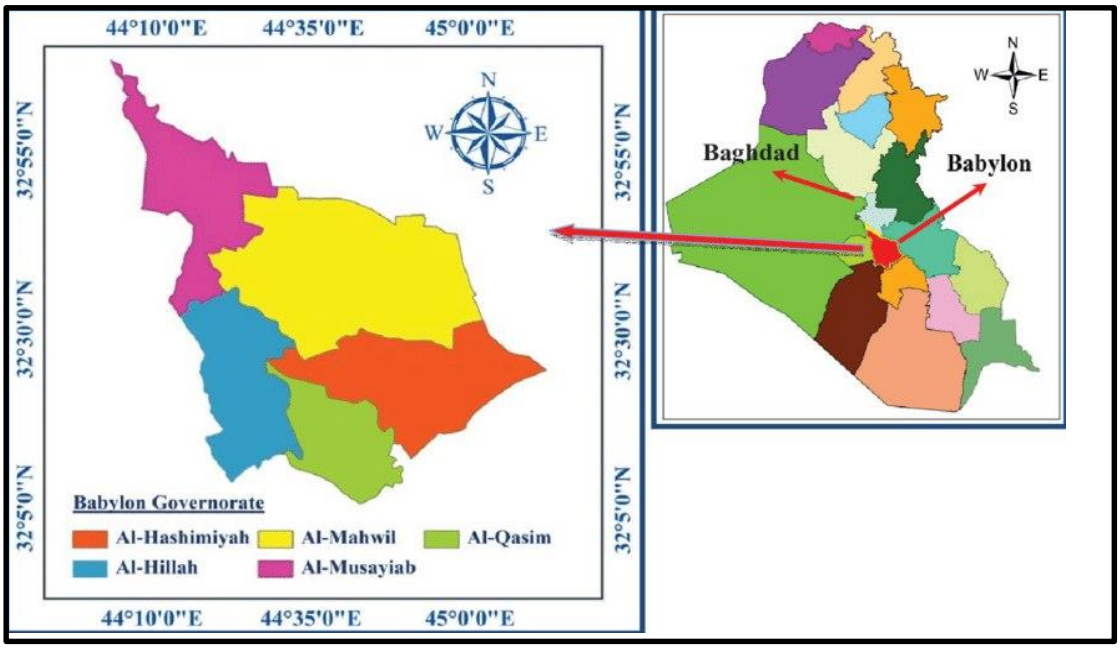

Figure (1 - 18): The region of study (Babylon), the right panel shows the position of Babylon with respect to Iraq, the left panel is zoom in to the red area (Babylon) in right panel showing the main districts [57].

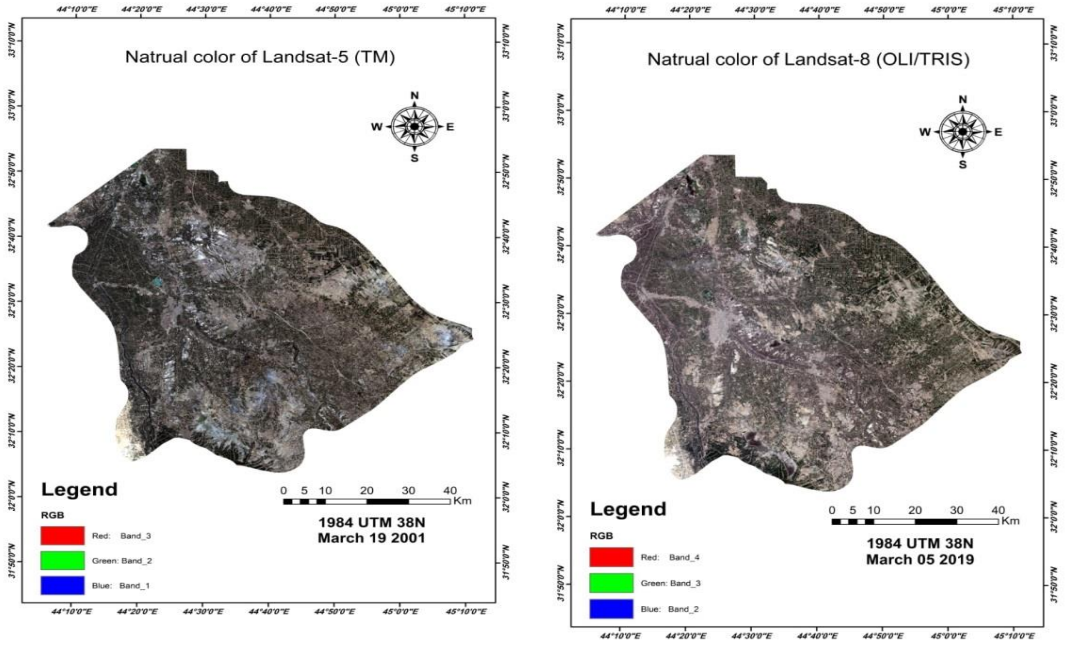

(a) (b)

Figure (1-19): (a) Satellite image of Babylon province by using Landsat5, (b) Satellite image of Babylon province by using Landsat8 [57].

4- Spatial Boundaries and Climate:

The spatial boundaries of the research for the province of Babylon, as it is considered one of the provinces of the middle Euphrates, bordered by the capital Baghdad from the northern side, Wasit province from the eastern side, the provinces of Najaf and Qadisiyah from the south side, and the provinces of Karbala and Anbar from the western side.

A desert climate prevails, characterized by a lack of rain in the winter and high temperatures in the summer, reaching 50C°, and a warm weather prevails in the winter.

1.12 Literature Review

Many studies dealt with some of the overlapping topics or similar to our work, including:

Al-Rijabo, (2011), this statement describes a study that examined the spatial variation of total solar radiation falling on a horizontal surface in Iraq. The study developed a mathematical model to estimate global solar radiation on a plane surface, which was a function of relative humidity, mean air temperature, and sunshine ratio. The study found that the model was highly accurate when applied, indicating that it could be useful for estimating solar radiation in Iraq. This information could be beneficial for a range of applications, including solar energy planning and agricultural production.

The development of the mathematical model highlights the importance of understanding the factors that affect solar radiation, as this knowledge can be used to estimate radiation levels accurately. The study's findings can help inform future studies on solar radiation and provide valuable information for decision-making related to solar energy planning and other activities that depend on solar radiation. [58].

Abdul Qayoom Jakhrani, *et al*, (2013), this statement discusses a study that aimed to examine the performance of tilted surface solar radiation models for estimating the amount of solar radiation. The study evaluated the results of different models using a one-sample statistical test.

The results of the study showed that the Reindl et al. model had the highest variation in estimated tilted surface radiations, while the Klucher model had the lowest error

according to the statistical test. Based on this evaluation, the study concluded that the Klucher model could be preferred for estimating tilted surface radiations.

This statement highlights the importance of selecting an appropriate model for estimating solar radiation on tilted surfaces, which can be useful for a range of applications, including solar energy planning and building design. The study's findings provide insight into the performance of different models and can serve as a guide for selecting the most suitable model for a particular application. [59].

E. Knight and G. Kvaran, (2014), studied "Landsat-eight Operational Land Imager Design, Characterization and Performance". This statement highlights the successful transition of the Landsat program to the pushbroom sensor era with the introduction of the Operational Land Imager (OLI). The design of the OLI has proven to be robust, and its extensive pre-launch characterization and calibration have resulted in high-quality data that meets the instrument's performance requirements, including low stray light, sharp edge response, and precision calibration.

The on-orbit performance of the OLI has been excellent, as demonstrated by stability trending and lunar views, indicating that the instrument is continuing the Landsat program's legacy of providing accurate and reliable Earth observation data. The OLI's success is a testament to the dedication and hard work of the program's engineers and scientists who have continued to push the boundaries of remote sensing technology.

Overall, this statement highlights the importance of the OLI in the Landsat program and demonstrates the program's commitment to providing reliable and high-quality Earth observation data for scientific research, resource management, and environmental monitoring. [60].

Taehong Sung, *et al*, (2015), this study proposes a mathematical model that incorporates weather variability in hourly solar radiation using the simple sky model. The model uses a superposition of trigonometric functions to investigate the effects of model variables on two important indices: clearness (kD) and probability of persistence (POPD).

The study also evaluates the model for all kD-POPD weather classes and compares its performance with the simple sky model using a simulation of a simple solar organic Rankine cycle system with thermal storage under actual weather conditions. The simulation results show that the proposed model provides more accurate system operation characteristics compared to the simple sky model. This finding suggests that the model can be used to improve the performance of solar energy systems that rely on weather-dependent factors, such as solar thermal storage and dispatchable power generation.

Overall, the study demonstrates the potential of the proposed model to provide more accurate predictions of hourly solar radiation with weather variability, which can help improve the design and operation of solar energy systems. The results can be used by researchers and policymakers to optimize the performance of solar energy systems and promote the use of renewable energy sources. [61].

Bibbins-Domingo K, *et al*, (2016), this study emphasizes the importance of early detection and prevention of melanoma, which has higher mortality rates compared to basal and squamous cell carcinomas. It highlights the need for increased public awareness and implementation of effective strategies to prevent and detect skin cancer. These strategies may include regular use of sunscreen, avoiding prolonged exposure to the sun, routine skin cancer screenings, and early treatment of suspicious

moles or lesions. By promoting these preventative measures and improving the early detection of melanoma, we can help reduce the number of skin cancer cases and prevent deaths from this disease. [62].

Ahmed A. Hameed, *et al* (2017), the study proposed a mathematical program that uses MATLAP to estimate the hourly spatial and temporal distribution of solar radiation incident on inclined surfaces with varying latitudes (25°- 40°) and longitudes (35°- 50°) using two mathematical models: the isotropic model and the anisotropic model. The program also takes into account the optimum inclination angle for solar energy collection at all times.

The results of the study indicate that the inclined surface receives more solar energy compared to the horizontal surface, and the amount of solar energy received increases as the latitude decreases. Furthermore, the anisotropic model was found to be more accurate than the isotropic model in estimating the spatial distribution of solar radiation incident on inclined surfaces.

Overall, the proposed mathematical program provides a useful tool for accurately estimating the spatial and temporal distribution of solar radiation incident on inclined surfaces in regions with varying latitudes and longitudes. The findings can be used by researchers and policymakers to optimize the design and installation of solar energy systems in these regions to maximize energy production. [63]**.**

Hilmi Cenk Bayrakçı, et al, (2018), "Development of Experimental Models for Estimating Global Solar Irradiation at the Horizontal Surface: A Case Study",

the study aimes to evaluate and compare different literary models for estimating global solar radiation in Muğla Province, Turkey. Using meteorological data collected on the campus of Muğla Sıtkı Koçman University between 2007 and 2015,

the researchers analyzed 105 models using the MATLAB program. The goal was to identify the most accurate models for estimating global solar radiation in this region.

The study found that some models were more accurate than others in estimating global solar radiation in Muğla Province. In particular, the Angstrom-Prescott (AP), Liu and Jordan (LJ), and Bristow and Campbell (BC) models were found to be the most accurate. By contrast, other models, such as the Hargreaves and Samani (HS) model, were found to be less accurate in estimating global solar radiation in this region.

Overall, the study highlights the importance of selecting the most appropriate model for estimating global solar radiation in a given region, as different models may perform differently depending on the location and atmospheric conditions. The findings can be used by researchers and policymakers to develop new models or refine existing ones for accurately estimating solar radiation in Muğla Province and other similar regions. [64].

Alberto Modenese, *et al*, (2018) ,"Solar Radiation Exposure and Outdoor Work: An Underestimated Occupational Risk", the review highlights that outdoor workers are particularly vulnerable to adverse health effects related to SR exposure, and that UV radiation is the primary cause of these effects. Furthermore, the review outlines the different methods available for assessing both short-term and cumulative exposure to UV radiation, and highlights the importance of using protective measures, such as sunscreen, protective clothing, and eyewear to reduce risk. The review also provides a comprehensive overview of the adverse skin and eye effects associated with SR exposure, including non-melanoma skin cancer, malignant

melanoma, cataracts, and photokeratitis. The evidence presented underscores the need for effective prevention strategies to reduce occupational SR exposure and the associated health risks.

Overall, the review provides valuable insights into the impact of SR exposure on outdoor workers and highlights the need for ongoing awareness and preventive measures to protect this vulnerable population. The findings can be used by policymakers, employers, and occupational health practitioners to develop and implement effective interventions that reduce SR exposure and improve the health and safety of outdoor workers [65].

Melina Arnold et al. (2018), "The worldwide burden of cutaneous dermatomes attributed to UV radiation in 2012", with the highest burden observed in high-income countries and particularly among women. Furthermore, the results showed that individuals aged 50 years and older were at a significantly higher risk of developing skin cancer due to excessive UVB exposure.

The study highlights the significant impact of excessive UVB exposure on the global burden of skin cancer, particularly among high-income populations and older individuals. The findings emphasize the need for interventions that target both population-level and individual-level UVB exposure reduction measures, such as promoting the use of protective clothing, sunscreen, and avoiding outdoor activities during peak UV radiation hours. The findings may help guide public health strategies for skin cancer prevention and control, particularly in populations at high risk for skin cancer due to excessive UVB exposure [66].

Ayatf, *et al* (2019), studied "Guess Solar Radiation Energy on Iraq by way of the usage of DEMS and ArcGIS Techniques" intervals and daily averages. The findings

show that the solar radiation energy ranges from 3000 to 8000 Wh/m2 per day. The regions with the highest solar radiation energy were found in the western and southern parts of Iraq, particularly in desert areas. On the other hand, the mountainous regions in the northern part of Iraq receive the lowest solar radiation energy due to the complex terrain and shading effects.

The study emphasizes the importance of using DEM data in estimating solar radiation energy in complex topography areas, as it provides accurate information about the slope, aspect, and altitude of the terrain. By combining the DEM data with satellite data, it was possible to produce high-resolution maps that can be used for various applications, such as solar power plant siting, urban planning, and agriculture.

Overall, the paper presents a valuable contribution to the field of solar radiation energy estimation in the region of Iraq, particularly in complex topography areas. The findings can be useful for decision-makers, urban planners, and researchers who are interested in utilizing renewable energy sources and adapting to climate change [67].

Junliang Fan, *et al* (2019), "Evaluation and development of empirical fashions for estimating each day and month-to-month imply day by day diffuse horizontal sun radiation for distinctive climatic regions of China", the results reveal that the accuracy of the models varies significantly depending on the climatic region and the model category. The linear regression models and the empirical models based on temperature, humidity, and sunshine duration show lower accuracy in all regions. The models based on clearness index and regression tree models perform relatively

better in most regions. Among the developed models, the artificial neural network (ANN) model consistently shows the best performance in all regions, with an average R2 value of 0.91 and a mean absolute error (MAE) of 5.54 W/m2.
Overall, the study provides valuable insights into the performance of different models for estimating diffuse solar radiation in diverse climatic conditions. The results can be helpful in selecting appropriate models for various applications, such as designing and optimizing solar energy systems, predicting plant growth, and assessing the impact of climate change on ecosystems [68].

E. Khanjer and W. Hassan et.al (2020), studied "Radon Distribution in Baghdad Province by Using Remote sensing techniques", using the Rad-7device, the Radon gas fixations for toxins conditions in Baghdad province were calculated in the soil, the water, and the air. All of these measurements were made using an Arc-GIS system and a Landsat satellite picture of Baghdad to create maps of radon distribution. The results showed that the highest value of radon concentrated in Air at Al-Zubidia and lowest at Sadar city, the highest value of radon concentrated in Water at Abo-ghreb and lowest at Kadhmiah city, the highest value of radon concentrated in soil at Dyilal Bridge and lowest at Karada. [69].

Sajjad Hussain et al. (2020), "Using GIS gear to discover land use/land cover changes over 40 years in the Lodran district of Pakistan", overall, the study found that the Lodran region has undergone significant LULC changes over the past 40 years due to various factors such as temperature, rainfall, and human activities. The transformation of barren soil into vegetated areas and built-up areas were major changes, which were mainly driven by the growing population and expanding infrastructure. The decrease in NDVI values over time indicates a decline in

vegetation cover, which is a cause for concern as it may lead to soil erosion, loss of biodiversity, and decreased agricultural productivity.

The findings of this study have important implications for land-use planners and policymakers in the Lodran region. They need to address the challenges associated with climate change, population growth, and urbanization while ensuring sustainable land use practices. The study highlights the need for a comprehensive land-use plan that balances economic growth and environmental sustainability. It is essential to monitor LULC changes regularly to identify potential land-use conflicts and intervene timely to mitigate their risks.

Overall, this study provides valuable insights into the complex relationship between LULC changes, environmental variables, and human activities in the Lodran region, and it underscores the urgent need for sustainable land-use practices and policies to ensure the long-term well-being of the region's ecosystem and people [70].

Miguel Rivas, et al, (2020), .the results suggest that the high levels of UV-A radiation in Arica may be one of the contributing factors to the high incidence of nonmelanoma skin cancer in this region. Therefore, it is important for residents of Arica and for visitors to take measures to protect themselves from UV-A radiation, such as using sunscreen, wearing hats and protective clothing, and avoiding prolonged exposure to the sun during peak hours. The findings of this study can also be useful for public health campaigns aimed at raising awareness of the risks associated with exposure to UV radiation and promoting prevention strategies to reduce the incidence of nonmelanoma skin cancer [71].

A f Abed1, *et al* (2020), studied "Evolution and installation the maps for sun radiation of Iraq the usage of Data remark and Angstrom model during month-to-

month ". In the first part, the Angstrom model was used to estimate the monthly solar radiation on a horizontal surface at various locations in Iraq. The model used the relationship between the extraterrestrial radiation, the duration of sunshine and the atmospheric transmittance to estimate the global radiation.

In the second part, the distribution of the estimated solar radiation was mapped over Iraq using interpolation techniques in Arc GIS software. The spatial distribution of the solar radiation was estimated using the inverse distance weighting method. The accuracy of the estimated values was evaluated by measuring the root mean square error (RMSE) between the estimated values and the observed values at the validation points.

The results show that the estimated solar radiation values are in good agreement with the observed values, with an RMSE of 0.089 MJ/m2/day. The spatial distribution of solar radiation over Iraq varied from a minimum of 16.71 MJ/m2/day to a maximum of 24.84 MJ/m2/day. The highest solar radiation is observed in the west and northwest regions of Iraq, while the lowest is observed in the southeast region.

In conclusion, this study provides valuable information on the spatial distribution of solar radiation in Iraq, which can be used for the planning and design of solar power projects [72].

H Ebru Colak, et al., (2020), "Optimal Site Selection for Solar PV Plants Using GIS and AHP: A Case Study of Malatya Province, Turkey" The study found that the most suitable location for a solar PV plant is in the eastern region of Malatya, particularly in the vicinity of the villages of Koklu and Sarioba. This area has high solar radiation potential, convenient access to roads and power transmission lines, and low risk of natural disasters such as floods and earthquakes. Furthermore, there

are no residential areas or protected areas that would conflict with the construction of the solar plant.

The study also recommends that the plant should be designed with a capacity of 20-30 MWp, and the modules should be mounted on single-axis tracking systems to maximize the energy yield. The estimated annual energy production of the plant is around 36 GWh, which could meet the electricity demand of about 15,000 households in the region.

The results of this study can provide valuable insights for policymakers and investors who are interested in developing renewable energy projects in Turkey. By using GIS and the analytical hierarchy process method, they can identify the most suitable locations for solar power plants based on multiple criteria and stakeholders' preferences. This approach could help to reduce the environmental and social impacts of energy development and ensure the sustainability of the energy systems [73].

Tao Hai , *et al*,(2020), the ELM model is compared with commonly used models such as artificial neural networks (ANN), support vector regression (SVR), and multiple linear regression (MLR).

The study uses data from three different locations with different climates and geographical features: Yakima, Washington; Greensboro, North Carolina; and Austin, Texas. The model is trained on 70% of the data and tested on the remaining 30%. The performance of the ELM model is evaluated based on three metrics: mean absolute error (MAE), root mean square error (RMSE), and coefficient of determination (R2).

The results show that the ELM model outperforms the other models in terms of MAE and RMSE for all three locations. The R2 values for the ELM model are also higher

than those of the other models, indicating better accuracy in predicting G. The study concludes that the ELM model can be a reliable and efficient tool for predicting G, making it useful for assessing the potential of solar energy generation in different locations.

Overall, this research contributes to the development of accurate predictive models for sustainable utilization of solar radiation as a renewable energy source, which can play a vital role in achieving global energy sustainability goals [74].

Mawloud Guermoui,*et al* , (2020)," A complete overview of hybrid models for sun radiation forecasting" The literature review highlights the use of different hybrid models such as Artificial Neural Networks, Support Vector Machines, Fuzzy Logic, Genetic Algorithms, and Gray System Theory. The performance of these models has been evaluated based on various parameters, including the Mean Absolute Error, Root Mean Square Error, and Correlation Coefficient. The review finds that the combination of two or more models can significantly improve the accuracy and reliability of solar radiation forecast.

Several studies have used hybrid models for solar radiation assessment in different climates and locations worldwide. The review identifies some promising models, such as the Adaptive Neuro-Fuzzy Inference System and Hybrid Support Vector Regression, that showed high accuracy and reliable performance in different locations and climates.

This paper provides important insights into the latest research trends in the application of hybrid models for solar radiation assessment. The findings of this study can be helpful for researchers, practitioners, and decision-makers in the renewable energy sector to identify the appropriate models and tools for solar radiation forecasting and assessment. This paper also highlights the need for further

research and development of integrated hybrid models for improved solar radiation assessment, especially in complex and dynamic climate conditions [75].

Laura Hudson, *et al,* (2020), "Individual and blended consequences of the infrared, visible, and ultraviolet mild components of sun radiation on harm biomarkers in human skin cells" It suggests that skin fibroblasts are more vulnerable to damage from solar-simulated light than keratinocytes, and that the inclusion of visible and IR components in solar-simulated light increases this vulnerability. Additionally, the synergistic effect of UV, Vis, and IR components in generating ROS in fibroblasts highlights the importance of multi-wavelength protection approaches when designing photoprotective interventions. Furthermore, these findings emphasize the need for further research on the differential responses of skin cell types to solar-simulated light and their potential implications for photodamage and photoprotection [76].

Ümit Ağbulut,*et al* ,(2021), "Prediction of day by day international solar radiation the usage of unique device getting to know algorithms: Evaluation and assessment" The results show that all of the machine learning algorithms can predict daily global solar radiation accurately. However, the ANN and DL algorithms perform better in terms of predicting the daily global solar radiation values in all provinces. The study also shows that the daily extraterrestrial solar radiation, day length, and solar radiation data of the provinces are the most important input variables in predicting daily global solar radiation.

Overall, this study demonstrates that machine learning algorithms can be successfully used to predict daily global solar radiation values with high accuracy.

The results can be used by the energy industry and policymakers in Turkey to better plan and optimize the use of solar energy resources and increase the renewable energy share in the country's energy mix [77].

1.13 Aims of the Study

1. Making maps of the distribution of solar radiation for the province of Babylon in four seasons (summer, autumn, winter and spring) and comparing them with the changes of climate factors air temperature (T_{air}) and relative humidity (RH) by adopting satellite images (DEM), and technology (ArcGIS). It will be based on the Radar Topography Mission Digital Elevation Model SRTM DEM of resolution (30X30) m for Babylon province region.
2. Calculating the land surface temperature of the Babylon province by making maps for the area under study by adopting satellite images and using (ArcGIS) technology to determine the changes in the LST during the four seasons, as well as the vegetation cover in the region.
3. Studying the effect of high concentrations of solar radiation on increasing the incidence of skin cancer by statistically the cases of infection throughout the province of Babylon.

CHAPTER TWO

Theoretical Concept

2.1 Introduction

Electromagnetic radiation is the beginning of the remote sensing process(RS), as it starts from the same satellite (active RS) or from the sun (passive RS), so it is possible to consider the RS technique with GIS as a field for modern modeling and integrating acquisition as well as managing and analyzing all the data referred to spatially. The incident radiation suffers from the process of reflection, as it is absorbed by the surface of the planet Earth during the interaction process, and these reflected radiations are measured by the satellite sensor Which contains all the terrestrial information, which contains all the information for all the terrestrial operations that occur when the satellite is overtaken at the site. Terrestrial processes include the process of vegetation cover, components of the hydrological cycle, interaction with water bodies and all other topography [78].

Each of the terrestrial processes can be sensitive to measurements at specific wavelengths and frequencies. Therefore, it has become necessary to select satellite remote sensing devices in proportion to the purpose. In addition, these measurements have a clear impact on the spatial, temporal, radiological and spectral resolution associated with the sensor. The development of modern technologies for geographic systems, which includes GIS and RS technique, they are basic and powerful tools have an effective impact in calculating, evaluating and monitoring land degradation [79].

2.2 The Remote Sensing

The concept of remote sensing began in the seventies of the last century, when humanity felt the need to explore the things that surround it. The term remote sensing or remote detection is applied to science and technology that monitors and collects data and information from long distances and interprets it using several methods, to study and find solutions to specific phenomena or problems from long distances without the need to approach or touch these phenomena or problems on the surface of the earth, when the human eye cannot reach it, whether it is day or night [80], the human senses of sight, hearing and smell are remote sensing means using natural devices that receive sound waves or light and even particles of materials chemical from its source, and the human eye can only see objects when there are light waves of certain lengths that are reflected from the objects, or if those objects themselves become radiant in fields of light. Hence, the main objective of remote sensing is to enable the institutions responsible for planning in any country to manage and use its natural resources effectively, as it is considered an effective, fast, accurate and less costly method than traditional methods [81]. It includes everything related to its images and data, for example, images taken by various satellites and aerial photographs, and to provide possible assistance for the optimal use of economic resources [82].

Through radar devices, the importance of remote sensing lies in exploring, monitoring and recording the various resources of water, minerals, vegetation, soil and subsoil, apportionment the amount of solar radiation reaching a surface of the planet, population density and other resources, and monitoring the changes that occur to these resources from time to time, whether this change was caused by man or nature, the goal is to predict changes, especially those related to negative effects

such as floods, drought, desertification, beach erosion, measure the amount of solar radiation, ultraviolet rays, pollution of all kinds, discover and exploit new resources and give indications for urban planning [83]. Satellite image information and data can also be used in the study and management of large projects that have an impact on the environment, such as constructing roads and dams, digging canals and wells, creating artificial lakes, drying natural lakes and exploiting mines, in light of their integration with the surrounding and far environment, access to the effects, and can also be followed up until their effects are processed within the framework of this integrated picture [84], Figure (2-1).

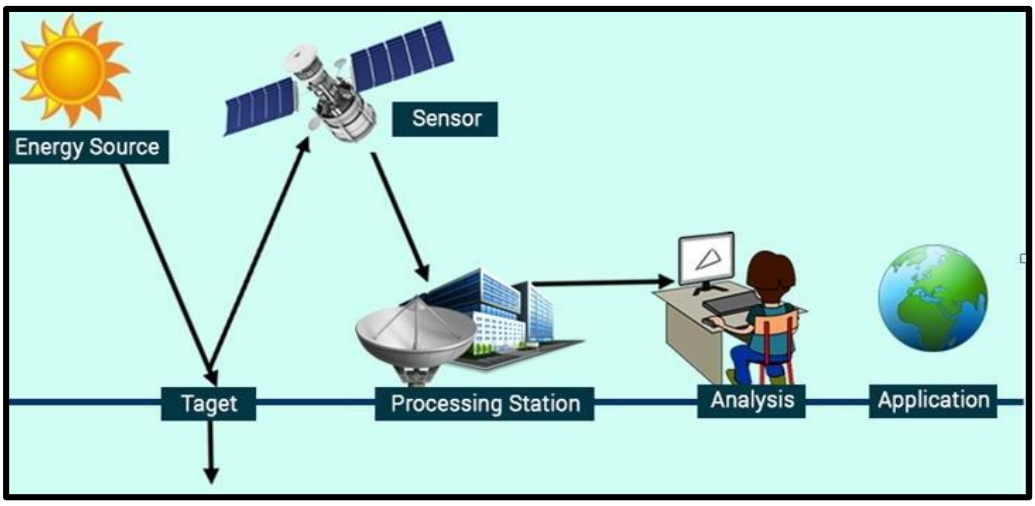

Figure (2- 1): The Remote Sensing Processes, representing the sequential steps of the remote sensing process to reach the results [85].

There are many definitions of this technique that appeared with its development over time [86]:

1- Remote sensing means the totality of operations that allow obtaining quantitative information about an object on the surface of the earth without direct physical contact between it and the information capture device.

2- The term remote sensing can be expressed as the science that uses everything that is reflected and emitted properties of electromagnetic waves by earthly bodies to obtain images and information about renewable and non-renewable natural resources.
3- Remote sensing means the combined effect of using modern remote sensing methods and data processing devices, in order to obtain an aerial and space survey of the Earth's surface.
4- The science of remote sensing is the knowledge of all data and information on the Earth by using a set of images taken from above by recording the amount of electromagnetic radiation emitted or reflected from the surface of the Earth.
5- Remote sensing can be expressed as the science through which we can collect data on the reflection of objects and the nature of their spectral behavior, and then convert them into information through processing processes.
6- Remote sensing is a tool or technique for collecting information from different distances ranging from several meters to hundreds of kilometers, and this information and data is stored in various forms (aerial photos, magnetic tapes, satellite data).

2.2.1 Types of Remote Sensing

Remote sensing is classified according to the type of data received into [87]:

1- Active remote sensing: the received data has spectral reflections, as the platforms carrying. The sensors send electromagnetic waves towards the targets to be studied, to collide with them and reflect them, so the sensors receive them and then send them to the ground receiving stations.

2- Passive remote sensing: It do not direct its own energy toward the surface or object being studied. Sunlight that deflect of the object is the origin of natural energies for negative remote sensing.

The basic operations of remote sensing can be explained according to Figure (2-2), as follows [88]:

1- power source (A): Remote sensing needs a source that emits energy through radiation, so it serves as a center that sends all waves and thermal radiation towards the target to be studied.
2- Energy transmission media (B): It is the atmosphere through which the waves pass, and a large part of them are absorbed through the gas envelopes around the earth, which are the majority and pass some of them, which are the visible rays and part of the infrared rays.
3- Interactivity with Objective (C).
4- Energy records by sensors (D).
5- Transmission, reception, processing (E): The reflected rays are sent through sensitive devices towards the receiving stations, after which the reflected rays are converted into magnetic intensity and then electric, and then the television picture is formed.
6- Annotation and analysis (F): The images recorded in the computer can be manipulated and entered to obtain information about the target.
7- Application (G): Data can be analyzed and controlled to obtain most of the information that helps us solve specific problems.

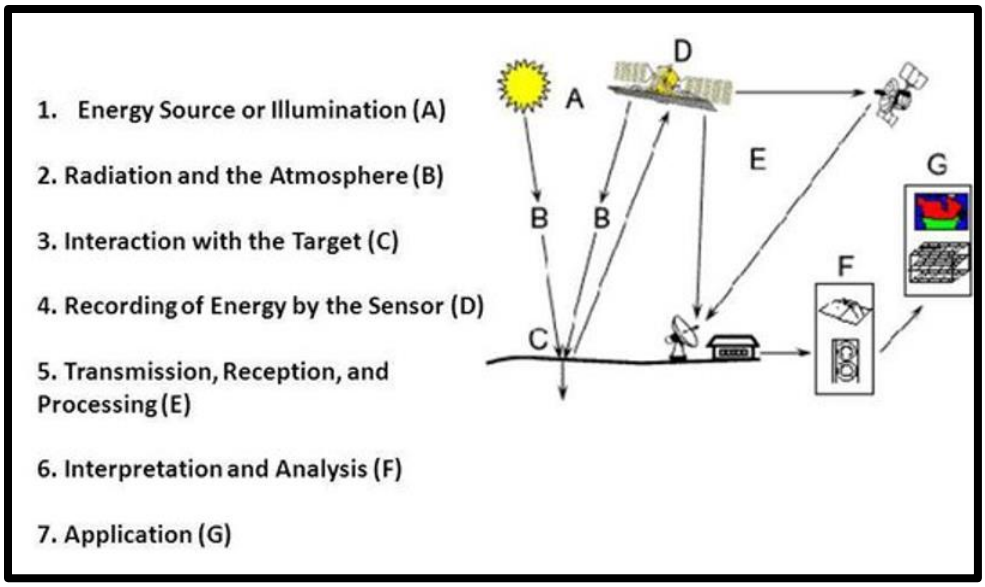

Figure (2-2): Stages and remote sensing processes [89].

2.2.2 Remote Sensing Data Products:

Sensor data is of two types, either pictorial data or digital data, as follows:

1. Digital data products: are a type of information format where the data is represented as a matrix of small cells. These cells contain quantitative values of electromagnetic energy emitted from all objects within a specific field of view. The result of this representation is a digital image, which is a two-dimensional matrix composed of individual picture elements, known as pixels. Each pixel within the image corresponds to a particular area on the Earth's surface and possesses a specific intensity value (represented by a number) and a location address (specified by a row and column number). The intensity value of a pixel represents the measurement of solar radiation within a specific wavelength range that is reflected from the Earth's surface. The location address of a pixel establishes a connection between its row and

column position within the matrix and the geographical coordinates (latitude and longitude) of the corresponding location on the Earth's surface. A digital image is typically defined as a matrix of large numbers, with the information being stored in magnetic tapes compatible with computers (TCC). Due to its digital nature, digital data can be easily converted into a photograph or visual representation using appropriate software and rendering techniques[90].

2. Pictorial data products: are information formats that provide clear visual representations of objects on the Earth's surface. There are two main types of pictorial data products: aerial photos and satellite imagery. Aerial photos are captured from aircraft using advanced cameras that utilize electromagnetic energy in the visible spectrum. These photos offer accurate depictions of the Earth's surface at a relatively lower scale. Aerial photographs can be either black and white or color, depending on the type of camera used in the aircraft. Satellite imagery, on the other hand, is obtained from sensors aboard satellites. These sensors capture both visible and invisible parts of the electromagnetic spectrum. Satellite images can also be black and white or color. In black and white images, different shades of gray are assigned to represent the data from each range. Monochrome images can be created by assigning different shades of blue, green, and red to their respective data ranges. Multi-color images can be obtained by combining three bands of data. For instance, when pictures are taken in blue, green, and red colors (representing the visible part of the electromagnetic spectrum) and then merged, a color image is generated. Another method involves capturing images in green and red colors (visible spectrum) along with the infrared band (invisible spectrum). In this case, blue, green, and red colors are assigned to the respective bands, and then they are combined to create a composite color image. It's important to note that while

composite color images derived from satellite imagery can be visually appealing, they do not provide the same level of accuracy as aerial photos. Interpreting satellite imagery requires expertise, and it may not be easily comprehensible to the average person. [91].

2.2.3 Characteristics of Remotely Sensed Data

The data collected by remote sensing systems can be divided into two types, as they are either analog format data or digital format data. Analog format data represents paper aerial photography or video data. As for digital format data, it represents a matrix of brightness values for the average radiation measured within an image pixel. Remote sensing data can be understood by four properties, which are spatial, spectral, radiometric, and temporal resolution [92]:

1- Spatial resolution: It is the minimum distance between two points, so that we can distinguish between them from each other in an image. This is measured for aerial photography. Spatial resolution is measured in linear pairs per millimeter. For other sensors, it is measured in meters. The area of land within the instantaneous field of view (IFOV) for a single detector within a row or pixel size. all spatial details are usually determined by the spatial resolution of the Earth's surface.

2- Spectral resolution:

Spectral resolution for a remote sensing device commonly refers to the number and size of the bands that can be recorded and this allows us all narrow bands at specific regions of the electromagnetic spectrum to distinguish between different properties easily. Therefore, we need a greater numbers of spectra, ie band, for every tight bandwidth, and it is assumed that the bands together cover the full spectral band.

3- Radiometric accuracy:

This accuracy refers to the sensitivity of the sensor to the incoming radiation, which is the amount of change in the value of the radiation reaching the sensor, before a change in the amount and value of the recorded brightness. Radiometric precision, using a few levels of brightness, records a clear scene of coarse resolution, which causes very high contrast, while radiometric precision records the same scene, but using several levels of brightness.

4- Temporal accuracy:

It is the amount of time that the sensor needs to return to one of the sites that it photographed previously, and thus the time accuracy has a clear and important effect in detecting change and monitoring the environment. Over time, environmental phenomena are constantly changing, for example, vegetation cover, weather, volcanoes, fires, etc. Weather sensors usually have a very high accuracy of measurement.

2.3 Remote Sensing Physics

When detecting and distinguishing surface objects, the process involves detecting the radiant energy and measuring its energy in relation to the rays that are reflected or emitted from those objects or materials. Different objects exhibit different energy levels in different bands of the electromagnetic spectrum when exposed to it. This variation depends on various factors such as the material's properties (structural, chemical, and physical), surface roughness, intensity of the energy, angle of incidence, and wavelength of the radiated energy.

Electromagnetic radiation represents a dynamic form of energy that propagates as a wave at the speed of light, which is approximately 3×10^{10} cm/sec. The characteristics

that differentiate waves are the wavelength (λ), frequency (ν), and speed (c), where the relationship between them is defined as $c = \nu\lambda$. According to the fundamental wave theory, electromagnetic energy is emitted and travels in a sinusoidal manner.

Wave theory effectively describes many properties of electromagnetic energy. However, there is another theory called particle theory that accurately explains how electromagnetic energy interacts with matter. It is commonly understood that electromagnetic radiation consists of discrete units known as photons or quanta. The energy of a photon can be calculated using the equations $E = hc/\lambda$ or $E = h\nu$, where h represents Planck's constant. These equations hold true at temperatures above absolute zero.

All objects are capable of radiating electromagnetic energy based on their atomic and molecular frequencies. The total amount of radiation emitted increases as the absolute temperature of the object rises and reaches its peak at shorter wavelengths. The sun is a major source of energy, radiation, and light.

The underlying principle for sensing electromagnetic radiation is based on the fact that everything in nature has its own distribution of reflected, emitted, and absorbed radiation Figure (2-3). These spectral properties can be utilized and leveraged in various scientific disciplines to differentiate between objects or obtain information regarding their size, as well as other physical and chemical properties [93].

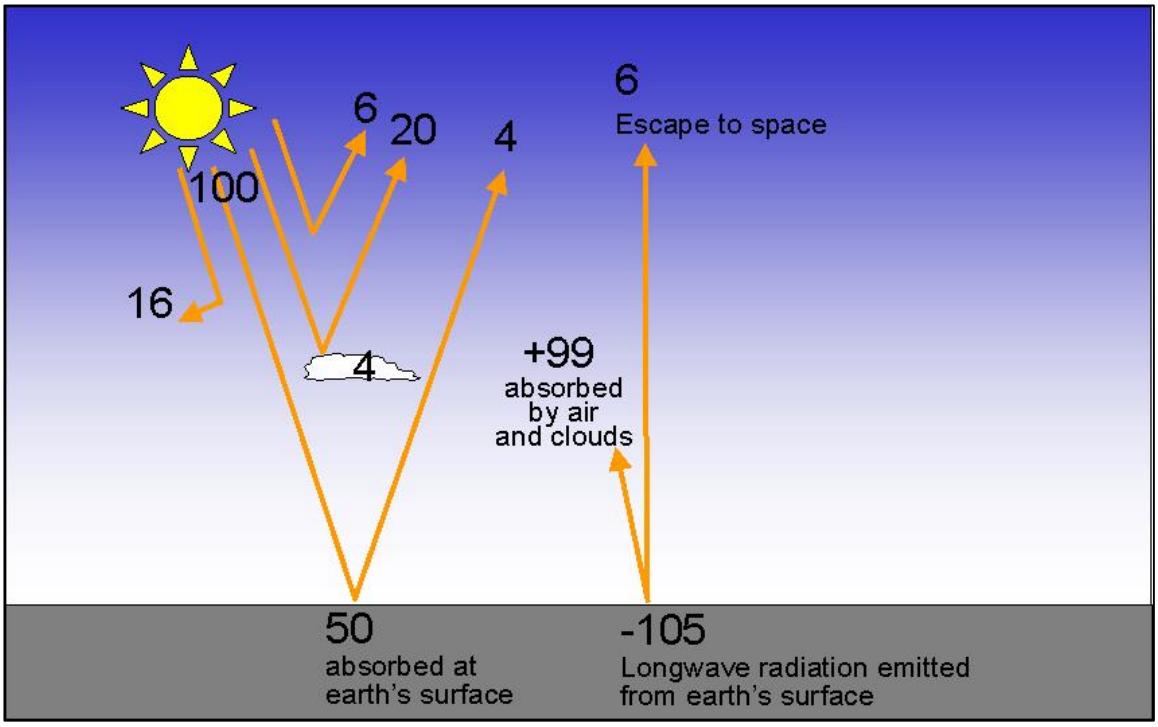

Figure (2-3): Remote Sensing Physics [93].

2.4 The Geographical Information Systems (GIS)

The GIS was first used over 60 years ago in North America for automated production of maps [94]. It transforms the real world into a virtual world that contains all the information and data we need by a computer [95], and contains powerful tools to capture, store, manage, retrieve, query, analyze and display spatial data to manage a wide range of information [96].

This system can develop and analyze explicit spatial variables, and the integration can become a powerful analytical toolkit that enables scientists to gain insight into the nature of the spatial structures of regional development [97].

All systems and software associated with the GIS is an effective model for spatial data preservation and retrieval and provide the possibility of final data mapping [98], Figure (2-4).

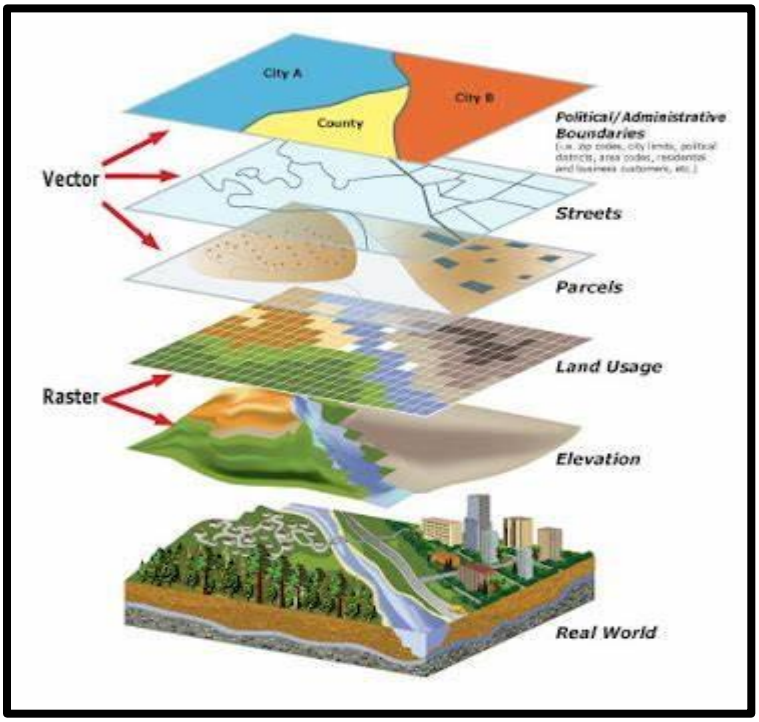

Figure (2-4): Geographic information systems courses, it shows which layers can be created and merged into a single image [99].

A geographic information system can provide four sets of capabilities for dealing with geo-referenced data, which are [100]:

1- Data capture and preparation.
2- Data management includes storage and maintenance.
3- Data analysis and processing.
4- Data display.

2.4.1 The Practical Benefit of the GIS Software

It can be concluded in two groups:

1- Drawing maps, buildings and putting information on them.
2- Collecting information from the truth and describing it in the maps in the form of layers, and the program can answer many questions through a database in the program, which is a set of information stored in the program [101].

2.4.2 Arc GIS Program

Geographical Information System (GIS) is a system for storage and processing of spatial data by using computers. It is a necessary means of assembling, processing, displaying and analyzing geographical data of a certain location, as well as being able to handle large volumes of data. The GIS is available in various computer systems where it is based primarily on the software programs that have given it its importance [102].

Arc GIS is type of GIS software which can create, edit, mapped, analyze and store data. It contains GIS viewer, GIS analyst, GIS editor. It is more suitable than other GIS software because it is scalable server architecture. It provides data in both the raster and vector format and combines data from multiple sources. ArcGIS is a perfect system for designing and managing solutions through the application of geographic knowledge. It has many aspects of cartography; it takes less time than other software for offering any map with better intelligence [103].

2.4.3 Types of Data Models Used in GIS

There are different types of data models:

1-Vector data model

This first model has another name, the object model, that is, it uses separate objects to represent features on the surface of Earth. There are three basic steps used to prepare vector data based on the above concept. The first step is that all spatial features can be classified into points, lines, and polygons on areas empty and this represents the location and shape of these features that use the points x, y and the second step structuring and arranging. All spatial relationships and properties of these geometric shapes that they are in the logical framework of the objects, the third step that all codes and stores data within the digital data files, which makes access, interpretation and processing possible and easy by computer. Vector data models for spatial features are represented using point, line, and polygon shapes by geometric objects. One of the most important components of raster features are raster files or a group of many points, given that the line is one-dimensional and has a property of lengths that is specific in addition to the location and line that has two points, and it can contain additional points between them to clarify and defining the shape of the line is a form Figure (2-5), this line may be a connection of straight segments or in the form of a smooth curve, usually the linear features consist of one line or a group of lines, and the most important and clear examples of that are public roads, borders and tables are the best examples of the features of the line. The area of the polygons is either self-contained or it shares borders with other polygons and it can have a hole in its scope. The feature consists of one polygon or a group of other polygons. Examples of them are cultivated areas as well as urban areas and also water bodies to indicate their

location. These points are Geographically represented by a pair of x-y coordinates [104].

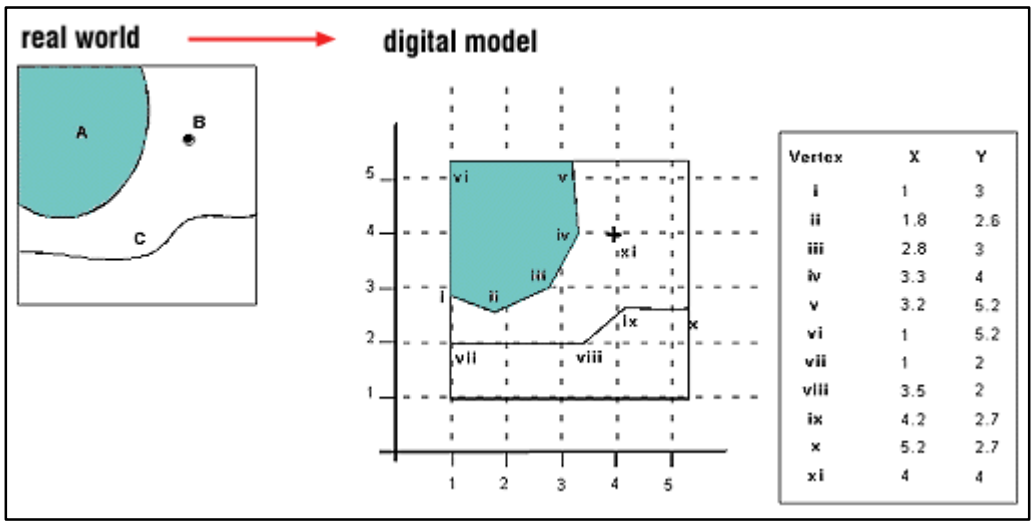

Figure (2-5): Vector data model [105].

2- Raster model: It may also be called a lattice or an images in (GIS). The raster represent a continuous surfaces, but for storing and analyzing data. The raster data is divided into rows and columns. As for the cells, they are called pixels in images. The rows represent the y coordinates and the columns the x coordinates, and the cell identifies in raster data through rows and columns. A raster consists of dots in the form of single cells, adjacent cells moving with lines, and polygons Figure (2-6). The raster model lacks the accuracy of the vector model in representation. The locations and boundaries of spatial feature have a clear advantage so that they have a fixed cell in computing algorithms. Raster data is treated on the basis that it is a matrix consisting of rows and columns, and the values of the cell are stored in two dimensions. Thus, raster data is much easier than processing, collecting and analyzing data with respect to the vector [106].

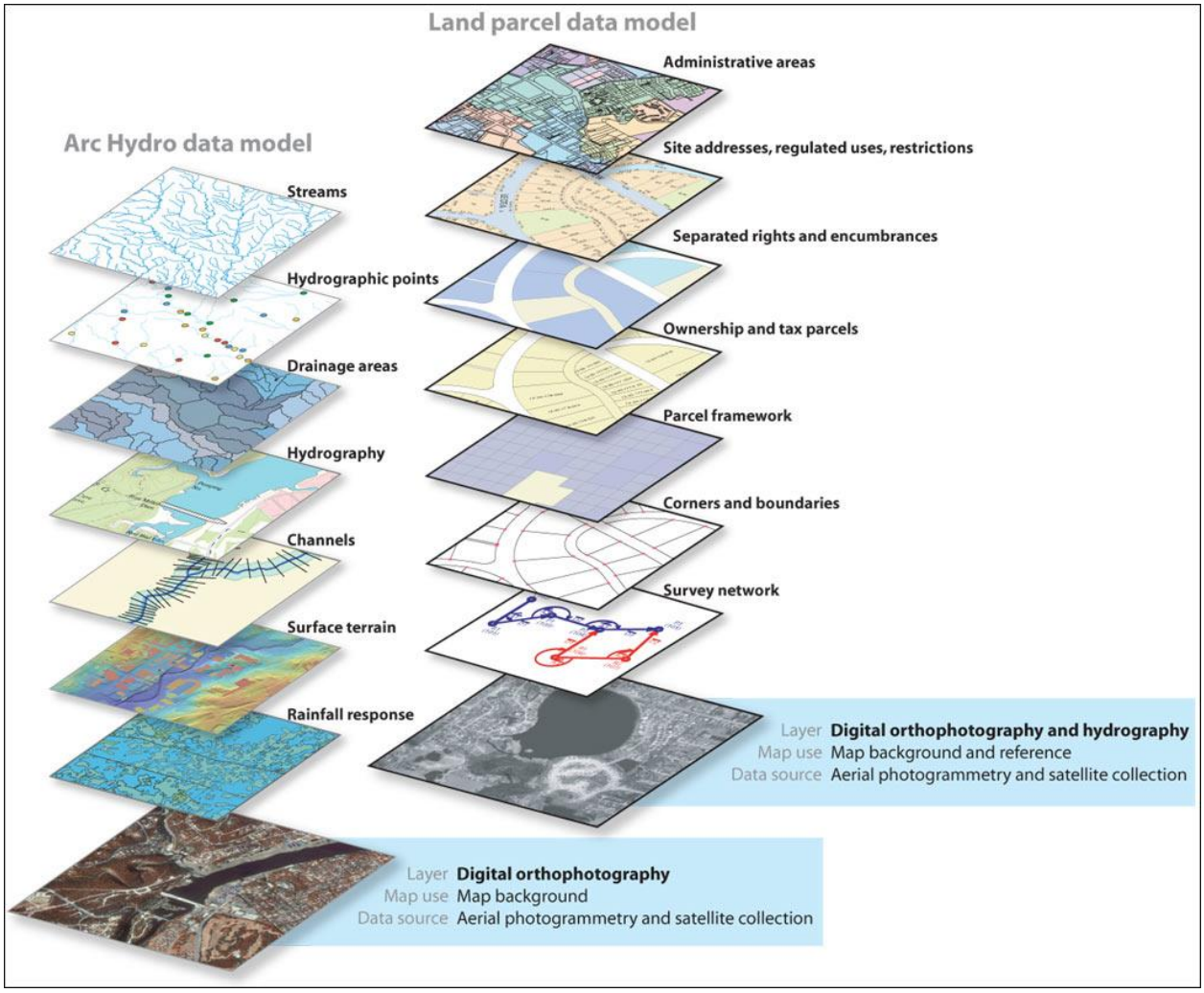

Figure (2-6): Raster data model [106].

2.4.4 Types of Used Data in the GIS

The GIS software uses two sets of data (spatial data and non-spatial data) [107]:

1- Spatial data: is a set of vector and point data prepared through field surveys or remote sensing data on the surface of the earth. These data sets include satellite images and coordinates, among other things, that are interpreted to produce objective maps that can be used in research.

2- Non-spatial data: these are features that are complementary to spatial data and describe what is present at a point on a line or in a factory and as social and economic characteristics from other sources.

2.5 Integration Between RS and GIS

There is a noticeable increase in the recent period in using of RS data for different types of resources, environmental and urban studies, geographic information systems to enable computer systems to deal with geospatial data in effective and more efficient ways. These geospatial data and techniques are useful for investigating natural and human systems as well as predicting them over time. The combination of RS and (GIS) is of great benefit due to the significant increase in the demand for the use of RS data with mapping data and other data obtained by (GIS). The (RS) system and geographic information (GIS) are the two main components of all geographic information sciences, and this is a broad and comprehensive field of endeavor in global positioning systems (GPS) and traditional mapping.

Although the (RS) system and the (GIS) have developed semi-independently, the compatibility between them has become increasingly clear. The (GIS) programs include tools for displaying and analyzing images, while the image processing programs contain options for analyzing auxiliary geospatial data.

The great progress that has been achieved in the integration of (RS) and (GIS) has been well summarized and this progress has been very rapid and beneficial. This integration defines that it is possible to use each technique to benefit the other as well, in addition to applying and using both methods in coordination and using modeling decision. Although the special literature related to the integration of remote sensing with geographic information systems is considered relatively

recent, the signs of integration go back to the early twentieth century when aerial holography and photographic and analog analysis were used. Modern digital and airborne remote sensing systems, in addition to satellites and all data analysis procedures such as digital photogrammetry, are among the important means through which GIS data are obtained and improved [108].

2.6 The GIS and Solar Radiation Program

The process of making calculations for point locations or entire geographic areas in GIS software involves four steps [109]:

1. Calculation of the ascending hemispherical field of view based on the terrain: This step involves generating an upward-facing hemispherical field of view for each location in the digital elevation model (DEM). It takes into account the topography and surface features of the area. The hemispherical field of view represents the visible sky and the sky directions obstructed by surrounding terrain and surface characteristics.
2. Overlay the field of view on the direct sun map to estimate direct radiation: Once the ascending hemispherical field of view is calculated, it is overlaid on a direct sun map. By doing this, the software estimates the direct radiation received by the location based on the position and intensity of the sun. This step helps determine the amount of direct sunlight that reaches the specific location.
3. Overlay the field of view on a diffuse sky map to estimate diffuse radiation. Similarly, the field of view is overlaid on a diffuse sky map in this step. The diffuse sky map represents the scattering of sunlight due to atmospheric

conditions. By overlaying the field of view, the software estimates the amount of diffuse radiation received by the location. Diffuse radiation refers to the sunlight that reaches the location after being scattered by particles in the atmosphere.

4. Repeat the process for each significant location to produce the insolation map. The above steps are repeated for each significant location within the geographic area of interest. This process helps generate an insolation map, which represents the solar radiation or insolation levels across the area. The insolation map provides valuable information about the spatial distribution of solar energy and can be used for various applications, such as solar energy potential assessment, environmental analysis, or urban planning.

Figure (2-7) displays a hemispherical image facing upwards, which provides a visual representation of the visible sky, as well as the sky directions obstructed by surrounding terrain and surface characteristics. This image resembles the view one would have from the ground when looking in all directions. It serves as a reference for understanding the calculation process and visualizing the impact of topography and surface features on solar radiation.

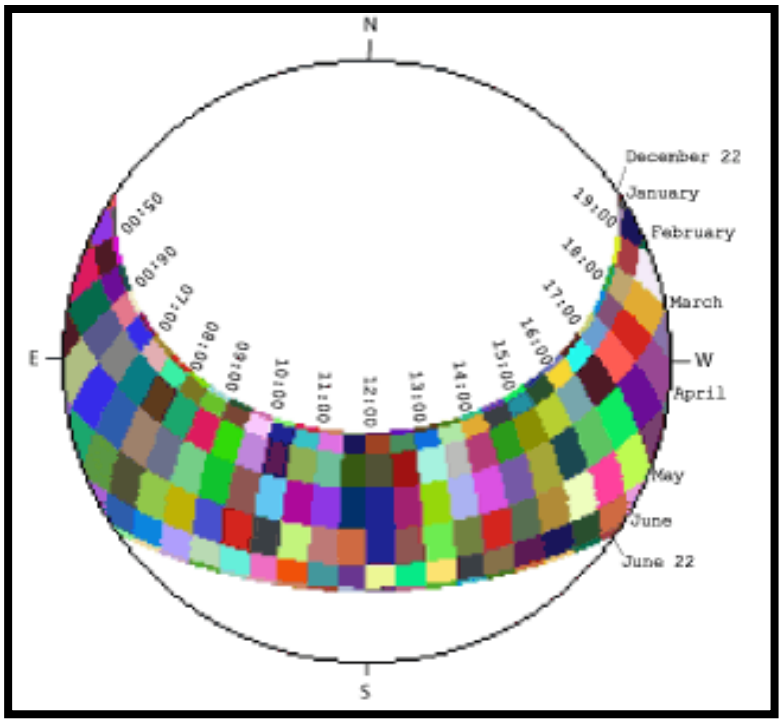

Figure (2-7) Shape of the Sun calculated from the winter solstice (December 21) to the summer solstice (June 21) for 45°N latitude [109].

2.7 Digital Elevation Model (DEM)

It is a data files that represents the data digitally, based on the raster formula that contains pixels. Each pixel has a specific numerical value that indicates the average height of the Earth surfaces in the region of each pixel. These files are usually found within the GIS program and are large in scale and useful for collecting purposes planning. This model uses either the geographical coordinates network, which is a network of longitudes and latitudes, when there is data that is constantly changing and separated due to the curvature of the surface of the globe, or it uses the (UTM) network of the Mercantile Global Transverse Projection System when there is a set of common data. Whenever the DEM scale is small, it is able to use geographical coordinates, but if the scale is large, it can use any type of them [110].

(DEM) always measures and clarifies the height of the terrain (meaning the height values of the bare land), which is abstract and devoid of natural vegetation, as well as normal phenomena that are not man-made, and this is unlike digital surface models, which represent the height of trees, towers, and all Phenomena that rise above the surface of the globe.

2.7.1 The Sources of Digital Elevation Model Output:

1- All satellite aerial visuals and photos [111]:

It is all the data for the three-dimensional aerial images using the cytroscopes manually or special graphics in digital format. As for the satellite images, there are several satellites that specialize in producing bitmap images representing (DEM) like what we see on the moon (Spot) with a spatial resolution of (2.5-4) m. Space Images (Strp) is more popular because it covers the countries of the world between 60°N and 90°S and is free.

There are high-quality models that use the (SAR) radar application, and one of its advantages is that it gives the (Z) height dimension with an accuracy of less than 10 m or more than 10 m, and it is able to detect all minor changes in all altitudes.

2- There are specialized organizations that produce bitmap elevation data, such as (GDEM) data, which are produced by the USGS with very high accuracy.

3- There are also different sources for the production of DEM, such as ground surveys and elevation data that are widely spread and obtained from GPS devices, as well as the numbering of topographic maps and contour lines in them.

4- There are also so-called interpolation methods, which are a set of mathematical algorithms that have samples with known heights for a specific

area, perform an arithmetic prediction process for all the heights of the region, and store the outputs in bitmap images.

2.7.2 Use of Digital Elevation Models

Digital elevation models can be used to help analyze and interpret many phenomena for many applications, including [112]:

Geology: by using the digital elevation model, it is possible to create maps and interpret their information and 3D geological detectors. It is possible to draw geological contact lines on the surfaces of the (DEM), or we use the (GPS) file, which contains digital files for the same area under study. And it is possible to use it with a map on the calculator, provided that it is digital. It is possible to obtain contour lines from the digital elevation model. This is done when matching a satellite image to the geological map and to the digital elevation model. This requires correction of elevations, especially when using satellite images, as well as adjusting all ground control points (Georefrencing) in them, being with a digital elevation model.

Geomorphology: all applications of digital elevation models contribute to topographic analysis, which keep pace with the evolution of the features of the Earth's surface. Therefore, using these models, it is possible to observe the topography of the Earth surfaces in a three-dimensional way, as it is able to convey a huge amount of information in the case of a normal topographic map.

2.8 Factors Affecting of Solar Radiation Distribution on the Earth's Surface

There are many factors affecting of solar radiation distribution on the surface of the globe [113]:

- The distance between the earth and the sun: The solar radiation reaching the surface of the globe increases by 7% during the period of solar apogee, and also that the distance between perihelion and the sun will increase in the northern hemisphere.

-Earth's rotation: as we have shown in the previous topics, the Earth revolves a complete cycle around the sun about every 365.25 days and revolves around itself once every 23.45 hours. about solar radiation.

- The angle of solar radiation: when the radiation falling on the earth's surface is vertical, its quantity is higher. There is a direct relationship between the angle of incidence of radiation and energy. By increasing the angle, the multiplier energy reaching the Earth's surface increases. For this reason, the equatorial regions have greater energy compared to the northern and southern regions of the equator. It is important and necessary to determine the direction and position of the sun for any point on the surface of the earth, and this is called the solar position [114]. The position of the sun can be determined by the following angles, as shoun in Figure (2-8).

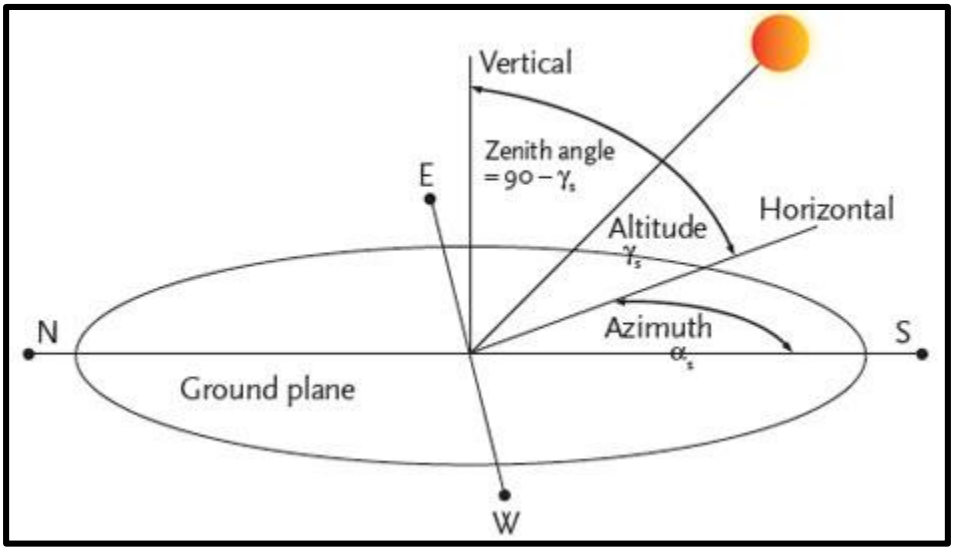

Figure (2-8): Solar angles [114].

-Solar elevation angle (H): The angle between the direction of solar radiation and the horizontal plane of the Earth surfaces is called the angle of solar elevation. It is important to know and determine the value of radiation that reaches the Earth surfaces.

- Zenith angle (Z): It is the angle between the solar radiation and the vertical to the horizontal surfaces, and it represents the sum of the angle of elevation of the sun and the angle of the head of 90 degrees.

- Solar azimuth angle (A): the angle made by the solar radiation at the level of the observer's horizon, measured towards the north, and it can be positive or negative, and its value ranges between (0-180), and it can be calculated through the relationship:

z= 360-d

z= azimuth.

d= distance from the north.

- Solar declination angle: the angle between the plane passing through the equator and the solar ray, and its value is relatively large, as it reaches (+23.5) at the summer solstice, and its value is (-23.5), i.e. relatively small during the winter solstice, but during the equinox period. Its value will be zero, as shown in the Figure (2-9).

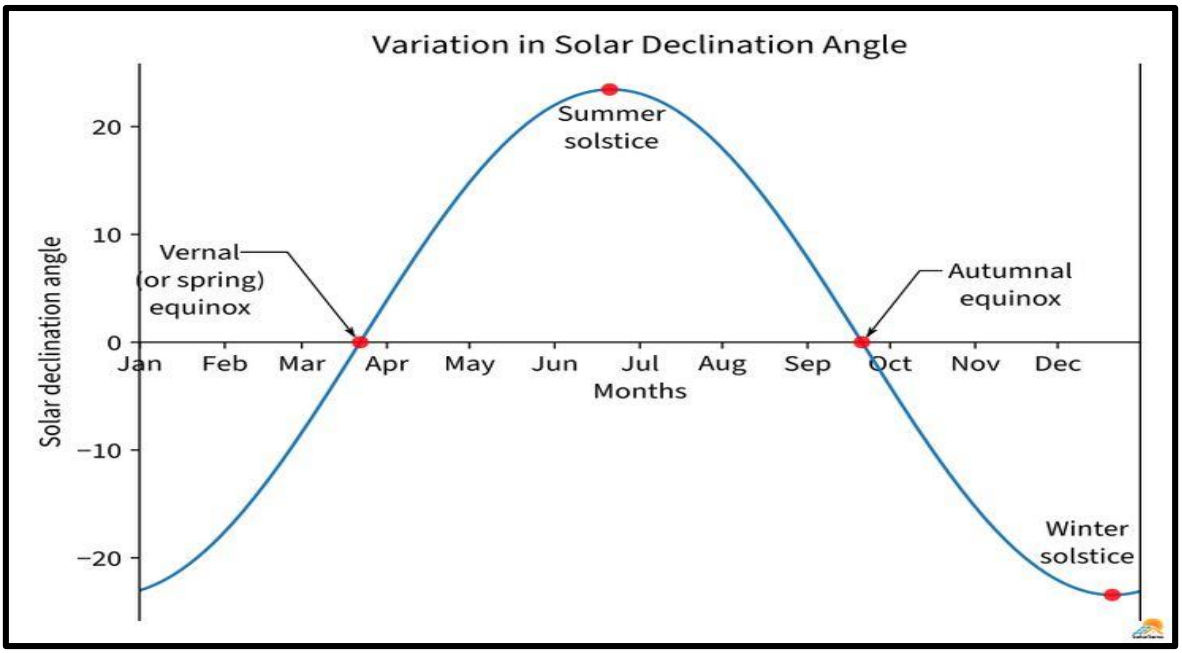

Figure (2-9): Change in the angle of the solar system by changing the sequence of the day [113].

- Hour angle (h): It is an angular measurement of time, equal to 15 degrees per hour, and a measurement of the position of the sun again. It can be calculated for any hour of the day through the following relationship:

$$h = 360/24\ (12-t) \qquad (2\text{-}1)$$

t= Hourly rate of time, measured from noon.

2.9 The Calculation of the Solar Radiation

Indeed, it is possible to calculate solar radiation, or insolation, across a landscape using various tools and algorithms specifically designed for this purpose. These calculations provide valuable information about the amount of radiation received at specific locations or across a region.

The calculation of solar radiation involves considering three components: direct radiation, diffuse radiation, and comprehensive (or global) radiation.

These calculations are performed repeatedly for each known location or any location on the topographic surface. By considering the specific characteristics of the terrain, such as elevation, slope, aspect, and obstructions, the insolation can be estimated at different points across the landscape.

The results of these calculations enable the generation of special insolation maps for a particular geographical area as a whole. These maps provide valuable information about the spatial distribution of solar radiation and can be used for various purposes, including solar energy potential assessment, agricultural planning, environmental analysis, and urban development. [115].

2.9.1 Global Radiation Calculation:

The calculation of global radiation (Global tot) involves summing the direct radiation (Dir tot) and the diffuse radiation (Dif tot) for all sectors of the sun map and sky map, respectively. The equations involved in these calculations are as follows [116]:

$$Global_{tot} = Dir_{tot} + Dif_{tot} \quad (2\text{-}2)$$

Total Direct Insolation (Dir tot):The total direct insolation (Dir tot) for any location is the sum of the direct insolation (Dir θ,α) for all sectors of the sun. It can be expressed as[116]:

$$Dir_{tot} = \Sigma\, Dir_{\theta,\alpha} \quad (2\text{-}3)$$

Thus, it is possible to calculate the direct insolation of the sun map (Dir θ,α) and of the midpoint with zenith angle (θ) and azimuth angle (α) through the following equation[116]:

$$Dir_{\theta,\alpha} = S_{Const} * \beta^{m(\theta)} * SunDur_{\theta,\alpha} * SunGap_{\theta,\alpha} * \cos(AngIn_{\theta,\alpha}) \quad (2\text{-}4)$$

- where:

S_{Const} : is the solar flux outside the atmosphere at the mean Earth-Sun distance, also known as the solar constant. A commonly used value for the solar constant is 1367 W/m^2.

β :is the transmissivity of the atmosphere (averaged over all wavelengths) for the shortest path in the direction of the zenith.

m(θ): is the relative optical path length, measured as a proportion relative to the zenith path length.

$SunDur_{\theta,\alpha}$: is the time duration represented by the sky sector. For most sectors, it is equal to the day interval (e.g., a month) multiplied by the hour interval (e.g., a half hour). For partial sectors near the horizon, the duration is calculated using spherical geometry.

$SunGap_{\theta,\alpha}$: is the gap fraction for the sun map sector.

$AngIn_{\theta,\alpha}$: is the angle of incidence between the centroid of the sky sector and the surface normal axis.

By summing the direct insolation for all sun map sectors, the total direct insolation (Dirtot) can be obtained. This, combined with the diffuse radiation, gives the global radiation (Globaltot), representing the total solar radiation received at a specific location or region. These calculations consider factors such as atmospheric transmissivity, optical path length, sky sector duration, sun gap fraction, and angle of incidence to estimate the insolation accurately.

The relative optical path length m(θ) can be determined based on the solar zenith angle (θ) and the height above sea level (Elev) using the following equation [117]:

$$m(\theta) = EXP(-0.000118 * Elev - 1.638*10^{-9} * Elev^2) / \cos(\theta) \quad (2\text{-}5)$$

- where:
    - **θ** - is the solar zenith angle.
    - **Elev** -is the elevation above sea level in meters.

This equation accounts for the effect of the angle of the sun's zenith and the elevation on the relative optical path length. It considers the attenuation of solar radiation through the atmosphere as it travels through different atmospheric layers.

To take into account the effect of surface orientation, the angle of incidence ($AngIn_{\theta,\alpha}$) between the intercepted surface and the sky sector, defined with the midpoint of the azimuth angle, can be calculated using the following equation[117]:

$$AngIn_{\theta,\alpha} = \text{acos}(\cos(\theta) * \cos(G_z) + \sin(\theta) * \sin(G_z) * \cos(\alpha - G_a)) \quad (2\text{-}6)$$

- where:
    - $\mathbf{G_z}$ - is the surface zenith angle. Note that for zenith angles greater than 80°, refraction becomes significant.

- $\mathbf{G}_a$ - is the surface azimuth angle.

The angle of incidence accounts for the angle at which solar radiation intercepts the surface, taking into consideration the orientation of the surface with respect to the sun's position.These calculations help in accurately determining the optical path length and the angle of incidence, considering factors such as elevation, solar zenith angle, surface zenith angle, and surface azimuth angle.

2.9.2 Calculation of Diffuse Radiation

To calculate the diffuse radiation, the following equation is used for each sector of the sky and the midpoint [118]:

$$Dif_{\theta,\alpha} = R_{glb} * P_{dif} * Dur * SkyGap_{\theta,\alpha} * Weight_{\theta,\alpha} * \cos(AngIn_{\theta,\alpha}) \quad (2\text{-}7)$$

- where:
  - $\mathbf{R}_{glb}$ - is the global normal radiation.
  - $\mathbf{P}_{dif}$ - It typically ranges from 0.2 for very clear sky conditions to 0.7 for very cloudy sky conditions.
  - **Dur** - is the time interval for analysis.
  - $\mathbf{SkyGap}_{\theta,\alpha}$ - is the gap fraction (proportion of visible sky) for the sky sector.
  - $\mathbf{Weight}_{\theta,\alpha}$ - is the proportion of diffuse radiation originating in a given sky sector relative to all sectors.
  - $\mathbf{AngIn}_{\theta,\alpha}$ -is the angle of incidence between the centroid of the sky sector and the intercepting surface.

The global normal radiation (R_{glb}) is calculated by summing the direct radiation from each sector and then correcting it by the direct radiation ratio ($1 - P_{dif}$)[118]:

$$R_{glb} = (S_{Const} \Sigma(\beta^{m(\theta)})) / (1 - P_{dif}) \quad (2\text{-}8)$$

For the uniform sky propagation model, the weight ($Weight_{\theta,\alpha}$) is calculated as:

$$Weight_{\theta,\alpha} = (\cos\theta_2 - \cos\theta_1) / Div_{azi} \quad (2\text{-}9)$$

- where:
    - $\boldsymbol{\theta}_1$ and $\boldsymbol{\theta}_2$ - are the bounding zenith angles of the sky sector.
    - $\mathbf{Div}_{azi}$ - is the number of azimuthal divisions in the sky map.

For the standard overcast sky model, the weight ($Weight\theta,\alpha$) is calculated as[118]:

$$Weight\theta,\alpha = (2\cos\theta2 + \cos2\theta2 - 2\cos\theta1 - \cos2\theta1) / 4 * Divazi \quad (2\text{-}10)$$

The total diffuse solar radiation for the site (Dif_{tot}) is obtained by summing up the diffuse solar radiation for all sectors:

$$Dif_{tot} = \Sigma\, Dif_{\theta,\alpha}$$

By performing these calculations, the diffuse radiation component can be determined, taking into account factors such as global normal radiation, proportion of diffused radiation, time interval, gap fraction, weight, and angle of incidence.

2.10 The Geospatial Data

All spatial features on the Earth's surface are covered by geospatial data, and these features can be identified. There is a geographical coordinate system that can be used, or a location can be used by using latitude and longitude and using an expected coordinate system. It is possible to use these systems to express the geographical coordination system. The geographic information system provides many coordinated systems expected, the most important example of which is the UTM system (Universal Transverse Merctor), where this global system divides the Earth's surface into 60 regions between 84 degrees north and 84 degrees south. Geographic information systems operate on a basic principle on the basis that the layers of maps represented by different geospatial data must be spatially coordinated, that is, they are spatially based. Figure (2-10), using vector data models for points, lines, and polygons, it is possible to represent all spatial features with clear spatial boundaries and locations such as streams, other locations on Earth, and vegetation areas. An identifier is used for each of these features and is associated with its attributes [119].

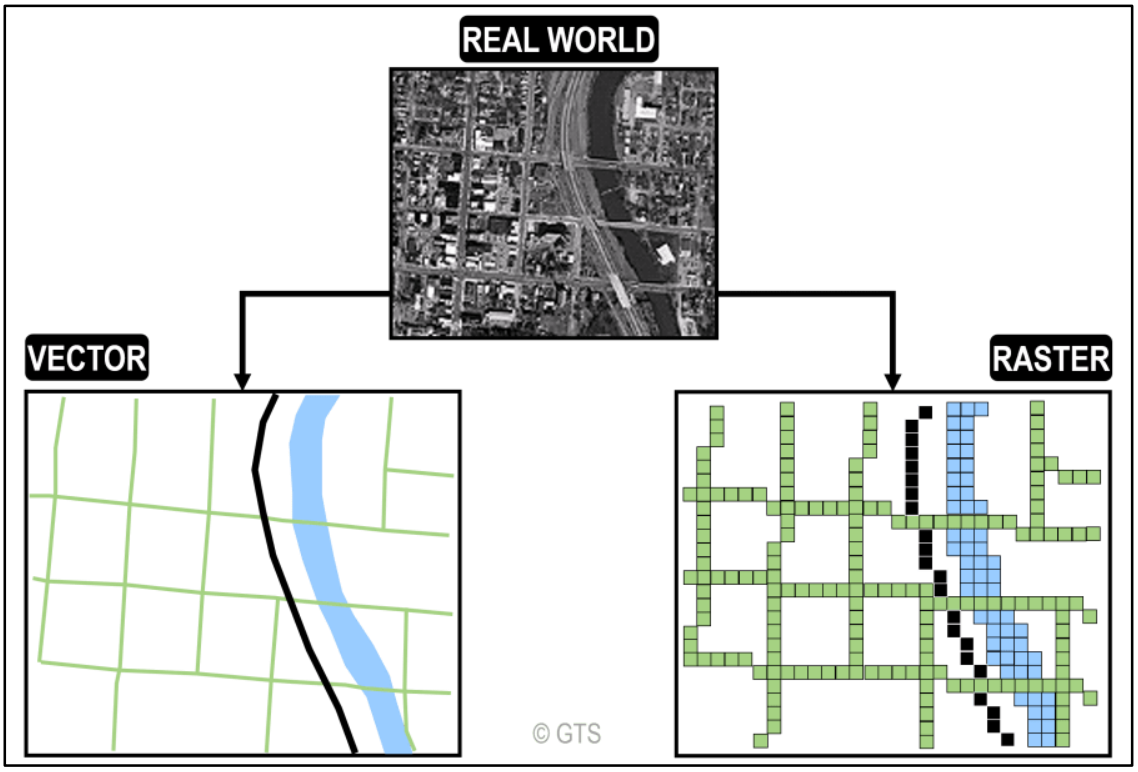

Figure (2-10): Geospatial data [119].

2.11 Landsat Satellite

There is a large group of satellites dedicated to monitoring and photographing the Earth. The Landsat program is one of this series of satellites by NASA and the USGS, in July 1972 the Landsat satellite was launched, as it was the only one of the satellite systems designed and built. It operates with the task of observing the Earth's surface periodically and with normal accuracy. The first Earth Resources Technology Satellite ERTS-1 was launched, later renamed Landsat 1, and its latest model is Landsat 8, which was launched in February 2013, all images and data This satellite is stored in Landsat stations in the United States of America and around the world, where this data is an important and unique wealth for research, applications, and changes in the geology of agriculture, mapping, forestry, education, regional

planning, and other applications through modern processing methods and algorithms, that computing with high accuracy and cloud-based It allows algorithms to be brought to the data and helps scientists and practitioners and enables them to generate a new vision as well as high-accuracy and powerful information products in most fields, as explained in the Landsat downloads. At the present time, satellites provide more than a million images per month, as there is a large user base working to implement integrated data analytics. In the Landsat satellite, there are sensors that see, record and photograph what the human eye cannot see. In addition, these sensors monitor and record the reflected and emitted light from the earth surfaces with specific wavelengths of infrared and visible waves [120].

2.11.1 Landsat 8

The Landsat 8 satellite was launched in February 2013, and it is the latest and last version of the Landsat satellite group. It carries the following tools:

1- Operational Earth Imager OLI with nine visible spectral bands VIS as well as the near infrared, NIR, and SWIR spectral regions. Figure (2-11) shows the structure of the OLI [121].

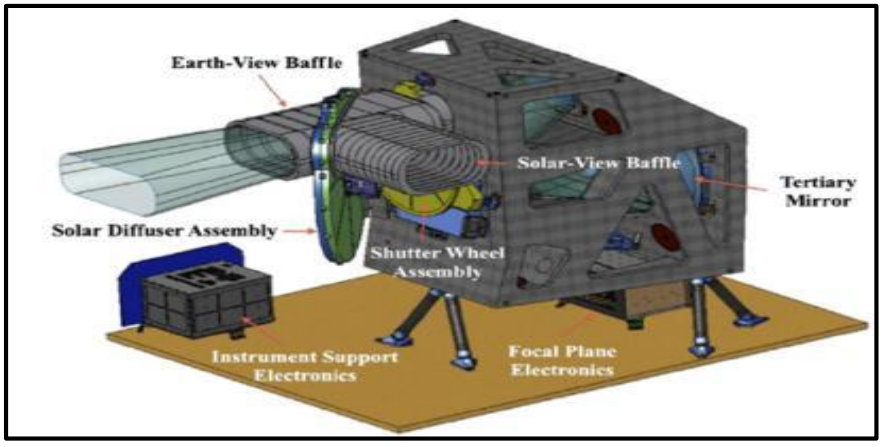

Figure (2 -11): OLI structure [122].

2- The TIRS infrared thermal sensor has two spectral bands in the LWIR. Figure (2-12) shows the TIRS sensor. The OLI sensor has nine spectral bands (1-9),

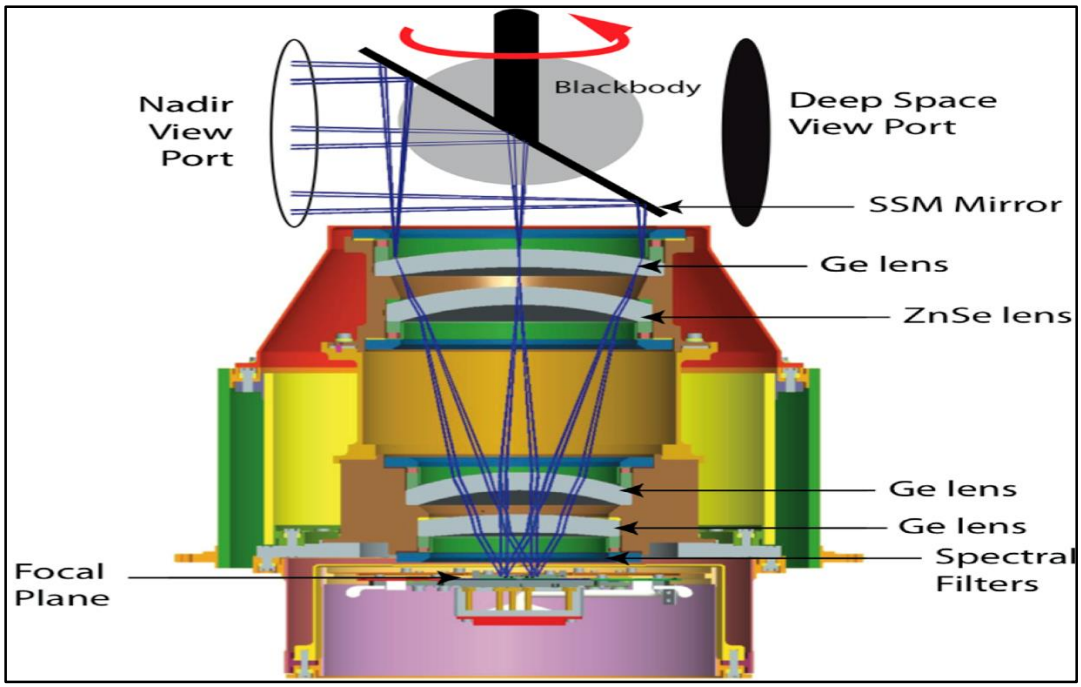

Figure (2 - 12): Thermal infrared sensor [123].

while the TIRS sensor contains two spectral bands (10-11), from band 2 to band 8, which are seven bands of OLI that are compatible with TM and ETM + sensors, while the remaining two bands of the OLI sensor, which are 1,9, measure water resources, investigate the coastal zone, and detect in cirrus clouds, the TIRS sensor can provide a thermal imager that measures the rate of evaporation. Figure (2-13) shows the components of Landsat 8.

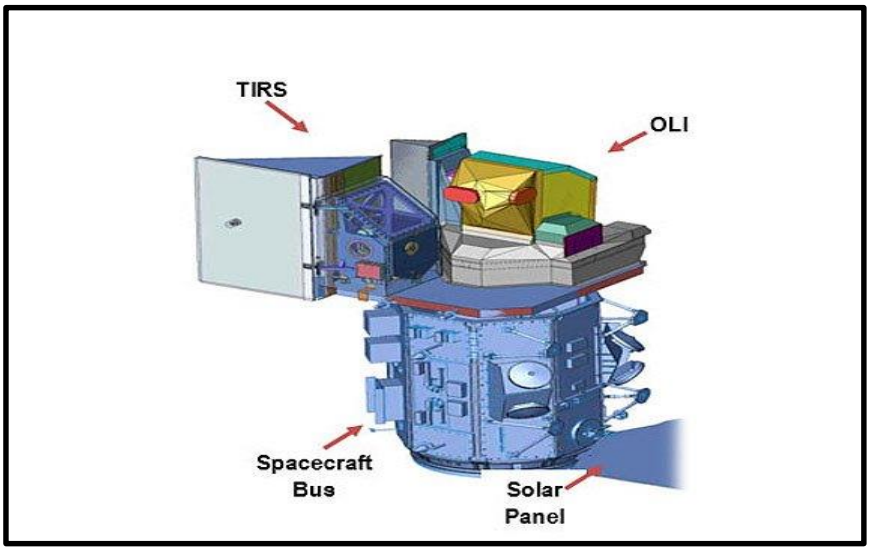

Figure (2 - 13): Landsat 8: satellite imagery overview [124].

2.11.2 The Types of Landsat 8 Satellite Bands

The landsat 8 satellite consists of 11 band [125]:

1- Band (1):

The first range of the Landsat 8 satellite uses the blue color to be able to detect the color of the ocean near the coastal areas, which helps scientists measure the concentration of chlorophyll (the color of the ocean) in coastal areas, and the reason for the presence of chlorophyll is the phytoplankton present in the oceans and known as Microorganisms resembling plants that live in surface waters. This analysis is necessary in the use of RS to know the quality and suitability of water. This range is called (coastal/ aerosol) and has a wavelength of (0.433 - 0.453) μm and has a resolution of 30 meters.

2- Bands (2, 3, 4):

These bands use blue, green and red colors and are called visible. They have wavelengths estimated at (0.450 - 0.515) μm for the second band, (0.525 - 0.600)

μm for the third band and (0.630 - 0.640) μm for the fourth band. The measurement accuracy is 30 m.

3-Band (5)

This range has a measurement accuracy of 30 m and has wavelengths of about (0.845 - 0.885) μm, which is the near infrared (NIR) range. NDVI values indicate the quality and health of plants more accurately than the visible greenery on their surface.

4-bands (6, 7)

These ranges are dedicated to the study of soil and its quality, and they cover different sections of the near infrared with short wavelength SWIR, either from the geological side, for example rocks and soil, these ranges have wavelengths as follows (1.560-1.660) μm for the sixth band and (2.100-2.300) μm for the seventh range, while the accuracy of measurement is 30 m.

5-band (8)

It is (panchromatic) and consists of a band of black and white colors that collects energy from the visible spectrum together, and for this reason the images are sharp and have a resolution of 15 m. One of its most important uses is in sharpening normal and low-resolution images. This range has wavelengths from (0.500-0.680) μm.

6-band (9)

This scope is capable of measuring short-wave infrared light. This new scope from OLI will be able to detect clouds in a way and with high accuracy better than other sensors of the Landsat satellite, as it is difficult to detect thin high clouds due to the interference of clouds and their shadows with the measurements. So Band 9

will be sensitive to the presence of thin clouds, characterized by wavelengths (1.360 - 1.390) μm, with accuracy, about 30 m.

7-bands (10,11)

These ranges are able to measure the temperature on the ground as they operate on TIR thermal infrared ranges, through which urban areas can be identified. The two bands show the effect of abstraction, and band 11 gives more instability values than band 10. These bands have wavelengths of (10.30 -11.30) μm for the tenth band and (11.50 -12.50) μm for the eleventh band, and they are measured with an accuracy of 100 m for both.

The Table (2-1) shows the characteristic of bands which observed by the sensors.

Table (2 - 1): The characteristic of bands which observed by the sensors [126].

Band	Resolution (m)	Wavelength (μm)	Description	Sensor
1	30	0.43 - 0.45	Coastal/Aerosol	Operational Land Imager (OLI)
2	30	0.45 - 0.51	Blue	OLI
3	30	0.53 - 0.59	Green	OLI
4	30	0.64 - 0.67	Red	OLI
5	30	0.85 - 0.88	Near Infrared	OLI
6	30	1.57 - 1.65	Short wave Infrared	OLI
7	30	2.11 - 2.29	Short-wave Infrared	OLI
8	15	0.50 - 0.68	Panchromatic	OLI
9	30	1.36 - 1.38	Cirrus	OLI
10	100	10.6 - 11.19	Thermal Infrared	Thermal Infrared Sensor (TIRS)
11	100	11.50 - 12.51	Thermal Infrared	TIRS

2.11.3 Satellite Sensor

Landsat 8 and Landsat 9 are both satellite missions that provide Earth observation data. Landsat 8 is equipped with the Operational Land Imager (OLI) and Thermal Infrared Sensor (TIRS), as Landsat 9.

The Landsat 8 OLI sensor has nine spectral bands with a spatial resolution of 30 meters. These bands are:

Coastal/Aerosol Band: This is the blue band (0.43-0.45) μm and is useful for coastal imaging and the study of aerosols.

Blue Band: This band (0.45-0.51) μm captures blue light and is used for various applications such as vegetation monitoring and water resource management.

Green Band: This band (0.53-0.59) μm captures green light and is also used for vegetation monitoring, land cover classification, and other environmental studies.

Red Band: This band (0.64-0.67) μm captures red light and is important for vegetation health assessment, urban studies, and other applications.

Near-Infrared Band: This band (0.85-0.88) μm captures near-infrared light and is used for vegetation analysis, soil moisture estimation, and other applications.

Short-Wave Infrared 1 Band: This band (1.57-1.65) μm is sensitive to vegetation moisture content and is useful for detecting vegetation stress and soil moisture conditions.

Short-Wave Infrared 2 Band: This band (2.11-2.29) μm captures longer wavelength infrared light and is used for geologic and mineralogical mapping.

Panchromatic Band: This band (0.50-0.68) μm has a higher spatial resolution of 15 meters and provides black and white imagery for various applications, including land cover mapping and change detection.

Cirrus Band: This band (1.36-1.38) μm is specifically designed to detect and assess thin cirrus clouds that can affect the accuracy of surface reflectance measurements.

Landsat 8's TIRS sensor consists of two thermal bands (10 and 11) with a spatial resolution of 100 m. These bands (10.60-11.19 and 11.50-12.51) μm are used for measuring land surface temperature and monitoring thermal anomalies.

The Landsat 9 mission continues the legacy of Landsat 8 and includes similar spectral bands. For specific details about the bands of Landsat 9, you can refer to

Table (2-2) in the relevant documentation or resources provided by the United States Geological Survey (USGS) or NASA, which are the organizations responsible for the Landsat program.

Table (2-2): Landsat 8,9 Thermal Infrared Sensor (TIRS) and Operational Land Imager (OLI) [127].

Bands	Wavelength (μm)	Resolution (m)
Band 1 - Coastal aerosol	0.43 - 0.45	30
Band 2 – Blue	0.45 - 0.51	30
Band 3 – Green	0.53 - 0.59	30
Band 4 – Red	0.64 - 0.67	30
Band 5 - Near Infrared (NIR)	0.85 - 0.88	30
Band 6 - SWIR 1	1.57 - 1.65	30
Band 7 - SWIR 2	2.11 - 2.29	30
Band 8 – Panchromatic	0.50 - 0.68	15
Band 9 – Cirrus	1.36 - 1.38	30
Band 10 - Thermal Infrared (TIRS) 1	10.6 - 11.19	100
Band 11 - Thermal Infrared (TIRS) 2	11.50 - 12.51	100

2.12 ALOS PARSAL Satelite

In the fall of 2006, Japan Aerospace Exploration Agency (JAXA) launched the IOS satellite, which is one of the advanced Japanese satellites for Earth observation. It is also an improved and good sensor that is also able to measure full polarization as well as ScanSAR operations. In addition, it was characterized by a completely new concept aimed at providing global coverage. coordinated spatially and

temporally. This satellite is one of the most important and largest satellites developed by the Japanese Space Agency, as it carries three sensor tools: the comprehensive color remote sensing tool for mapping stereoscopic PRISM with a high accuracy of 2.5 m, and an advanced visible radiometer with an accuracy of 10 m and near infrared of the second type, AVNIR2, and the synthetic aperture radar of the type of L_band PAL Phased Array L_band.

The weight of the satellite is about 4000 kg and is in a sun-concurrent orbit at an elevation of 691 km. This satellite also has the ability to calculate DEM units high-resolution digital elevation images. This satellite provides accurate and detailed monitoring in all air fields, day and night, and has the ability to calculate repeated interference. All these data were obtained through multiple monitoring modes with display accuracy, flat display, variable polarization, and off-perspective angle. In the first half of 2011, the Japanese Space Agency discovered that this satellite began to lose its energy, suggesting the reasons for the deterioration of its solar arrays. The reasons may be due to meteorites hitting large parts of it, according to the scientists' report. At the end of 2011, JAXA sent orders to the satellite to shut down, and then Lost contact with the satellite [128], as shown in Figure (2-14).

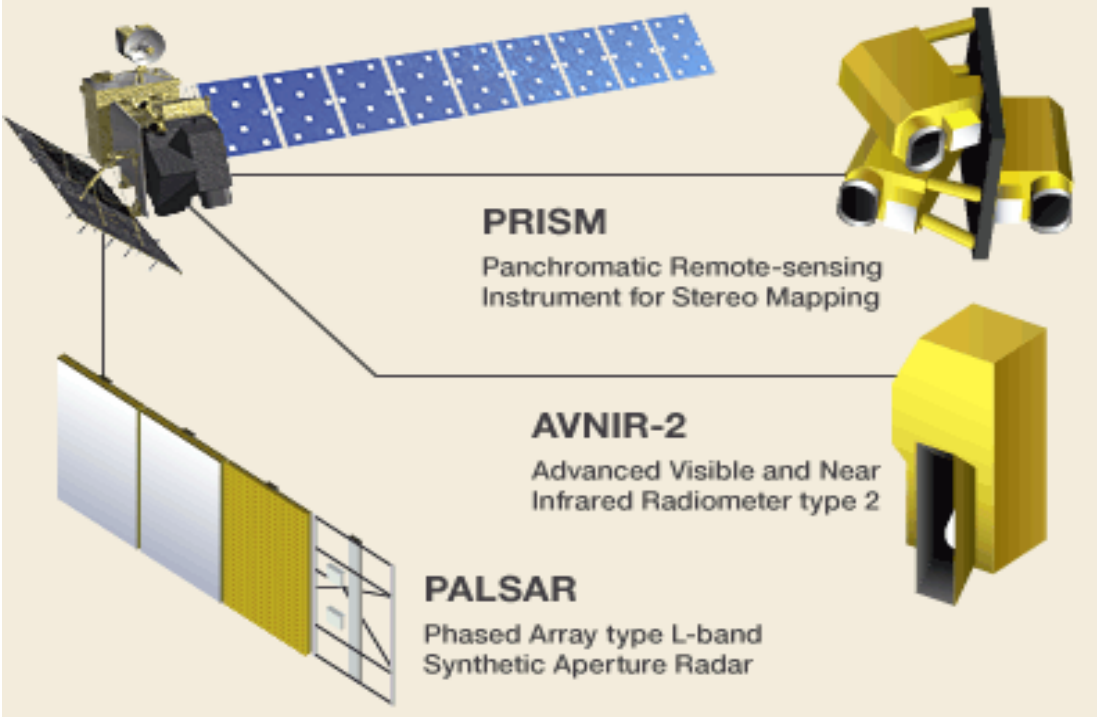

Figure (2-14): Diagram of the ALOS Satellite and it's on board sensors [128].

CHAPTER THREE
Results and Experimental Work

3.1 Introduction

In this chapter, information about the used satellites will be introduced, as well as a detailed explanation of how to deal with satellite images in terms of spatial corrections and atmospheric corrections. The merge of satellite images and the process of clip raster process of the study area (Babylon province) were also dealt with in detail. Two flowcharts were presented about the method of work that used in calculating the spatial distribution of solar radiation, as well as the process of calculating the Earth's surface temperature. The information related to the study area in terms of the geographical location, its area, and the administrative units it includes, was mentioned earlier in the chapter 1Table (1.1).

3.2 Data Acquisition

The SAR aperture radar of PALSAR, and its assistance in weather conditions at night times, and the radar mission began from 2006 to 2011, and its tasks also carry out frequent interferometric measurements, as this radar jointly with Alaska, to participate in the collection of industrial data in one of the most important and largest collection Donations, also in this project and from the ASF website downloaded 12,5" x 12,5" DEM images.

Landsat 9-8 TIRS / OLI group, these images are all with a resolution of 30 m, and they were obtained from the USGS, the data obtained from the European Center for Medium-Range Weather Forecasts ECMWF represents climate information, as it

studies all weather data and forecasts for meteorology for all countries members of the ECMWF are all accredited.

3.3 The Solar Radiation Methodology

The process of calculating the solar radiation for the Babylon province was summarized in the illustrative diagram, that shown in Figure (3-1).

Figure (3-1): The flowchart shows the steps that were used in calculating the solar radiation for Babylon province for each season**.**

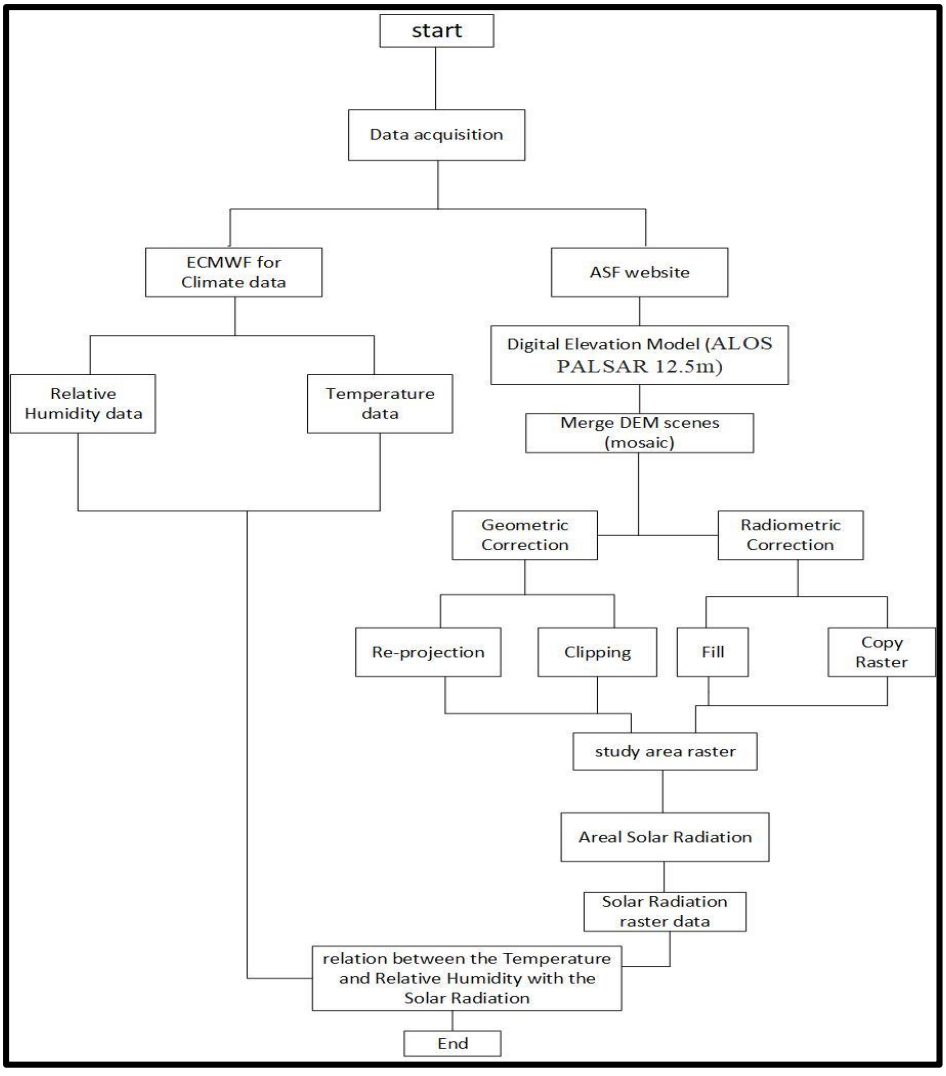

The study area (Babylon province) needs five scenes to be covered. Then five DEM were downloaded from the USGS. In this case the five scenes require to be merged.

Table (3-1): ALOS PALSAR satellite data (DEM) specification for Babylon province.

Scene	Path/Frame	Scan-time	Absolute Orbit	Datum/UTM Zone
1	584 / 640	11/26/2010, 19:29:19	25786	WGS84/UTM Zone 38N
2	584 / 630	11/26/2010, 19:29:11	25786	WGS84/UTM Zone 38N
3	585 / 650	07/28/2010, 19:33:20	24021	WGS84/UTM Zone 38N
4	585 / 640	07/28/2010, 19:33:12	24021	WGS84/UTM Zone 38N
5	585 / 630	07/28/2010, 19:33:04	24021	WGS84/UTM Zone 38N

3.4 The Mosaic Process

It represents merge five raster datasets into a new raster dataset. In this case, we merge 5 scenes DEM imagery to cover all study area boundary, in ArcMap, by using the tool (mosaic to new raster), select the number of bands (that the output raster will have) used 1 band and chose the pixel type (the bit depth, or radiometric resolution

of the mosaic dataset) depending on the raster that be used. The used five raster datasets and the new raster dataset, which was produced from merging the five raster datasets, were shown in Figure (3-2).

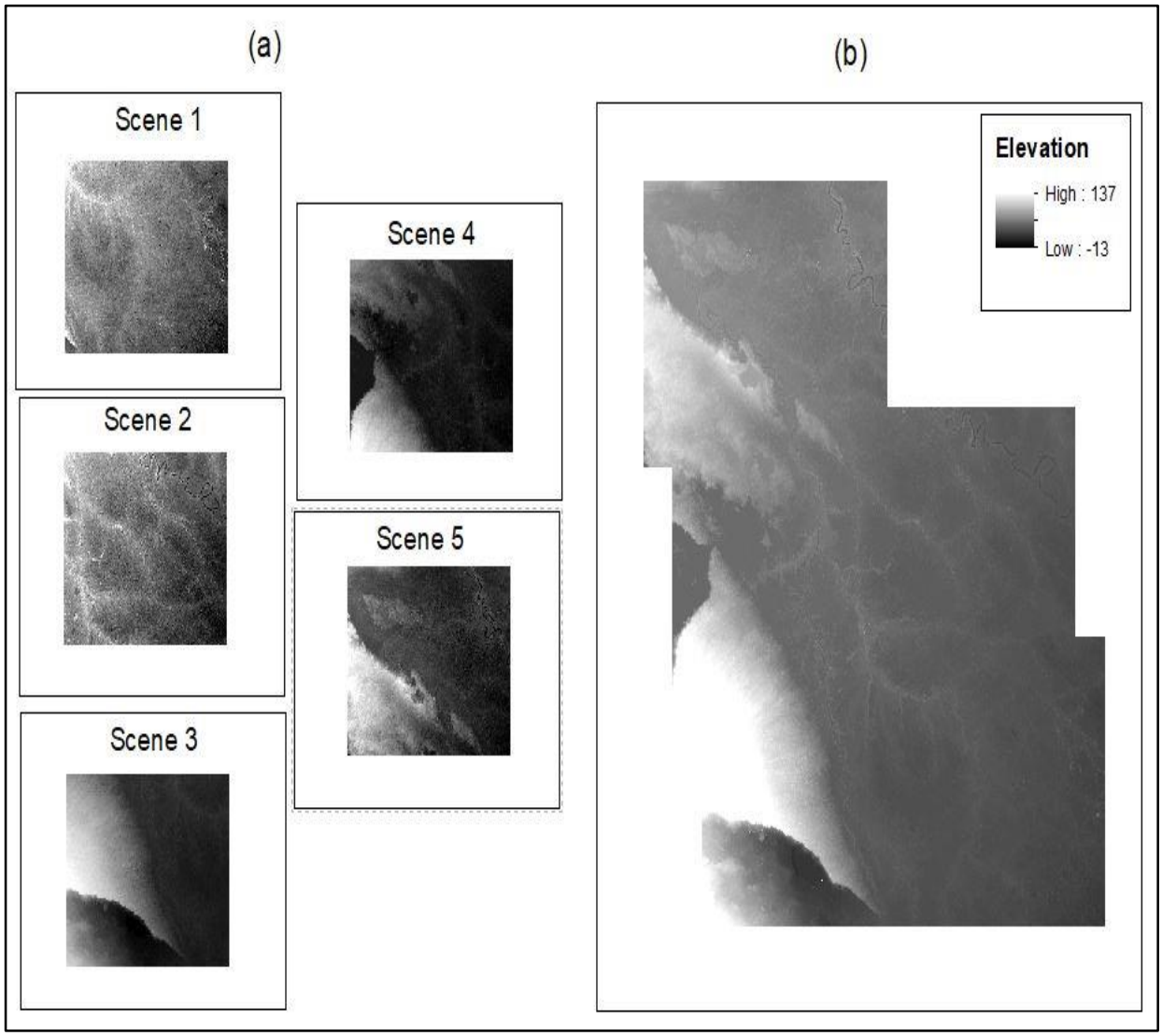

Figure (3-2): The Mosaic Process: (a) the 5 scenes DEM from ALOS PALSAR, (b) the DEM scene after mosaic.

3.5 Geometric Correction

The correction of errors in remotely sensed data, such as those brought on by sensors that stray from the main focus plane or by satellites or airplanes that don't maintain a consistent altitude. Resampling is frequently used to compare images to ground control points on precise basemaps in order to determine exact positions and the right pixel values.

3.5.1 The Clip Raster Process

Clipping raster allows you to only work on or display a certain area of interest. It could be defined a boundary from a vector shapefile, or it could be defined by the extent of the window, after merge DEM scenes we extract Babylon province using Babylon vector shapefile as boundary definition. The Figure (3-3-A) shows the image that resulted from the mosaic process, and the panel (B) represents the province of Babylon after clip raster process.

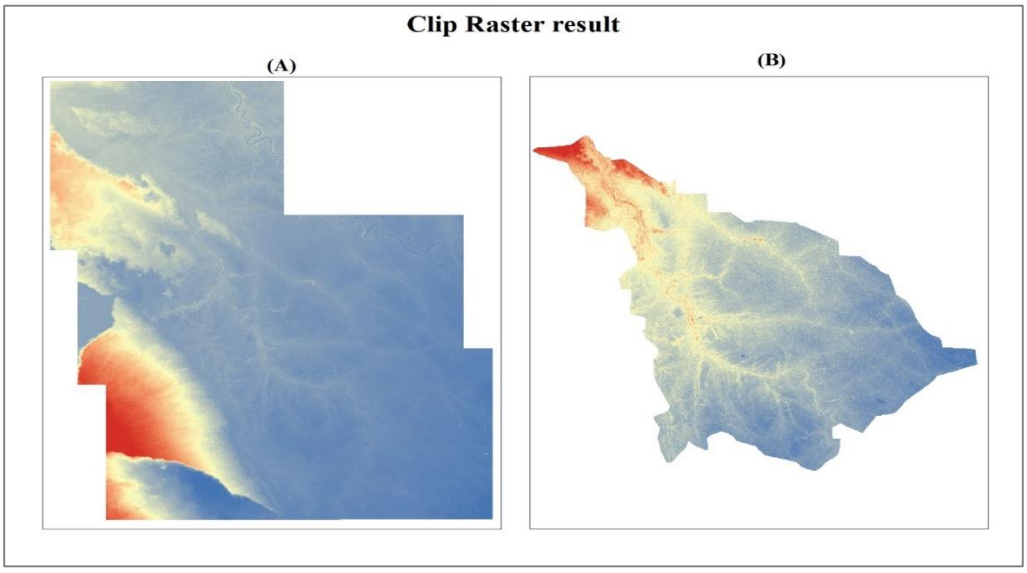

Figure (3-3): The Clip Raster Process: (A) the merged DEM by the mosaic process, (B) the clipped DEM as the shape of the Babylon province.

3.5.2 The Re-Projection Process

Transforms the raster dataset from one projection to another, in Arcmap, we use the tool (project raster) to convert the DEM from geographic coordinate system to

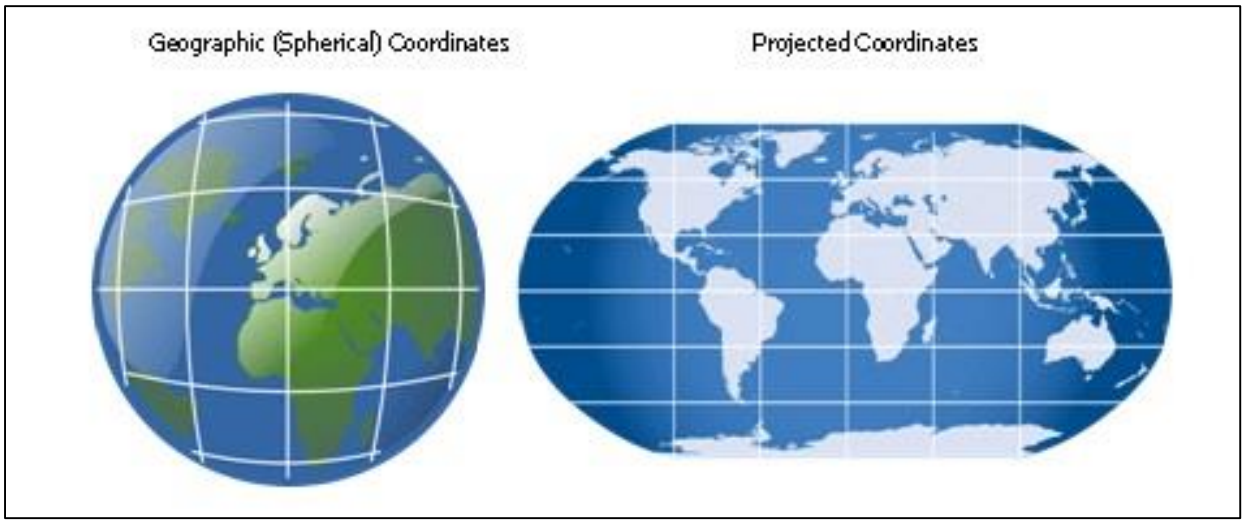

Figure (3-4): It represents the geometric and projected coordinate systems.

projected coordinate system in meter unit to facilitate calculations and achieve accurate results, Figure (3-4) represents the geometric and projected coordinate systems.

3.6 The Radiometric Correction

One of the many image processing techniques used today to analyze remote sensing imagery is radiometric correction. The procedure involves matching or directly comparing a group of images after normalization. The general goal of absolute radiometric (atmospheric) correction is to turn the digital brightness values (or DN) recorded by a remote sensing system into scaled surface reflectance values.

3.6.1 The Copy Raster

This command saves a specific copy of a raster data set or converts mosaic data into a single raster data set. Another use of this tool is to measure the type of pixel from one bit depth to another. In the case of measuring the pixel depth, a raster scan displays the same values, but with different values. To the new depth of the new bit taking into account ignoring the amount of background to avoid errors in the scene.

3.6.2 The Fill

There are small defects in the data and they still fill the basins in the surface raster, and each cell in the data with an unlimited drainage direction is called a basin. The flow point is defined as a boundary cell with the minimum height of the basin area. When the basin is filled with water, then this will be the point that spills It contains water, and by using fill it is also possible to remove the vertices, where the vertex is defined as each cell that does not contain adjacent cells higher than it, and the method used to remove the vertices is by using the subtraction tool by inverting all the raster data of the input surfaces, so that we determine the highest value for the surface raster which is considered as a first entry and the surface points as a second entry, after which the filling takes place.

And the last step is to flip the results, after which we get a pure surface that contains the values of the original lines and without peaks. This process can be applied to the (Z) limit, and if nothing is specified for the Z-Limit, then all peaks will be removed. The apparent difference is only in the value of g for the peak region and the values of the highest neighboring neighbor to it are greater than the boundary g and that peak cannot be removed.

3.7 The Solar Radiation Estimation in Arc GIS (10.5)

To derive the incoming solar radiation to the earth by using the Arc GIS program, we need to choose Spatial analyses tools from the Arc Toolbox then the Solar Radiation.

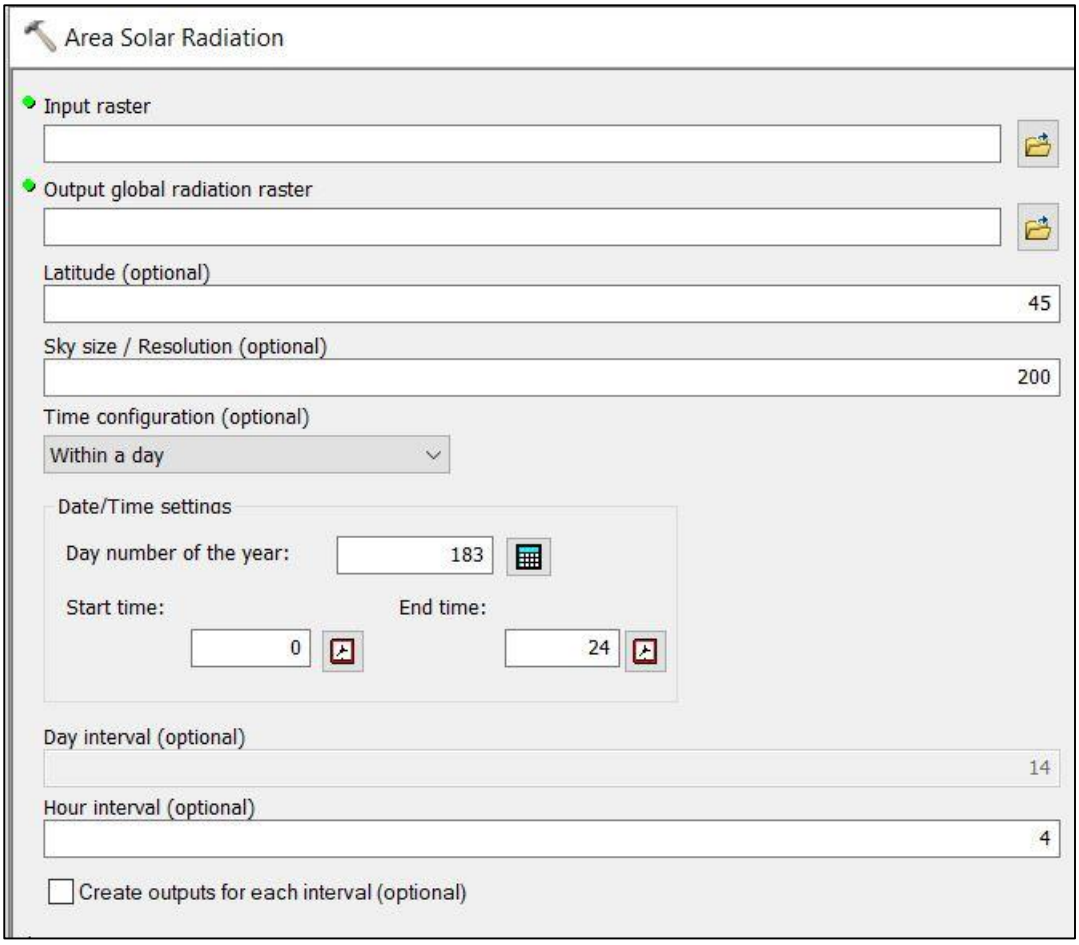

Figure (3-5): It represents the Arc Toolbox of the area solar radiation.

This selection suggests two choices: point (points) solar radiation and area solar radiation. In this study the second choice was chosen, and the toolbox in this tool we used DEM dataset for the study area and define the date and time of solar radiation data and other parameter, this tool used global solar radiation formula.

- Input raster data: it is defined as the raster of the surfaces to be able to enter the DEM height after it has been corrected.
- Latitude: It is used for the area of the site and is in units of decimal degrees, with positive and negative values for the northern hemisphere and the southern hemisphere, respectively.
- The size of the sky: it can be defined as the size of the sky for the scope of vision, its accuracy, the map used for the sky, and the raster map of the sun, and its units are made up of cells created from the default numbers of 200 x 200 cells.
- Time composition: To perform solar calculations, a specific time period is determined within one day.
- Day separator: It can be defined as the time period within one year, which is used to calculate the areas of the sky for the map of the sun and in units of days.
- Hour interval: It is the period of time used to calculate the sky sector in maps of the sun, and its units are hours.

Then we create outputs and results for the time intervals to determine whether we want to calculate one complete insolation value for most of the sites or multiple values for the specified time interval during the hour or day, after clicking on the OK button to start the calculation process.

3.8 The Land Surface Temperature Methodology

The Figure (3-6) shows the methodology of estimating the LST for the Babylon province. In this part of study, five months were chosen to cover the four seasons of 2021 (January, April, July, August and October). After, creating an account on the site: (https://earthexplorer.usgs.gov/), the needed Landsat 8-9 OLI/TIRS satellite images data were downloaded. To estimate the brightness temperature, TIR band 10 was used, while bands 4 and 5 were used for NDVI calculation. As mentioning before, the Babylon province needs two scenes to be covered then the mosaic process was applied to merge these images into a single image.

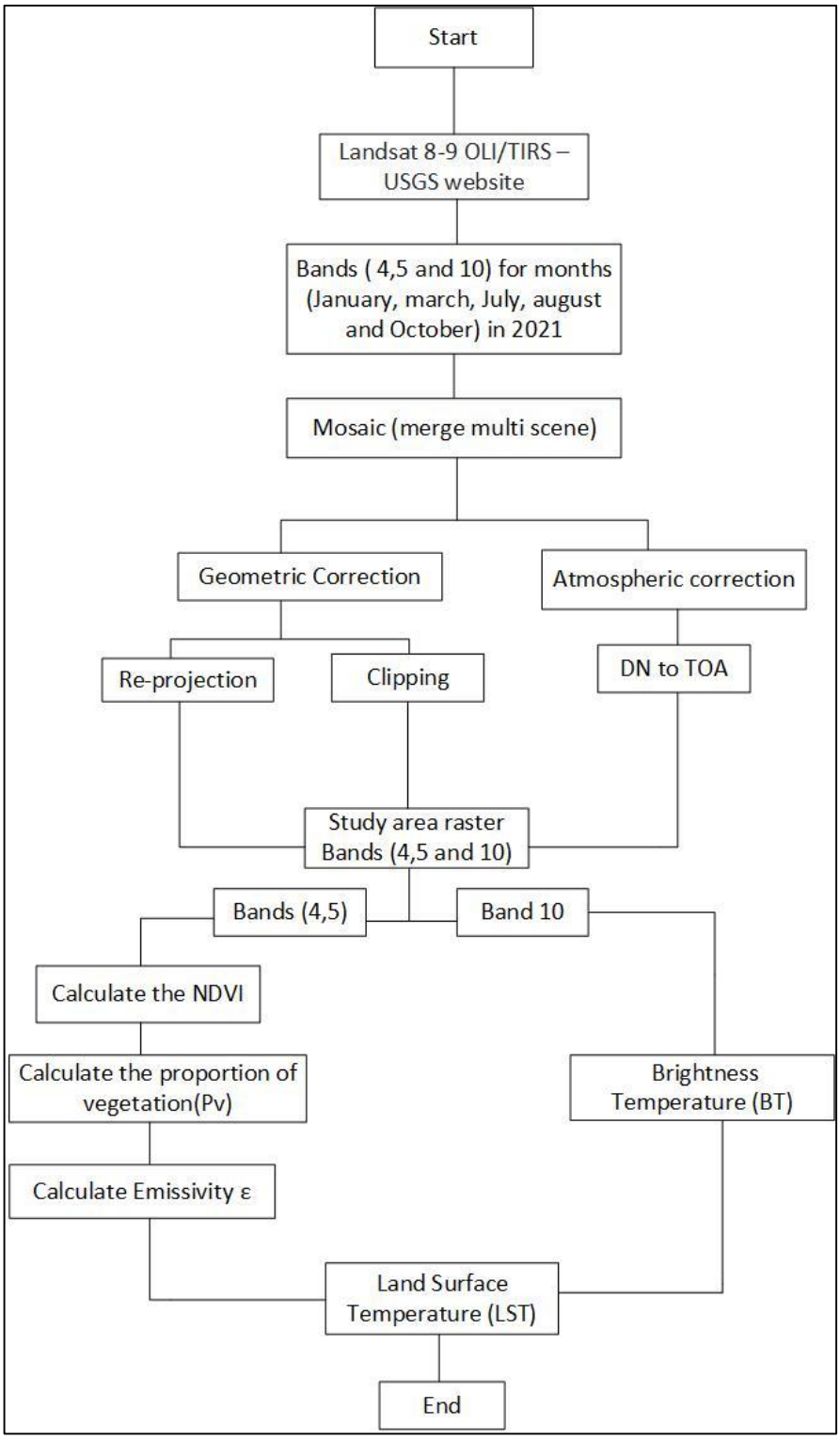

Figure (3-6): The flowchart shows the steps that were used in calculating the LST radiation for Babylon province for each season.

Table (3-2): Landsat 8-9 OLI/TIRS satellite data specification for Babylon province.

Seaso	Scene	Path/Row	Dates	Scan-time	Sun-azimuth (º)	Sun-elevation (º)	Datum/UTM Zone
Winter	1	168 /037	15/1/2021	2021-01-12 07:39:44.27 / 2021-01-12 07:40:16.04	154.38182159	30.80485052	WGS84/UTM Zone 38
	2	168 / 038	15/1/2021	2021-01-21 07:33:53.96 / 2021-01-21 07:34:25.73	152.07519049	33.29673565	WGS84/UTM Zone 38
Spring	1	168 /037	15/3/2021	2021-03-10 07:33:15.66 / 2021-03-10 07:33:47.43	143.79197589	46.39884364	WGS84/UTM Zone 38
	2	168 / 038	15/3/2021	2021-03-10 07:33:39.56 / 2021-03-10 07:34:11.33	142.50717122	47.40077265	WGS84/UTM Zone 38
Summer	1	168 /037	15/7/2021	2021-07-16 07:33:16.34 / 2021-07-16 07:33:48.11	114.34366784	66.40189859	WGS84/UTM Zone 38
	2	168 / 038	15/7/2021	2021-07-16 07:33:40.23 / 2021-07-16 07:34:12.0	110.91378437	66.72755441	WGS84/UTM Zone 38
	1	168 / 037	15/8/2021	2021-08-17 07:33:30.62 / 2021-08-17 07:34:02.62	128.79993054	61.46713057	WGS84/UTM Zone 38
	2	168 /038	15/8/2021	2021-08-17 07:33:54.75 / 2021-08-17 07:34:26.52	126.24154260	62.14663339	WGS84/UTM Zone 38
Autumn	1	168 / 037	20/10/2021	2021-10-20 07:33:47 / 2021-10-20 07:34:19.	155.87692146	43.25241602	WGS84/UTM Zone 38
	2	168 / 038	20/10/2021	2021-10-20 07:34:11 / 2021-10-20 07:34:43	154.93286178	44.45529064	WGS84/UTM Zone 38

3.9 The Geometric Correction

3.9.1 The Mosaic Process

It represents merge multiple raster datasets for a new raster dataset. In this case, we merge multi spectral imagery to cover all study area boundary, in ArcMap, by using the tool (mosaic to new raster), select the numbers of band (in which the resulting raster will be) used 1 band and chose a pixel type (represents the bit depth as well as the radiometric resolution of the mosaic dataset) depending on the raster that be used. The used bands in this thesis (band 10, band 5 and band 4) are shown in Figure (3-7) before and after the mosaic process.

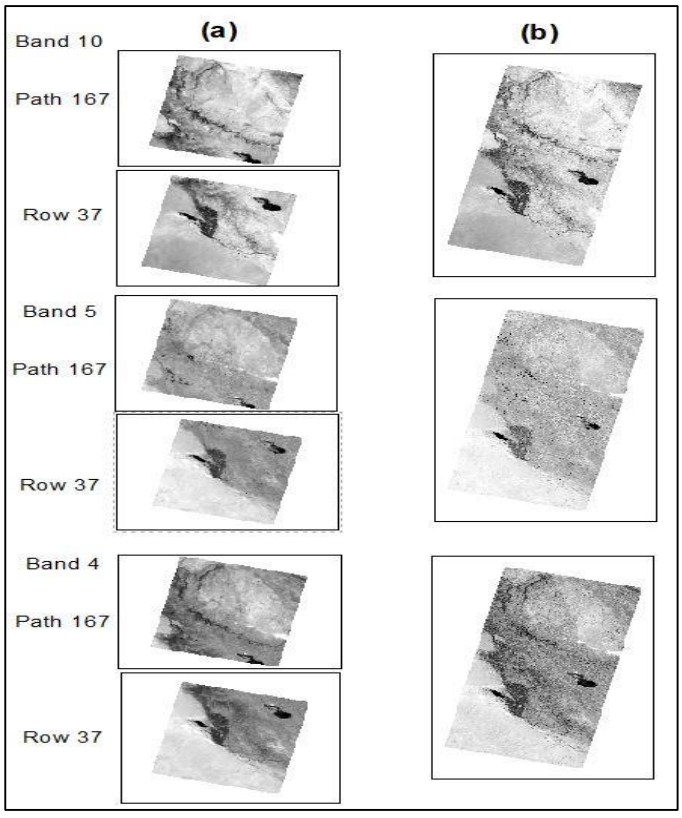

Figure (3-7): (a) Shows the band 4, band 5 and band 10 from landsite 8 15/7/2021. (b) Bands scene after mosaic.

3.9.2 The Clipping Process

The produced image from the mosaic process for the Landsat 8-OLI satellite images (the first scene with path and Row (168,37) and second (168,38)) was shown in Figure (3-8-A). This image needs to be clipped as the shape file of Babylon province. The produced image after the clipping process is shown in Figure (3-8-B).

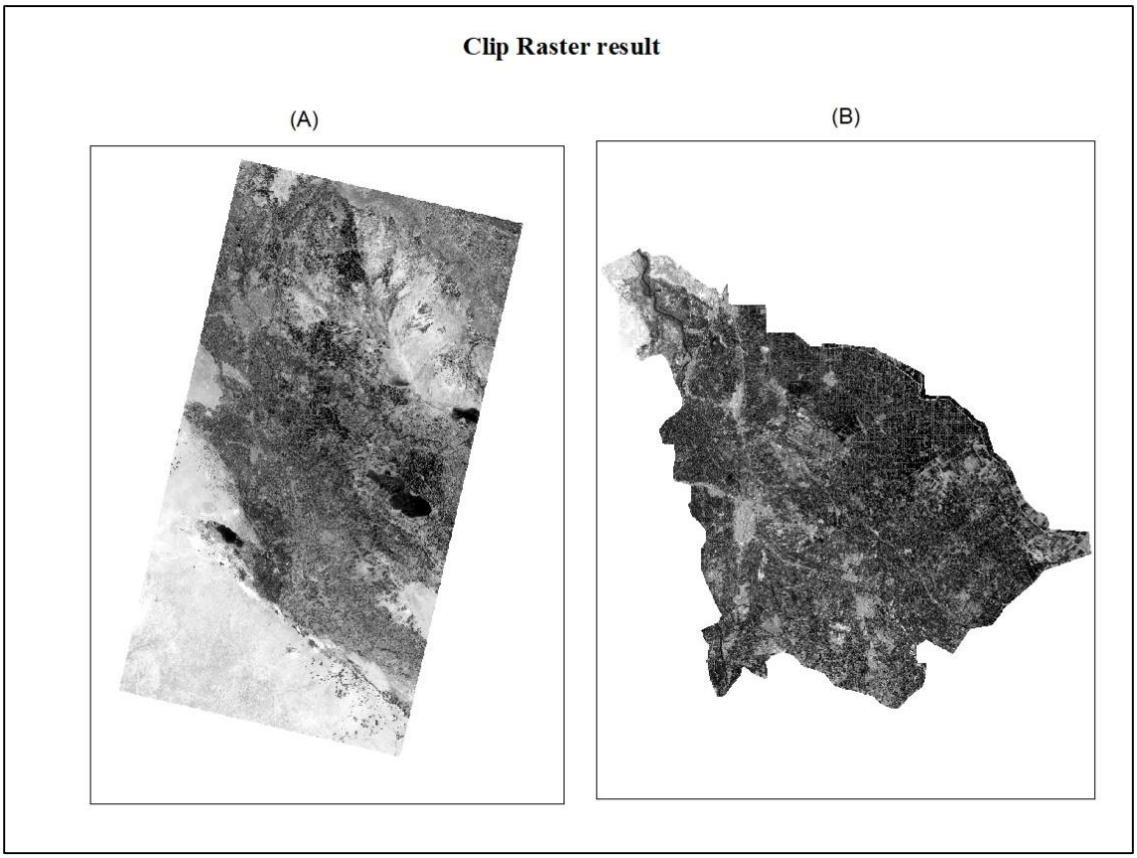

Figure (3-8): The clipping process: (A) show the merged image by the mosaic process for Band4, (B) after the clipping process as shape file of Babylon province.

3.10 Atmospheric Correction

Usually, changes occur in the solar radiation reflected from the Earth's surface to satellites due to the interaction of solar radiation with the atmosphere. This is due to the concealment of atmospheric effects from satellite images, so the correction of the atmosphere aims to ascertain the true values of surface reflection. Any emission from atmospheric correction, probably the most crucial step in the pre-processing of satellite remotely sensed data, leads to inaccurate results:

- **Convert the Digital Number (DN) to the Top of Atmosphere (TOA) Radiance:**

The DN in remote sensing systems represents a pixel-specific variable consisting of a binary integer in the range (0-255) (i.e. bytes). As for the range of energies examined in a remote sensing system is broken into 256 bins. The TOA is a unitless measurement which provides the ratio of the reflected radiation to the incident solar radiation on a given surface, to calculate TOA radiance we used the formula below[129]:

$$L_\lambda = Ml \times Q_{cal} + A_l \quad (3\text{-}1)$$

Where:

L_λ : Is TOA spectral radiance (Watts/(m^2 srad μm)).

M_L : Is The Band-specified multiplicative rescaling factor from the metadata (RADIANCE_MULT_BAND_x, where x is the band number).

A_L: Is The Band-specified additive rescaling factor from the metadata (RADIANCE_ADD_BAND_x, where x is the band number).

Q_{cal} : Is Quantized and calibrated criterion product pixel values (DN).

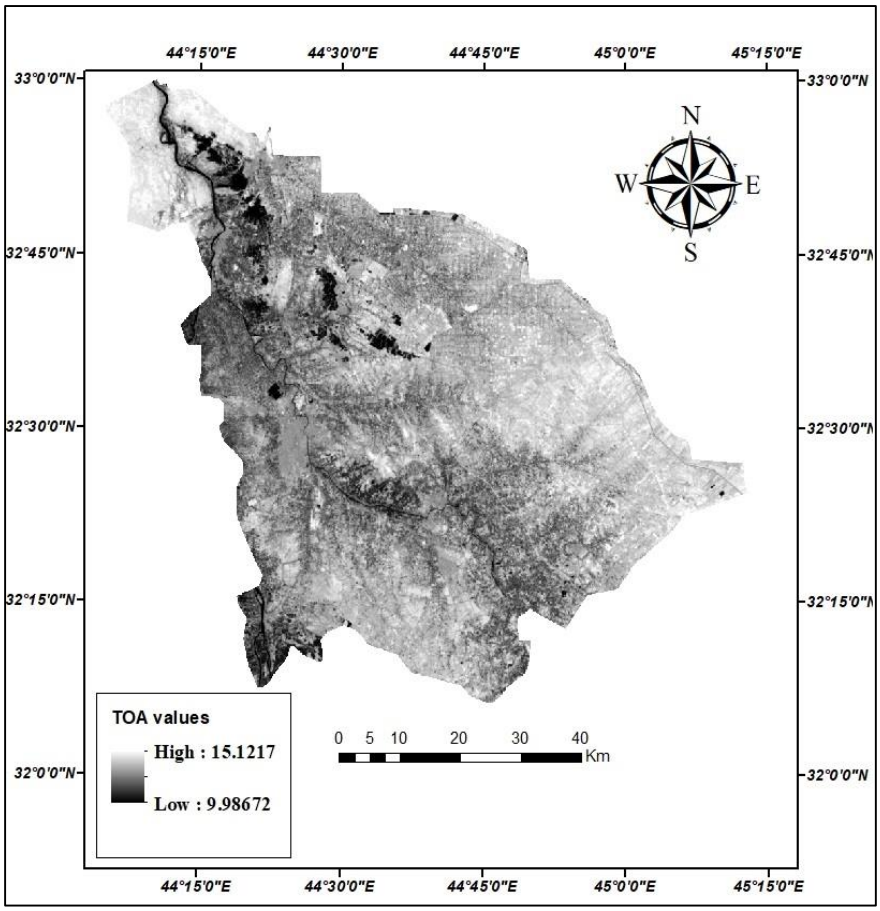

Figure (3-9): The top of atmosphere (TOA) radiation top of atmosphere values for 15-7-2021**.**

- **The Convert of the Top of Atmosphere (TOA) radiation to Top of Atmosphere Brightness Temperature (BT)**

The next step will be converted the LS to BT by using Planck's Law and the calibration constants of the Landsat8,9. The following equation will be used [129, 130]:

$$BT = \frac{K_2}{In(\frac{K_1}{L\lambda+1})} - 273.15 \quad (3\text{-}2)$$

Where:

K_1 and k_2 represent the thermic constant of the thermal infrared radiation, and saved in the meta data file which already connect with the satellite images.

K_1 = 774.8853.

K_2 = 1321.0789.

3.11 The Calculation of the Normalized Difference Vegetation Index (NDVI)

One of the most important uses of the vegetation index is to estimate and evaluate the greenness of vegetation, as well as to calculate and understand the density of vegetation, to know and evaluate all changes in the state of healthy plants, and to calculate the NDVI index, all visible ranges were used, which are somewhat close to infrared, and the importance of NDVI estimation is associated with The fact that the amount of vegetation cover is very important, and from the use of NDVI it is possible to deduce the state of the total vegetation cover, and after that it is possible to calculate the percentage of vegetation cover (PV), which has a close relationship and correlation with NDVI, as well as the urgent need to calculate the emissivity (ε), associated with PV.

$$NDVI = \frac{NIR-R}{NIR+R} \quad (3\text{-}3)$$

Where: NIR : Is near-infrared band.

R : Is red band In Landsat 8.

$$NDVI = \frac{BAND\ 5-BAND\ 4}{BAND\ 5+BAND\ 4} \quad (3\text{-}4)$$

Where: BAND 5 : NIR

BAND 4 : R

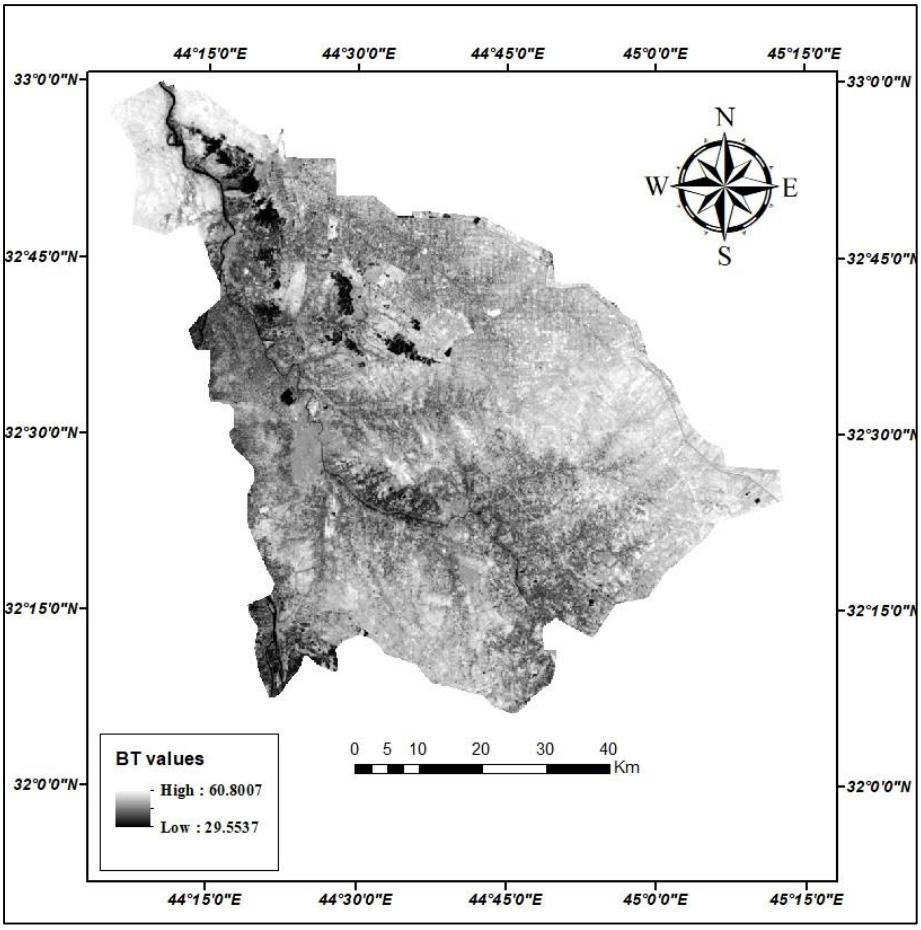

Figure (3-10): Show the BT value of Babylon province.

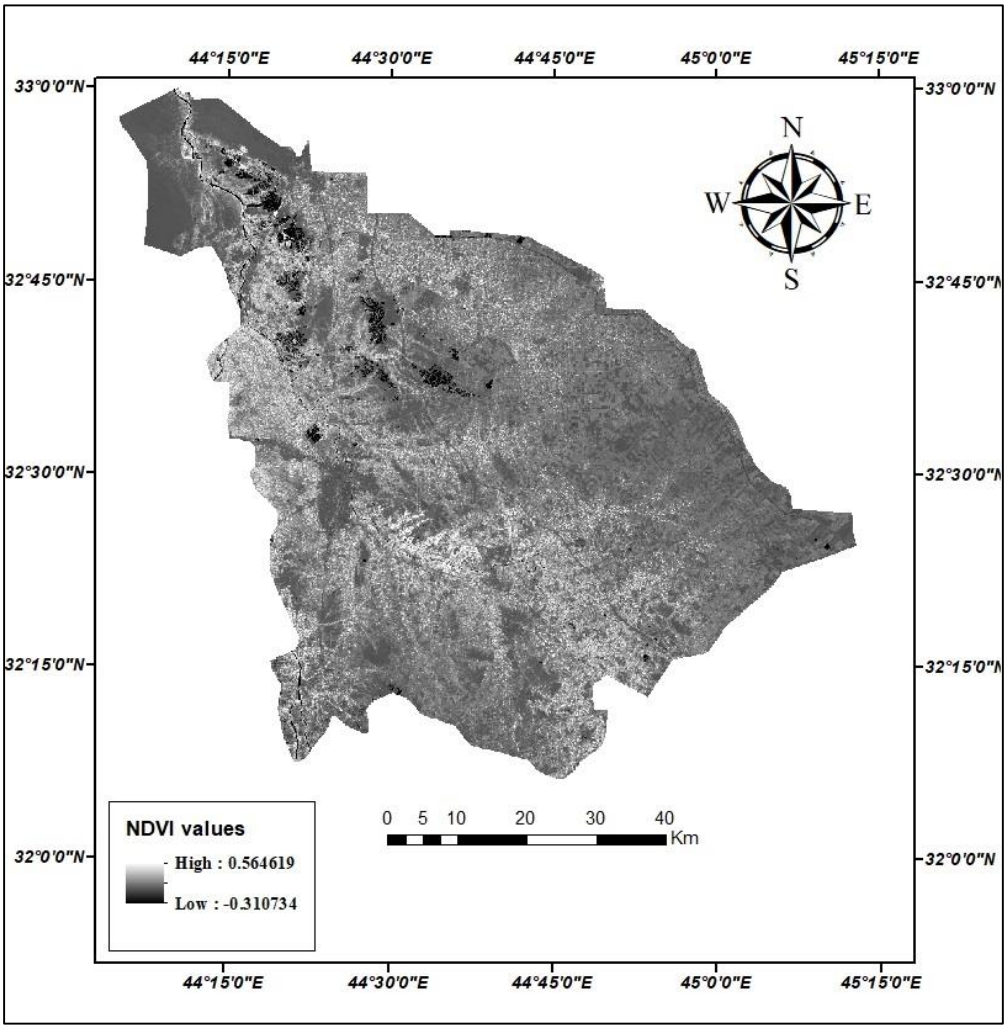

Figure (3-11): The special distribution of the NDVI for 15-7-2021.

3.12 The Calculation of the Proportion of Vegetation (PV)

Through the equation below it is possible to calculate the PV using the maximum and minimum values of NDVI:

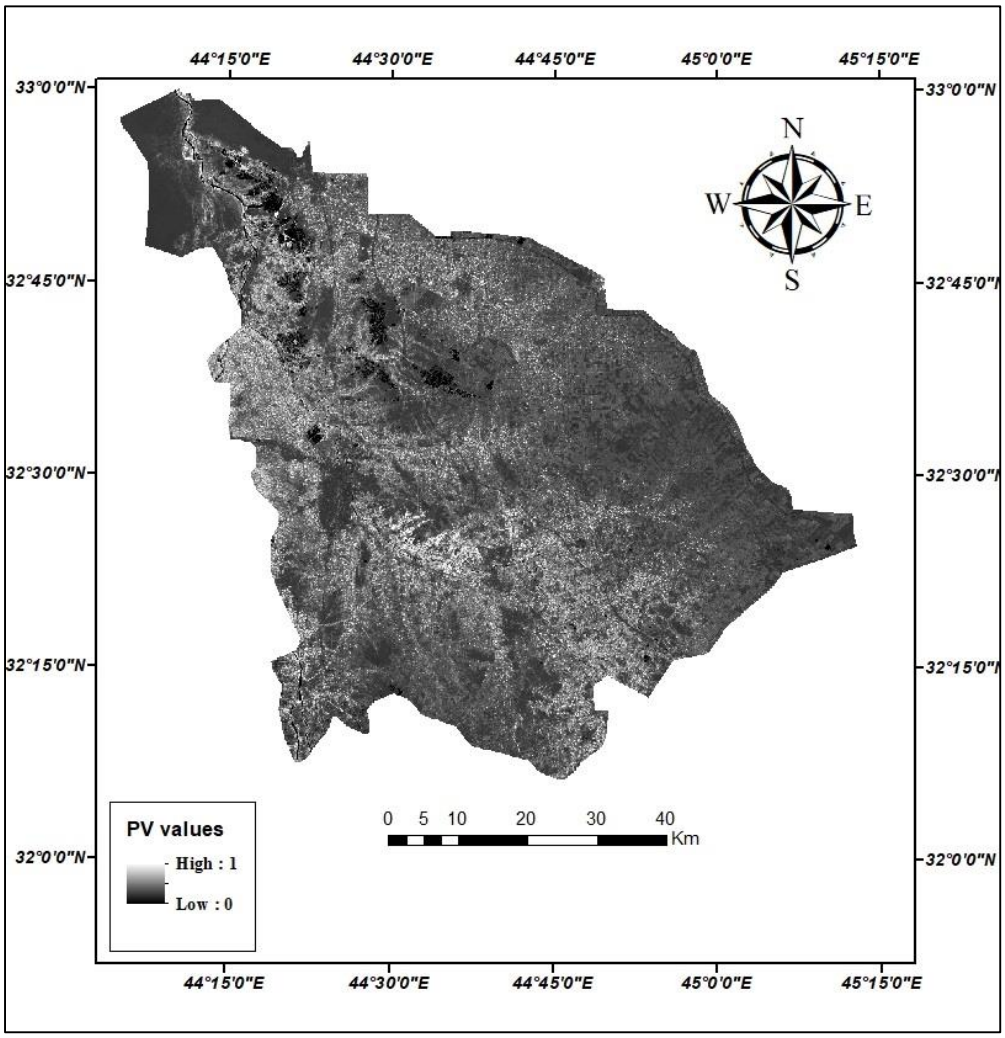

Figure (3-12): The special distribution of the PV for 15-7-2021.

$$PV = \left(\frac{NDVI - NDVI_{min}}{NDVImax + NDVI_{min}}\right)^2 \quad (3\text{-}5)$$

3.13 The Calculation of the Land Surface Emissivity (LSE (ε))

According to Planck's law for predicting radioactive emissions, the LST is a proportional factor that measures the black body radiation, as well as the thermal energy transfer factor from the Earth's surface to the atmosphere, so we need to know

the estimate of the LST, and the terrestrial emission is determined clearly and conditionally as follows:

$$\varepsilon = 0.004 \times PV + 0.986 \quad (3\text{-}6)$$

Where: (0.004) represent the vegetation emissivity, PV represents the proportion of the vegetation and (0.986) refers to the surface roughness.

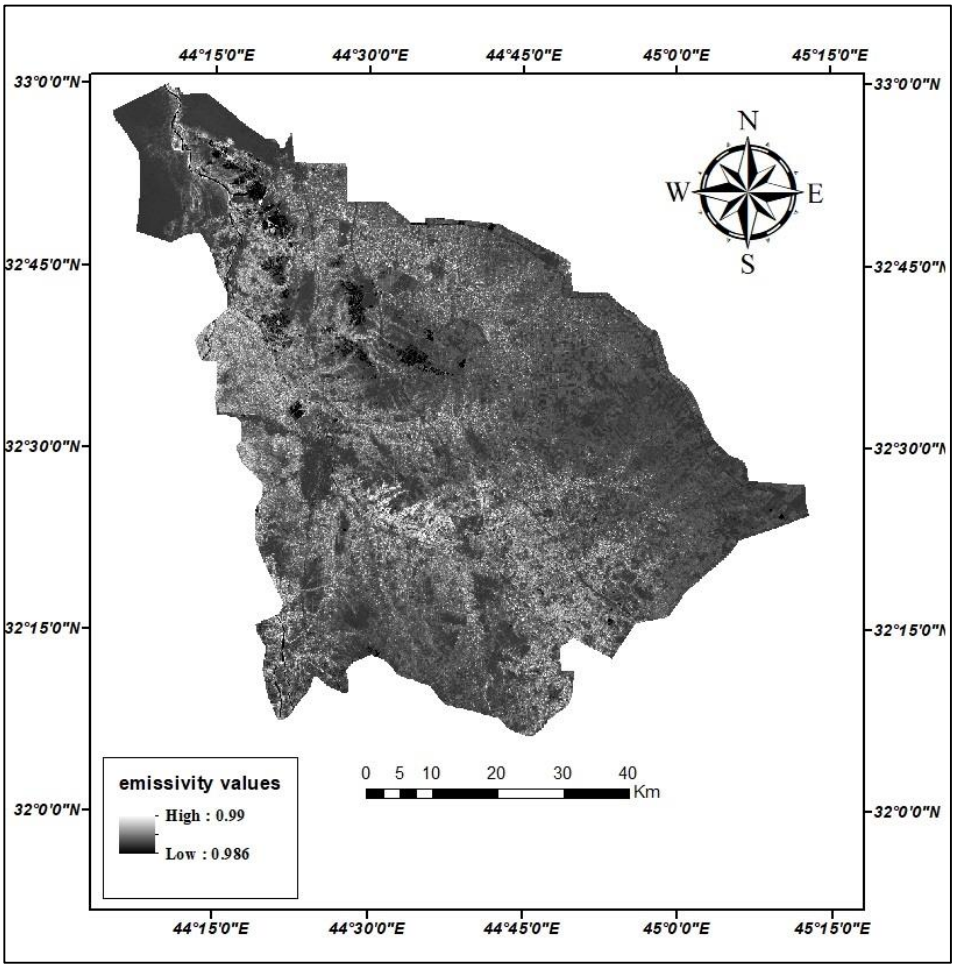

Figure (3-13): The special distribution of the emissivity for 15-7-2021.

3.14 The Calculation of the Land Surface Temperature

The emissivity-corrected surface temperature is calculated from the last step of the LST recovery and is as follows:

$$LST = \frac{BT}{1 + [(\frac{\lambda BT}{\rho})ln\ \varepsilon\lambda])} \quad (3\text{-}7)$$

Where LST represents the Earth's surface temperature in degrees Celsius, and BT represents the sensor in degrees Celsius, λ represents the wavelength of the amount of radiation emitted (for which the peak response and average wavelength are used) and the value of (λ =10.895), ε_λ is the emissivity calculation in (3-6), and ρ=h *c/σ = 1.438 × 10^{-2} m K

Where σ the Boltzmann constant (1.38 × 10^{-23} J/K), h the Planck's constant (6.626 × 10^{-34} J s), and c is the velocity of the light (2.998 × 10^{8} m/s).

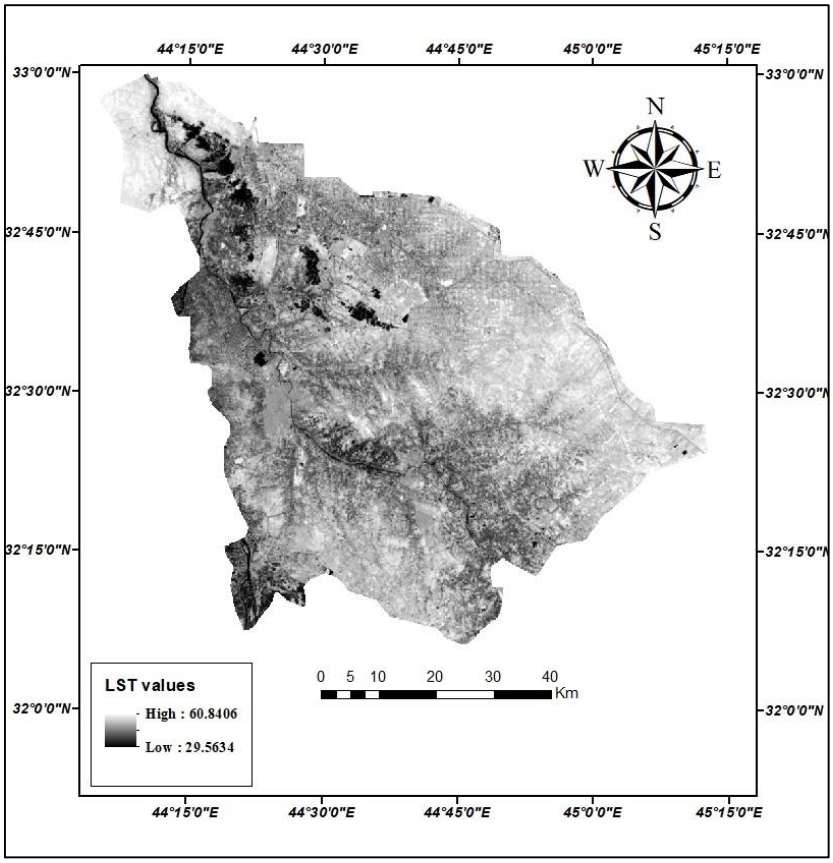

Figure (3-14): The special distribution of the Land surface Temperature for 15-7-2021.

CHAPTER FOUR

Results and discussions

4.1 Introduction

The solar radiation and the LST of the study area were calculated in five months (January, March, July, August and October) of the year 2021 to cover the different seasons of the year.

4.2 The Solar Radiation in January

The important information about the state of the climate in the observing day is listed in Table (4-1). The day time length was divided in three periods, four hours for each one. Then the areal solar radiation was determined in each period by using DEM from the USGS for the specified time period in the study area (Babylon province) Table (4-2). Figures (4-1-A) represents the spatial distribution of the solar radiation through the first period and Figure (4-1-B) shows the distribution of the solar radiation in histogram form in order to a present statistical way. The histogram shows how many pixels that have a specific value of the solar radiation. The maps and histograms of consecutive periods are presented in Figures (4-2) and (4-3). In Figure (4-4), the average distribution of the solar radiation during the day of observation. The attitude of the rate value of the solar radiation and the calculated temperature during the day of observation was presented in Figure (4-5) upper panel, while the attitude of the rate value of the solar radiation and the relative humidity was shown in Figure (4-5) lower panel.

Table (4-1): The climate state was taken from ECMWF for the time of observation.

The observing day	The Day time length hour	Temperature Cº	Relative humidity	Precipitation mm/day
15/1/2021	10.15	10.5	53.94 %	0.3

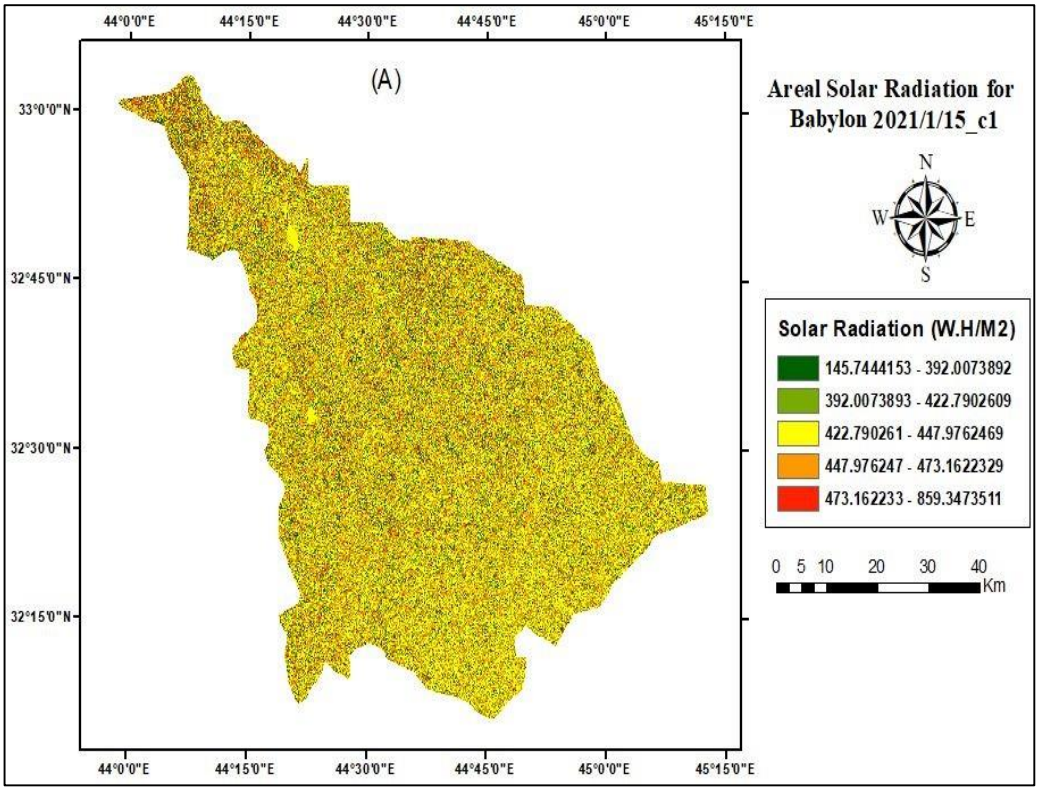

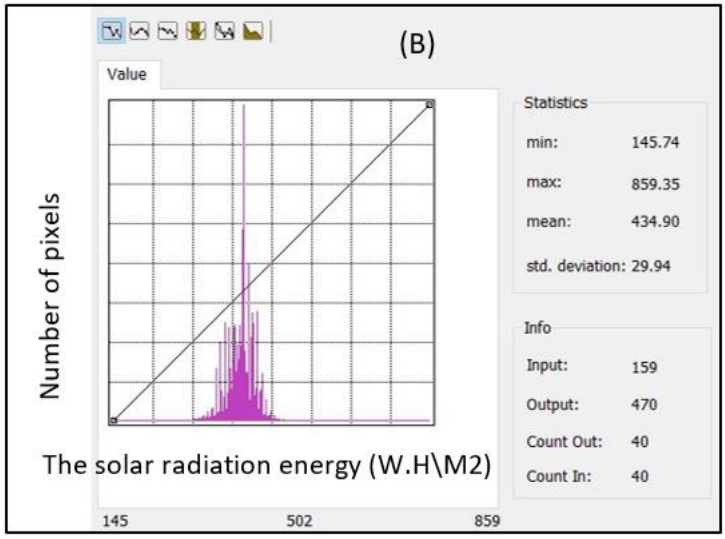

Figure (4-1): (A): The distribution of the solar radiation energy for Babylon province in the first period in (15-1-2021). (B): The histogram for the numbers of the pixels and the values of the solar radiation energy that belong to it.

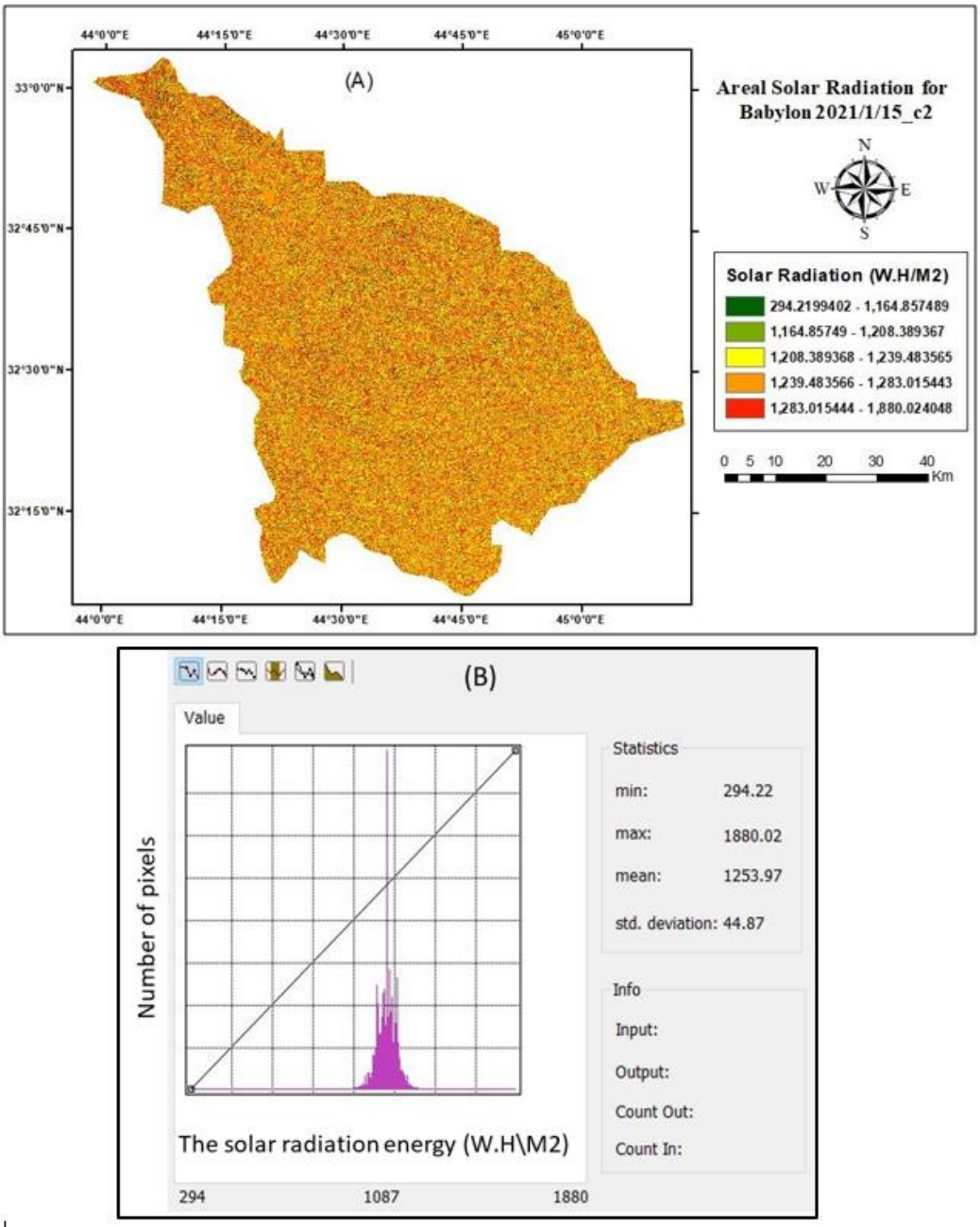

Figure (4-2): (A): The distribution of the solar radiation energy for Babylon province in th second period in (15-1-2021). (B): The histogram for the numbers of the pixels and the valu of the solar radiation energy that belong to it.

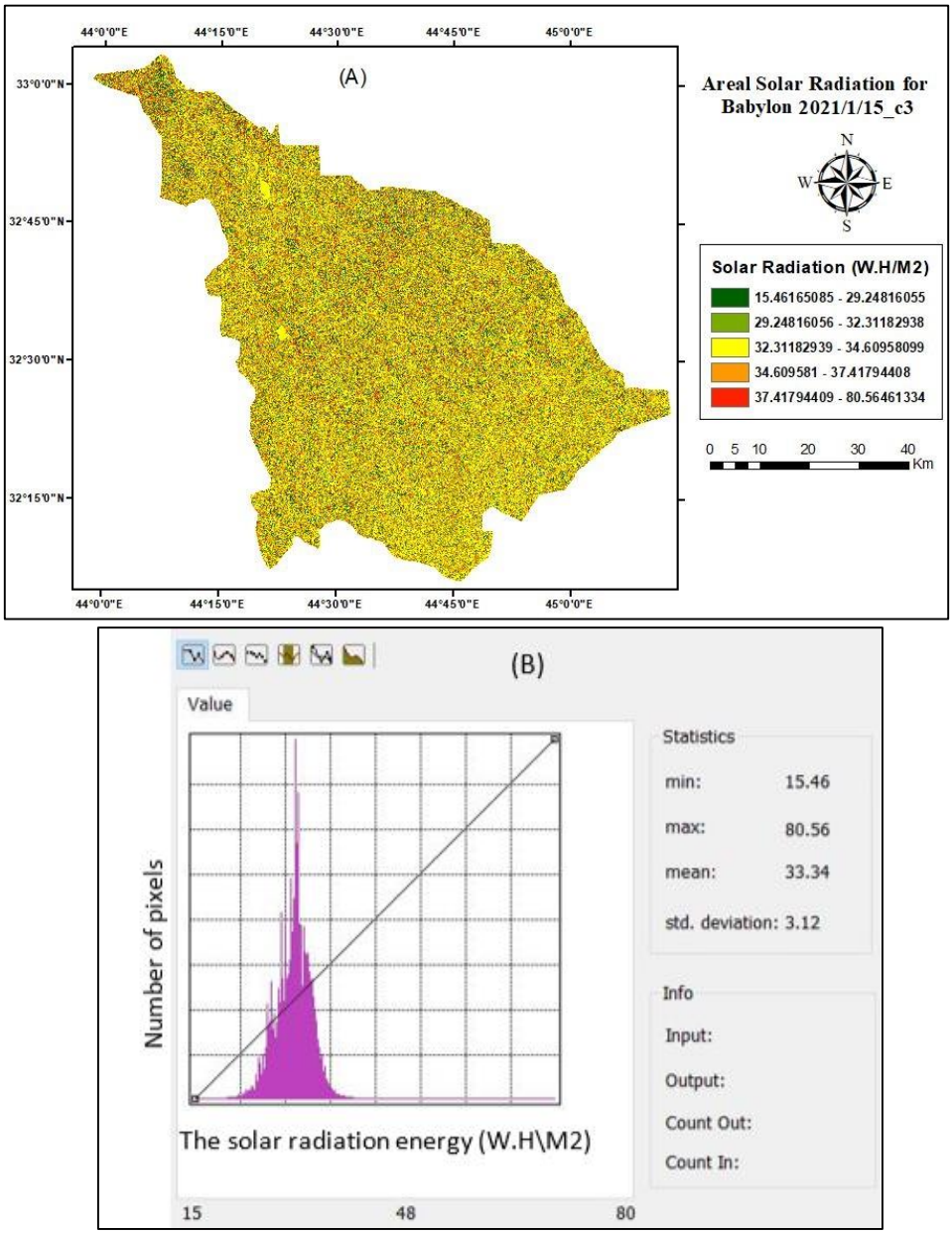

Figure (4-3): (A): The distribution of the solar radiation energy for Babylon province in the third period in (15-1-2021). (B): The histogram for the numbers of the pixels and the values of the solar radiation energy that belong to it.

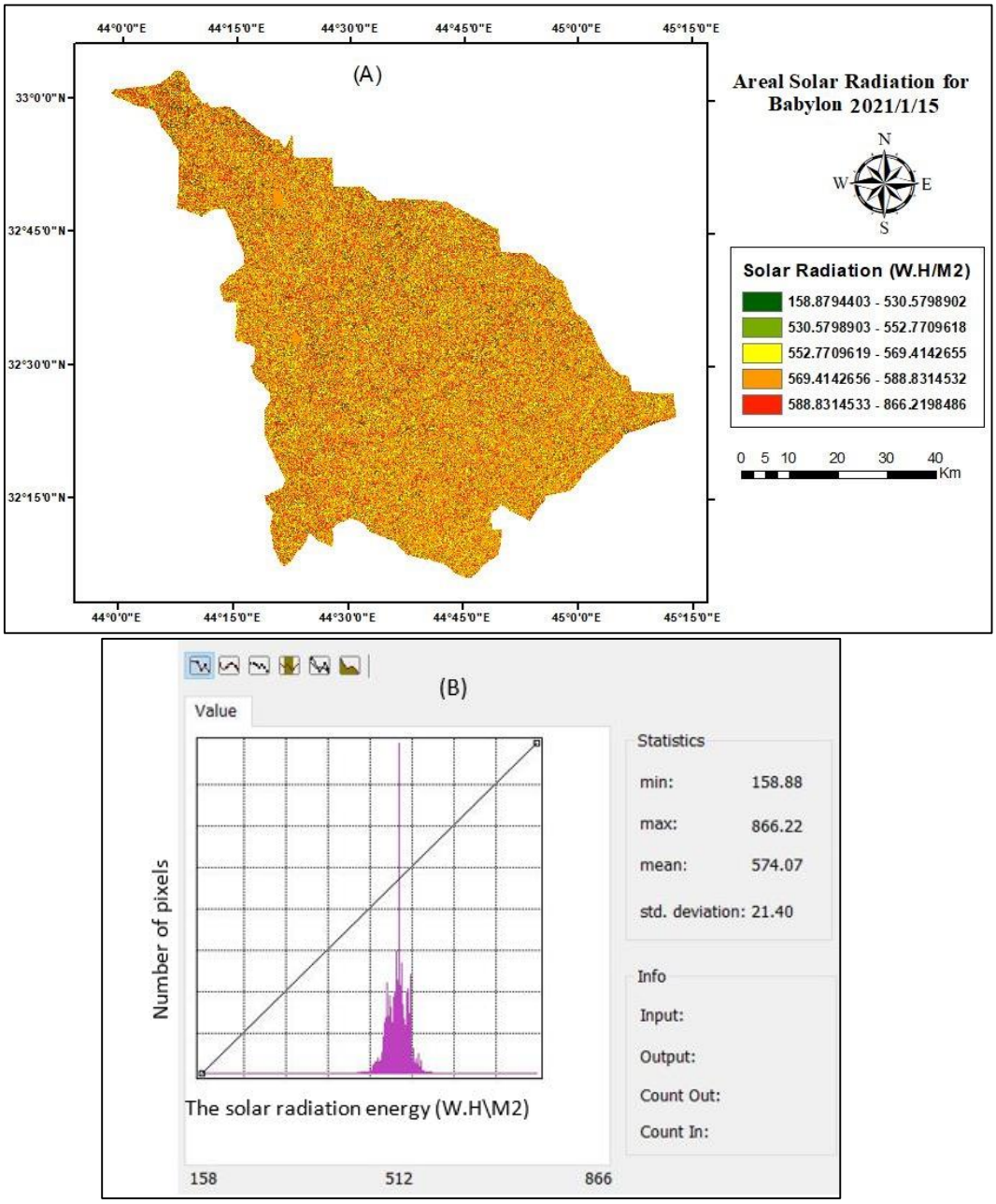

Figure (4-4): (A): The average distribution of the solar radiation energy for Babylon province during (15-1-2021). (B): The histogram for the numbers of the pixels and the values of the solar radiation energy that belong to it.

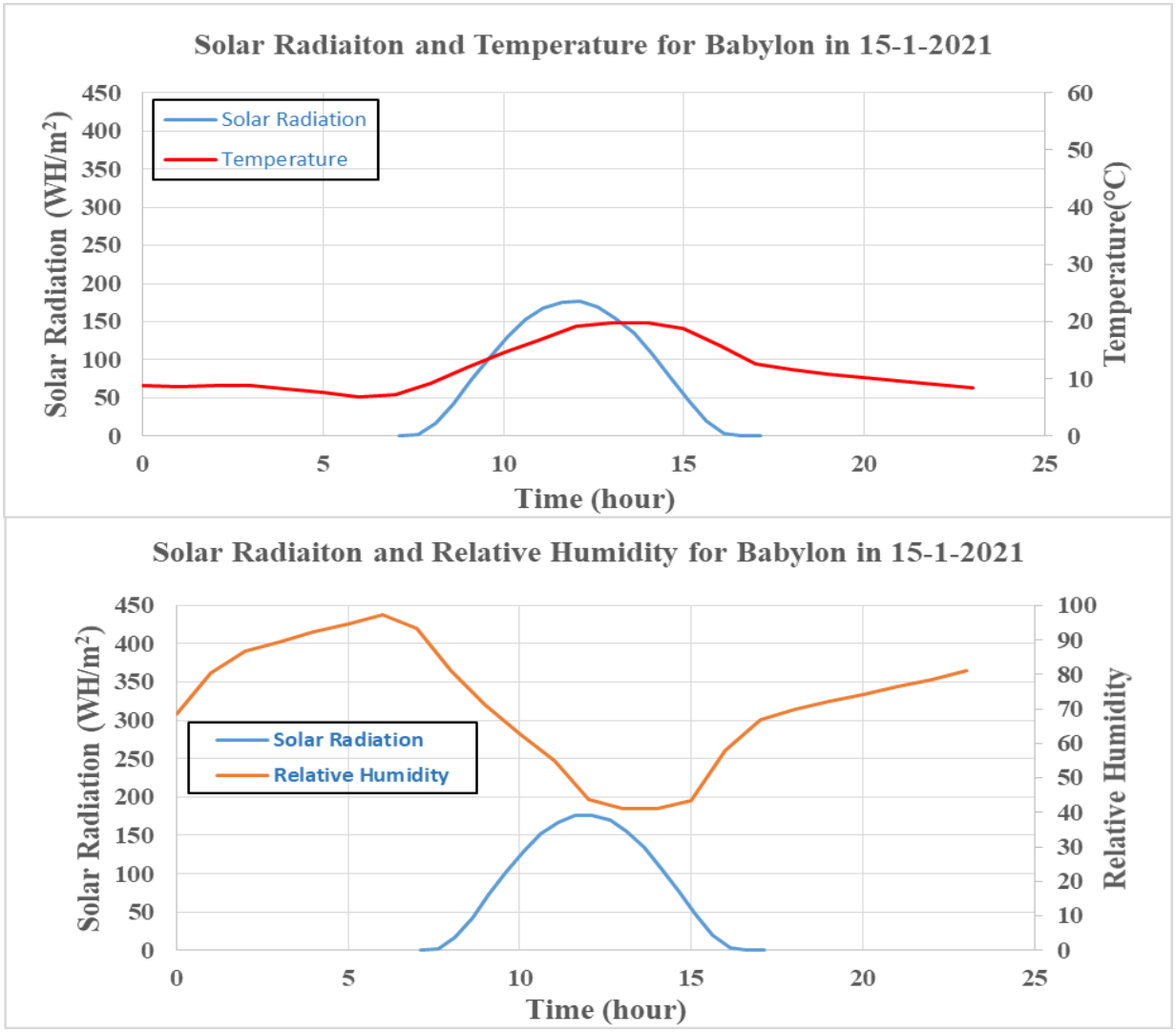

Figure (4-5): The relation between the Solar Radiation with temperature and relative humidity for Babylon during the day (15-1-2021).

Table (4-2): The solar radiation energy with sun duration day length for 15-1-2021 is (10.15 h) for one point in Babylon province.

Solar Radiation W.h.m^{-2}	Sun duration h	Solar Radiation	Sun duration
0.002739	7.116	169.4187	12.616
2.604113	7.616	155.1493	13.116
16.83256	8.116	134.2889	13.616
42.70205	8.616	107.9959	14.116
73.16707	9.116	78.084	14.616
103.4268	9.616	47.38522	15.116
130.4368	10.116	20.37337	15.616
152.2517	10.616	4.026595	16.116
167.625	11.116	0.020614	16.616
175.8	11.616	1.89E-07	17.116
176.4067	12.116		

4.3 The Land Surface Temperature (LST)

To determine the distribution of the LST, there are several steps that need to be calculated, that were presented in the flow chart Figure (3-6). The LST of the study area was calculated in five months (January, march, July, August and October) of the year 2021 to cover the different seasons of the year for Babylon province.

4.3.1 The Results of the LST in January

Figure (4-6) shows the maps of the TOA, NDVI, PV, Emissivity and BT in panels (A), (B), (C), (D), and (E) respectively and calculate from equation (3-1),(3-3),(3-5),(3-6),(3-2) respectively in January 15/1/2021.

Figure (4-7) shows the spatial distribution of the LST for Babylon Province, where the highest temperature was 15.9Cº and the lowest was -2.3 Cº.

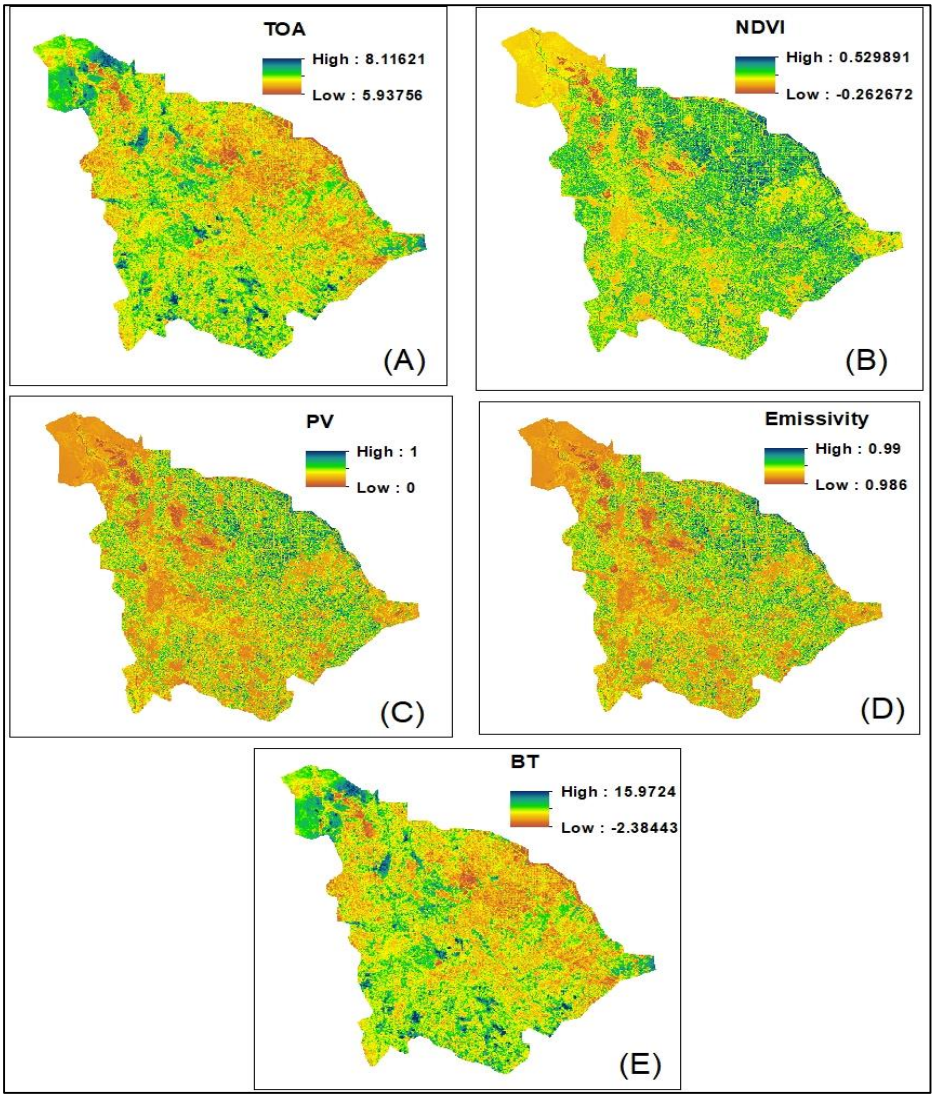

Figure (4-6): The maps of the TOA, NDVI, PV, Emissivity and BT are shown in panels (A), (B), (C), (D), and (E) respectively of Babylon province 2021-1-15.

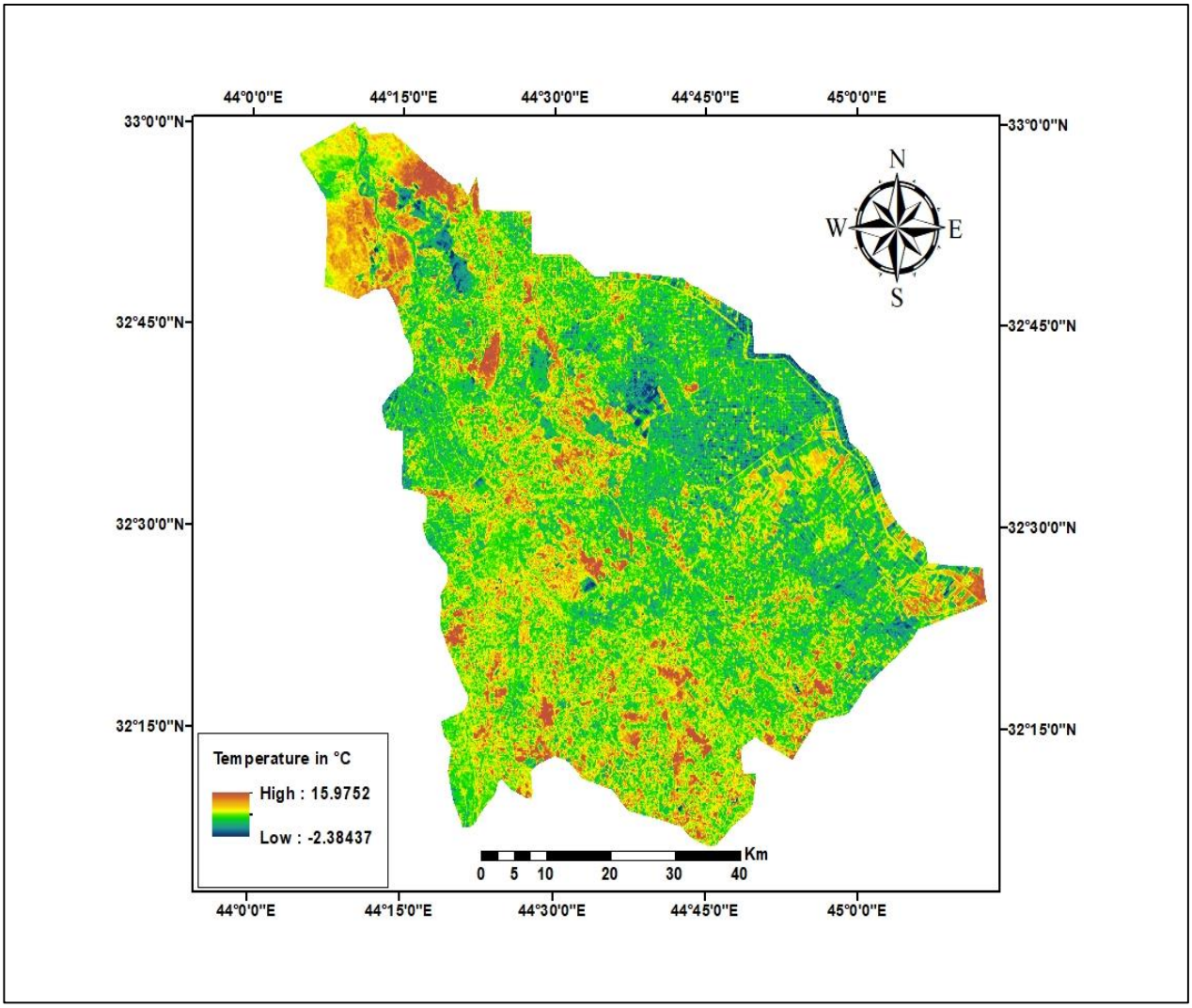

Figure (4-7): The special distribution of the Land Surface Temperature values of Babylon province the highest temperature reach to 15.9 Cº and lowest values reach to -2.3 Cº in 15-1-2021.

4.4 The Solar Radiation in March

Table (4-3) shows all the information about the state of the climate, and using the DEM, the spatial solar radiation was determined after dividing the observation day into three periods and distributing four hours for each period for the study area, based on USGS information Table (4-4). Figure (4-8) A, which represents the spatial distribution of solar radiation for the first period, and Figure (4-8) B shows the distribution of solar radiation in the form of a histogram. As for Figures (4-9) and (4-10), maps and graphs are presented for all used periods. Figure (4-11) show the rate distribution of solar radiation during the observation day. The upper part of Figure (4-12) show the rate value of solar radiation and the temperature calculated during the observation day, while the lower part of the same Figure show the rate value of solar radiation and relative humidity.

Table (4-3): The climate state was taken from ECMWF for the time of observation.

The observing day	The Day time length hour	Temperature C^o	Relative humidity	Precipitation mm/day
15/3/2021	12	17.65	40.38 %	0

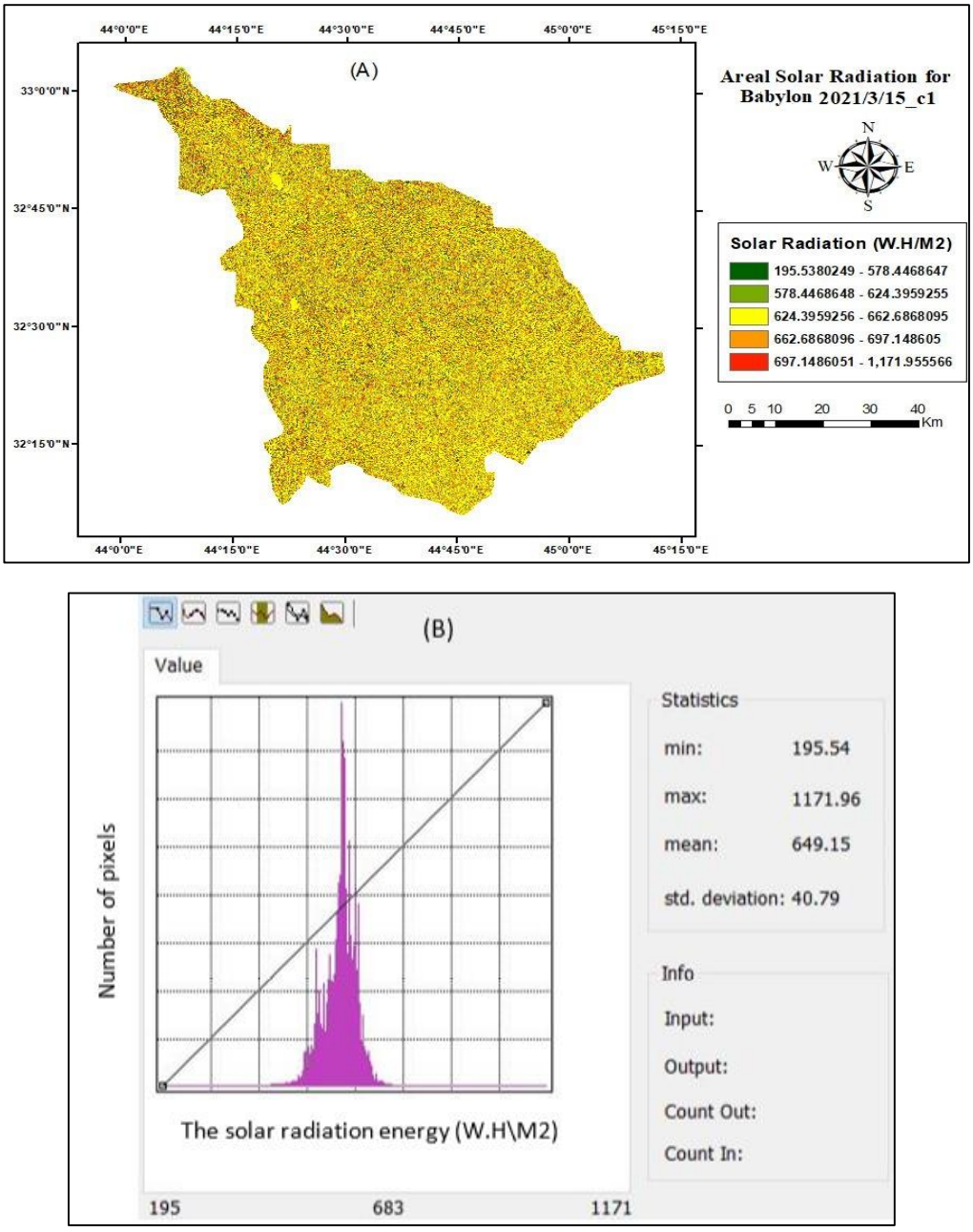

Figure (4-8): (A): The distribution of the solar radiation energy for Babylon province in the first period in (15-3-2021). (B): The histogram for the numbers of the pixels and the values of the solar radiation energy that belong to it.

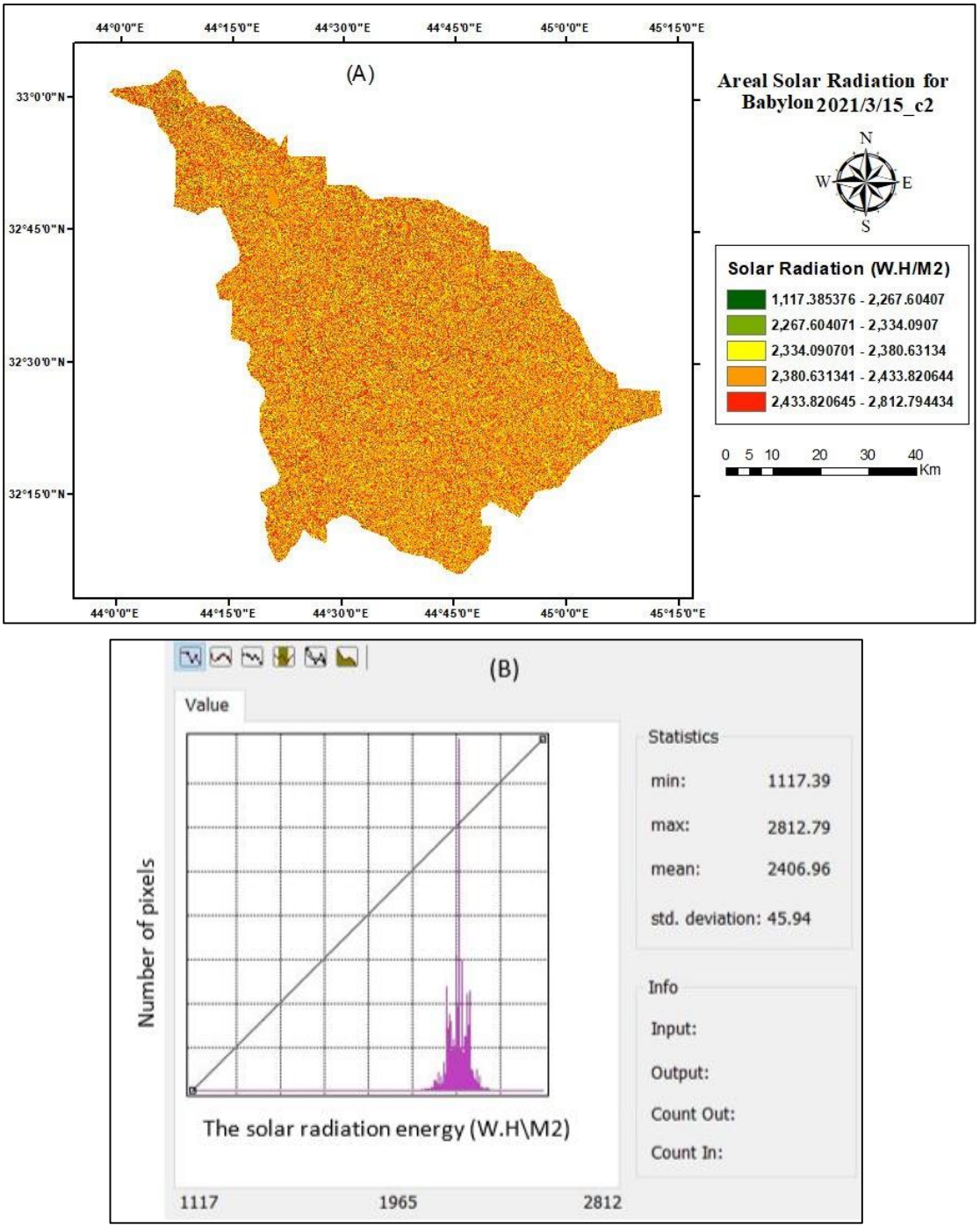

Figure (4-9): (A): The distribution of the solar radiation energy for Babylon province in the second period in (15-3-2021). (B): The histogram for the numbers of the pixels and the values of the solar radiation energy that belong to it.

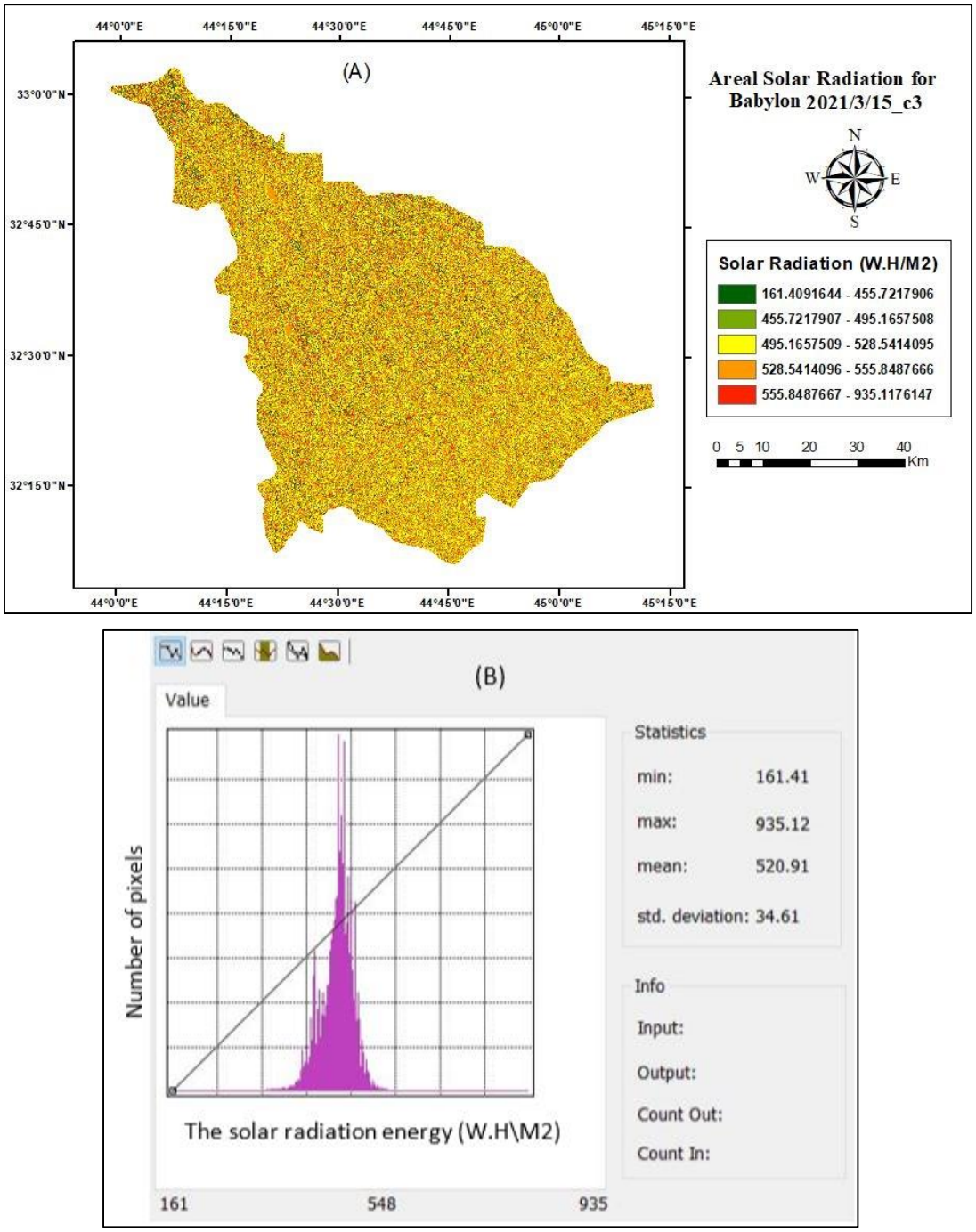

Figure (4-10): (A): The distribution of the solar radiation energy for Babylon province in the third period in (15-3-2021). (B): The histogram for the numbers of the pixels and the values of the solar radiation energy that belong to it.

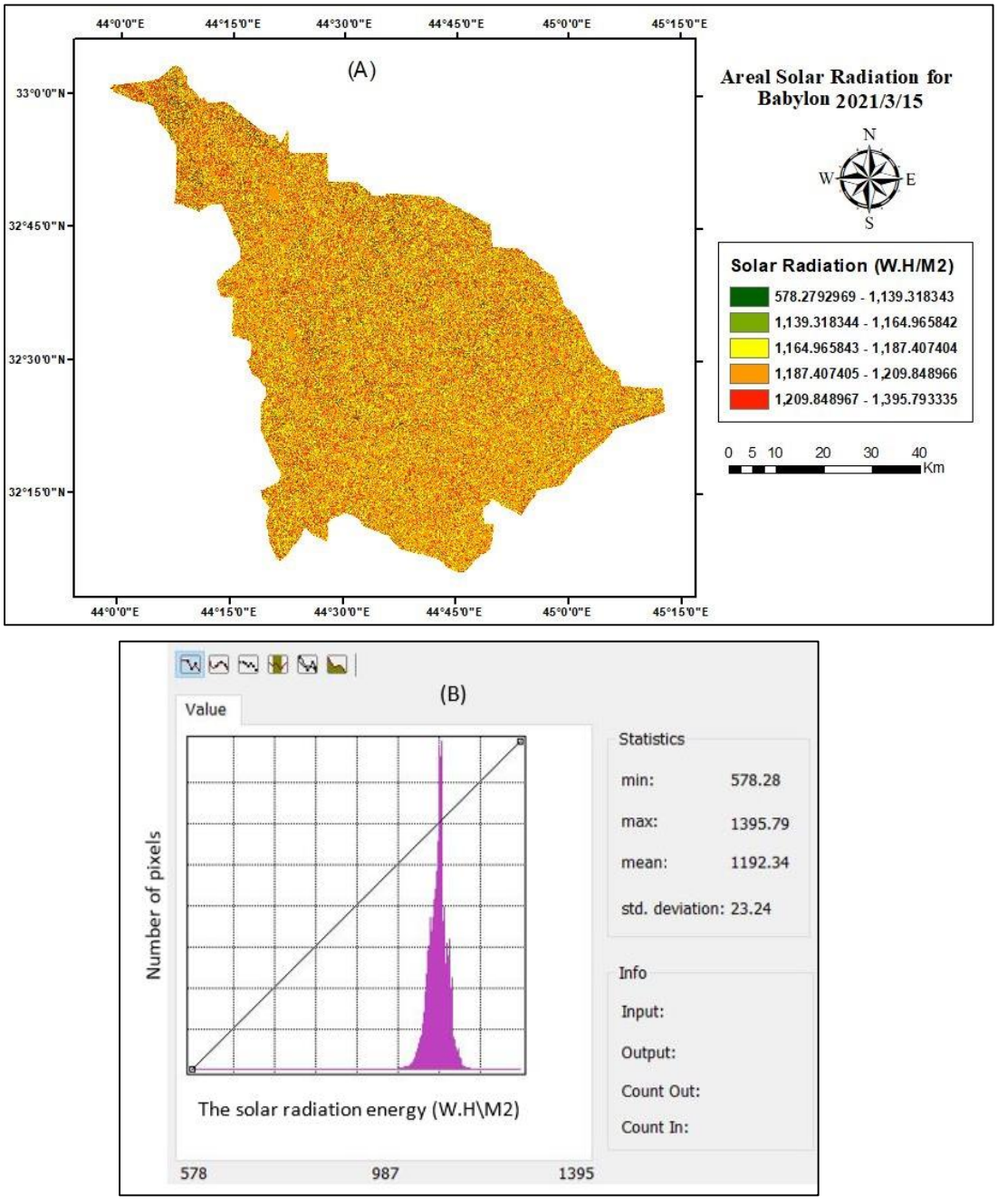

Figure (4-11): (A): The average distribution of the solar radiation energy for Babylon province during (15-3-2021). (B): The histogram for the numbers of the pixels and the values of the solar radiation energy that belong to it.

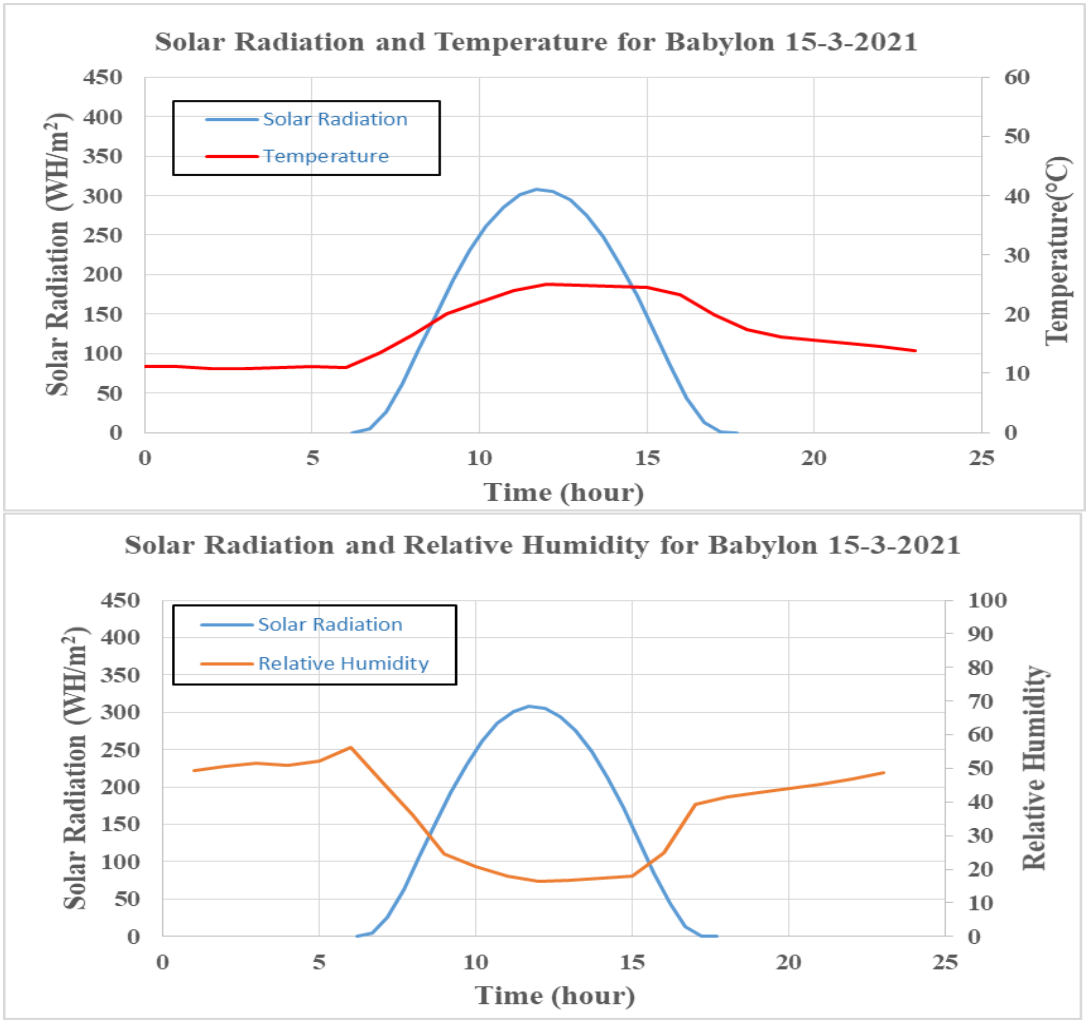

Figure (4-12): The relation between the Solar Radiation with temperature and relative humidity for Babylon during the day (15-3-2021).

Table (4-4): The solar radiation energy with sun duration day length for 15-3-2021 is (12 H) for one point in Babylon province.

Solar Radiation W.h.m^{-2}	Sun duration h	Solar Radiation	Sun duration
0.00612591	6.2	305.5398	12.2
4.335755556	6.7	294.5396	12.7
25.7758155	7.2	275.0159	13.2
62.61681412	7.7	247.5818	13.7
106.124442	8.2	213.1762	14.2
150.7513109	8.7	173.1462	14.7
192.99104	9.2	129.4103	15.2
230.5156472	9.7	84.78373	15.7
261.7094541	10.2	43.61988	16.2
285.435766	10.7	12.81229	16.7
300.9194212	11.2	0.665097	17.2
307.687345	11.7	1.54E-05	17.7

4.5 The Land Surface Temperature (LST)

The LST was calculated for the study area of Babylon Province for five months of the year 2021 in order to cover the different seasons of the year, which were presented through the flow chart (3-6).

4.5.1 The Results of the LST in March

Figure (4-13) shows the maps of the TOA, NDVI, PV, Emissivity and BT in panels (A), (B), (C), (D) and (E) respectively and calculate from equation (3-1),(3-3),(3-5),(3-6),(3-2) respectively in march 15/3/2021.

As for Figure (4-14), it shows the highest and lowest temperature recorded on 15-3-2021, where the maximum temperature was 31.5Cº and the minimum was 13.7Cº.

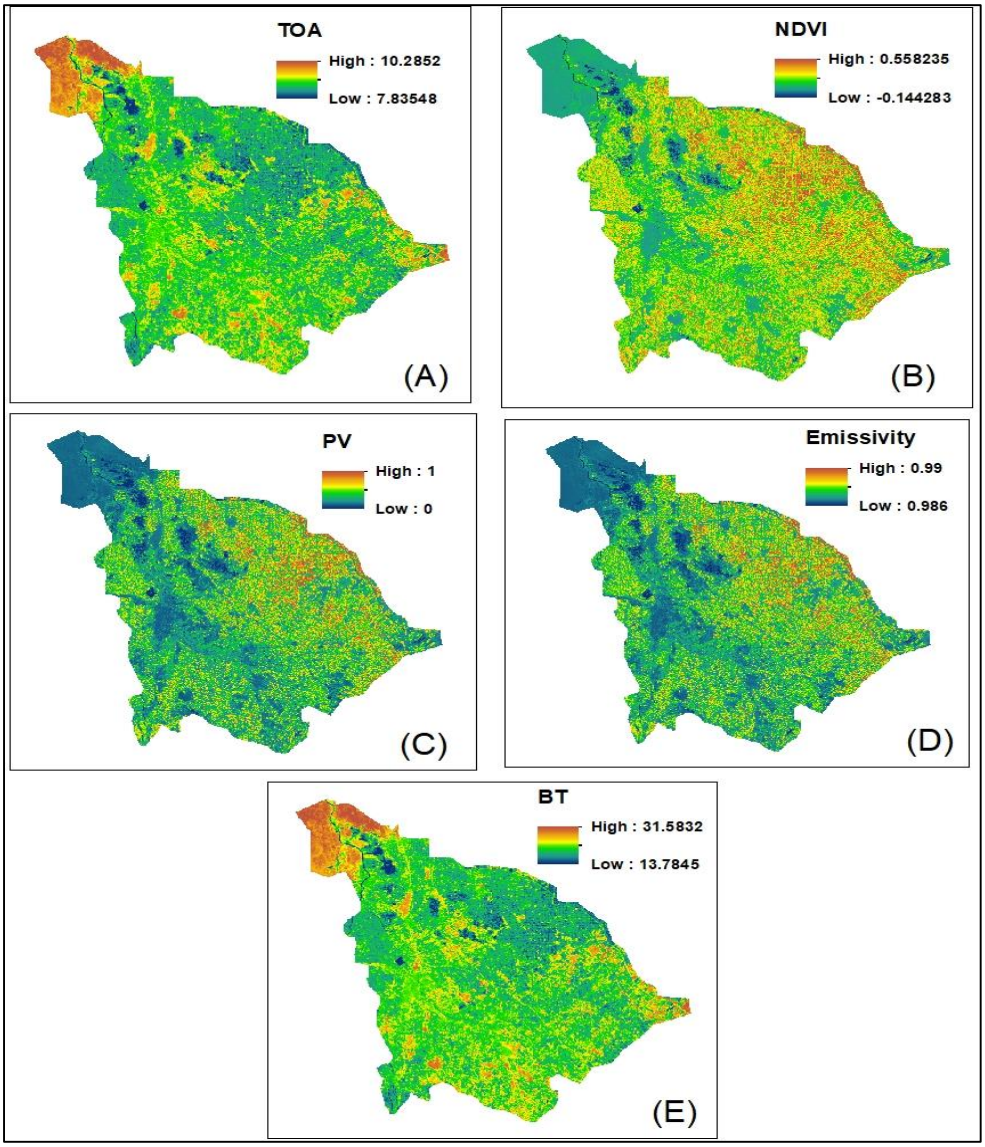

Figure (4-13): The maps of the TOA, NDVI, PV, Emissivity and BT are shown in panels (A), (B), (C), (D) and (E) respectively of Babylon province 2021-3-15.

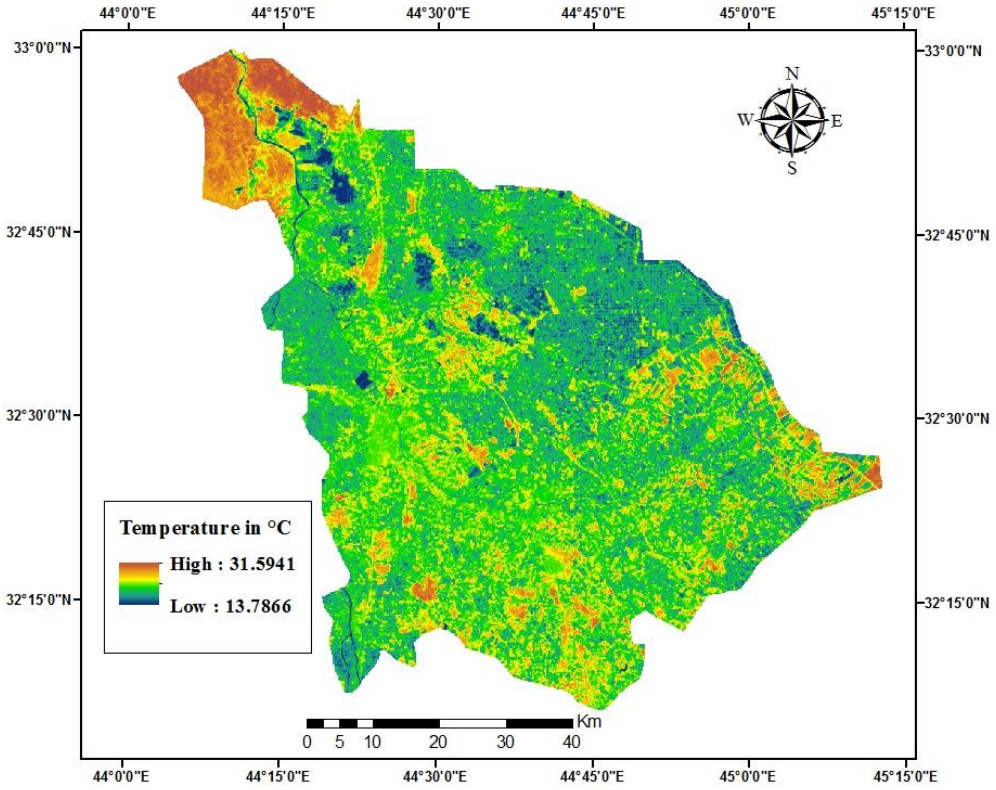

Figure (4-14): The special distribution of the Land Surface Temperature values of Babylon province the highest temperature reach to 31.5Cº and lowest values reach to 13.7 Cº in 15-3-2021.

4-6 The Solar Radiation in July

Table (4-5) contains all the important information about the state of the climate on the observation day for the month of July. The day was divided into four periods, given that the sunrise hours on this day are 14 hours. Each of these periods was divided into four hours, except for the last two hours, using the elevation model. The numerical solar radiation was determined by the USGS for the study area Table (4-6). Figure (4-15) A, which shows the spatial distribution of solar radiation for the first period, and Figure (4-15) B shows the distribution of solar radiation in the form of a histogram. The graph shows the number of pixels that It has a solar radiation value. Figures (4-16), (4-17) and (4-18) show maps and graphs for successive periods. Figure (4-19) show the rate distribution of solar radiation for the observation day. Figure (4-20) The upper part of it represents the rate value of solar radiation and the calculated temperature, while the lower part of the same figure shows the rate value of solar radiation and relative humidity for the study area on the same observation day 7-15-2021.

Table (4-5): The climate state was taken from ECMWF for the time of observation.

The observing day	The Day time length hour	Temperature C^{o}	Relative humidity	Precipitation mm/day
15/7/2021	14	39.75	15.38 %	0

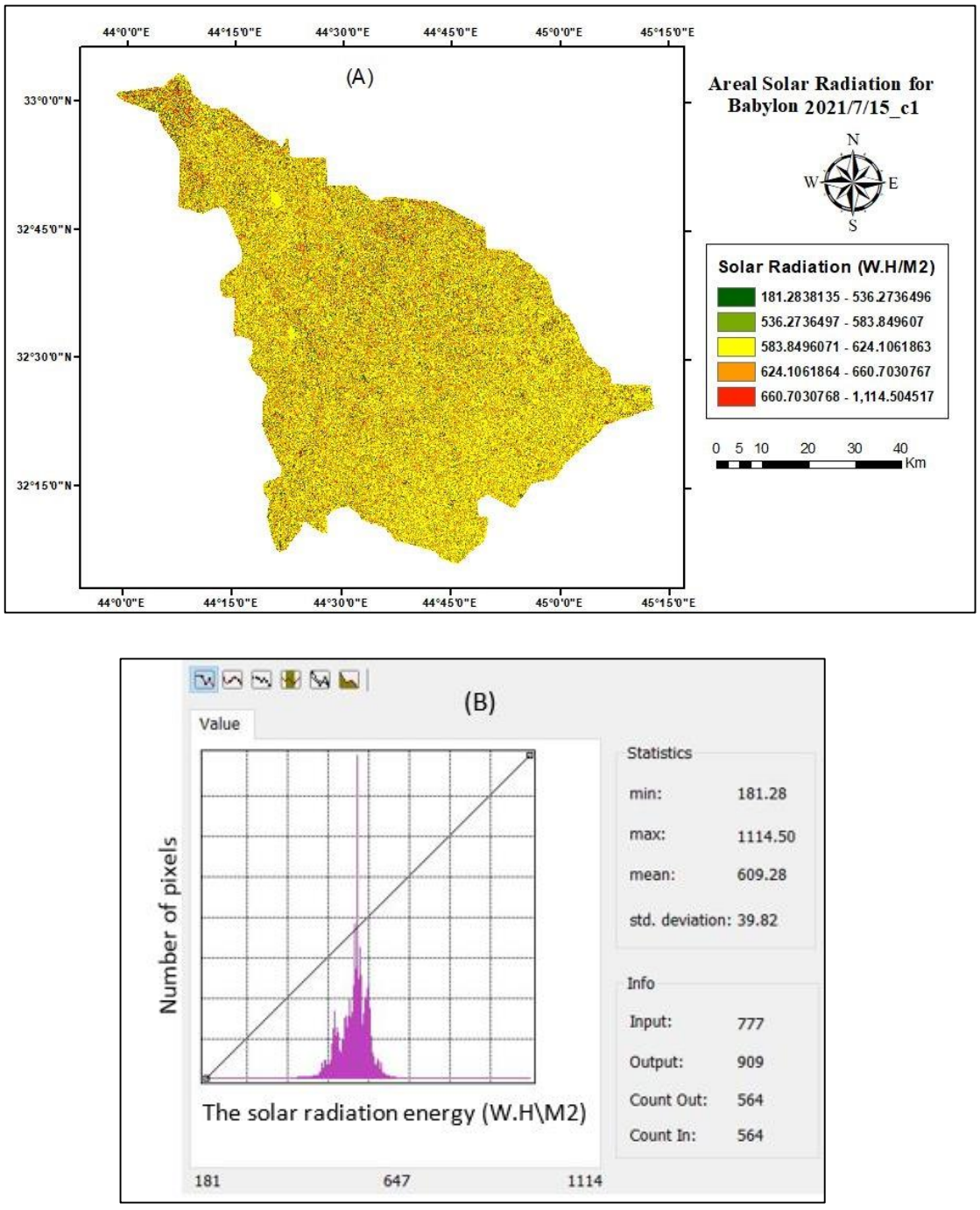

Figure (4-15): (A): The distribution of the solar radiation energy for Babylon province in the first period in (15-7-2021). (B): The histogram for the numbers of the pixels and the values of the solar radiation energy that belong to it.

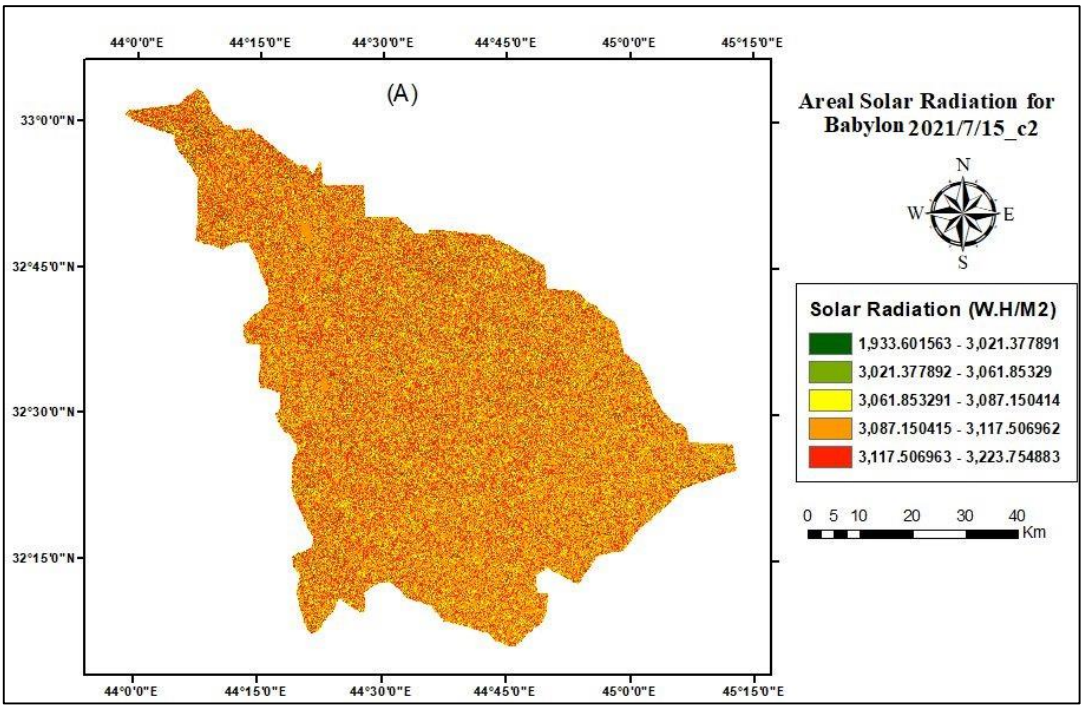

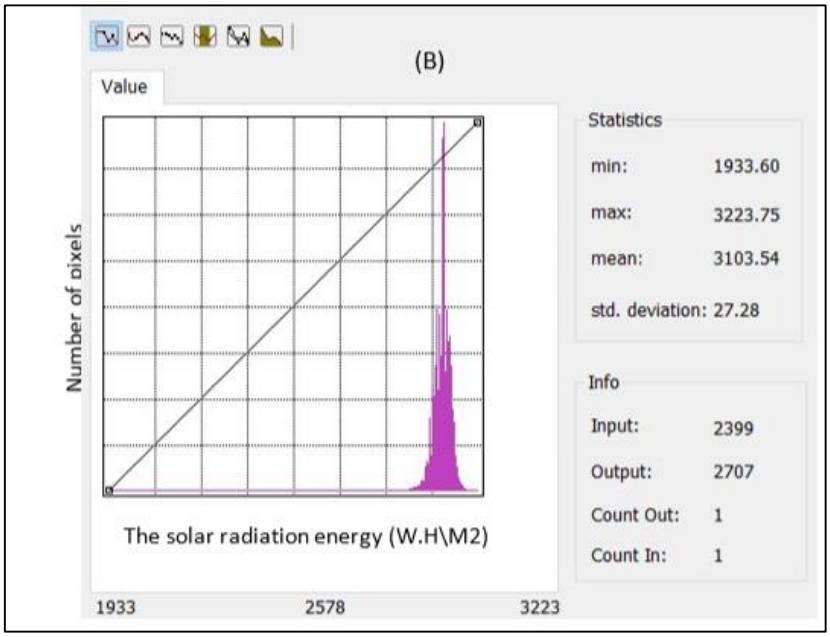

Figure (4-16): (A): The distribution of the solar radiation energy for Babylon province in the second period in (15-7-2021). (B): The histogram for the numbers of the pixels and the values of the solar radiation energy that belong to it.

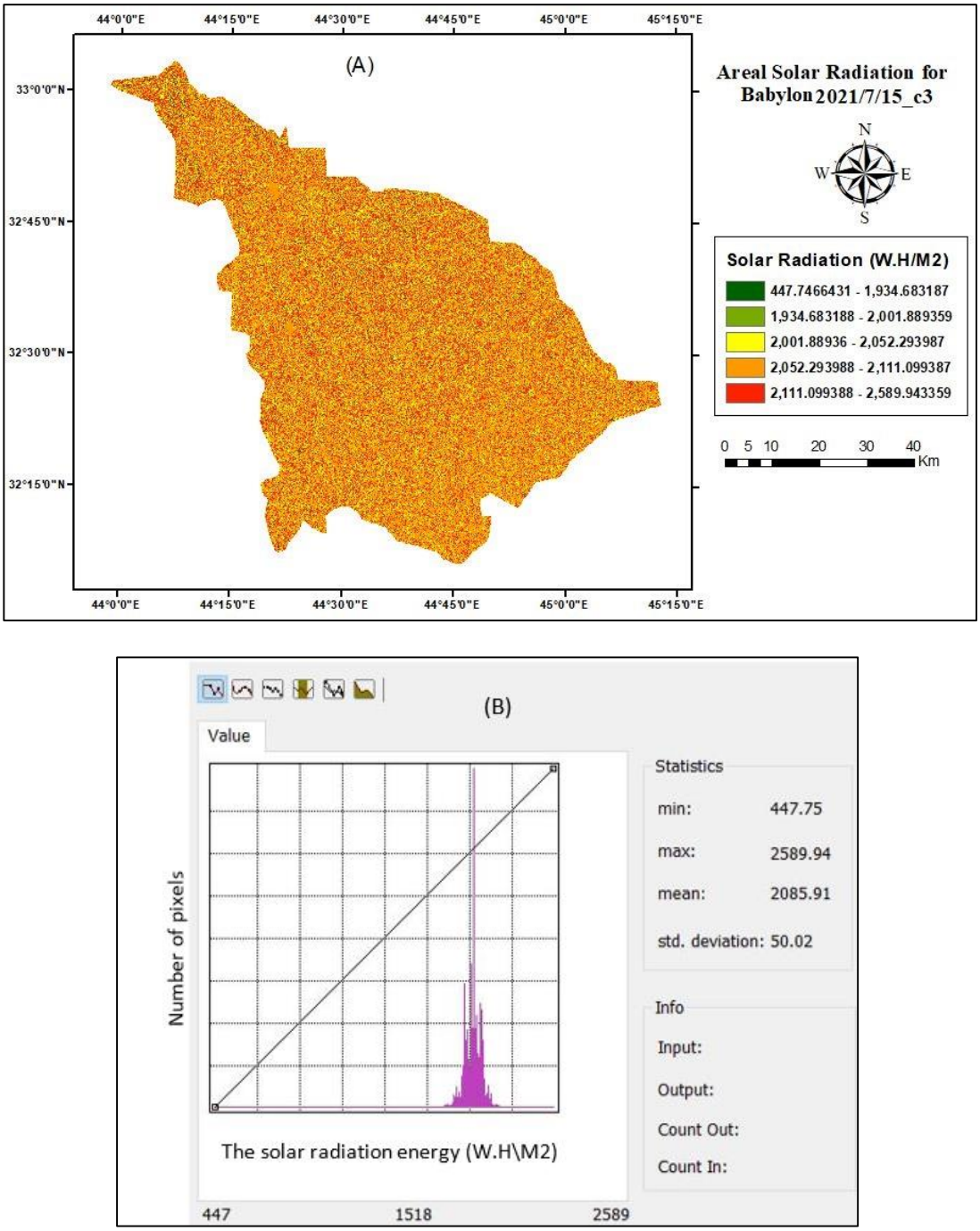

Figure (4-17): (A): The distribution of the solar radiation energy for Babylon province in the third period in (15-7-2021). (B): The histogram for the numbers of the pixels and the values of the solar radiation energy that belong to it.

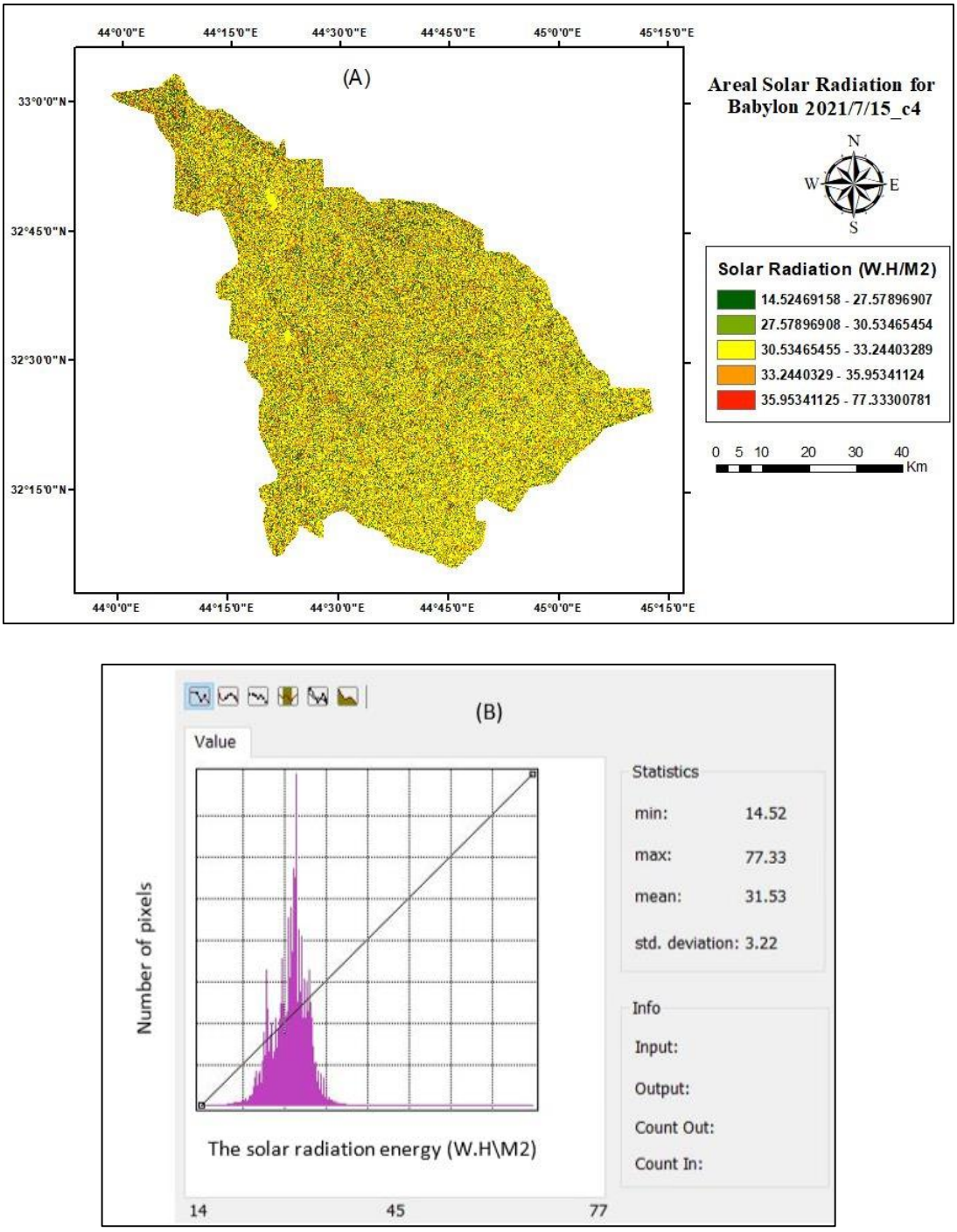

Figure (4-18): (A): The distribution of the solar radiation energy for Babylon province in the fourth period in (15-7-2021). (B): The histogram for the numbers of the pixels and the values of the solar radiation energy that belong to it.

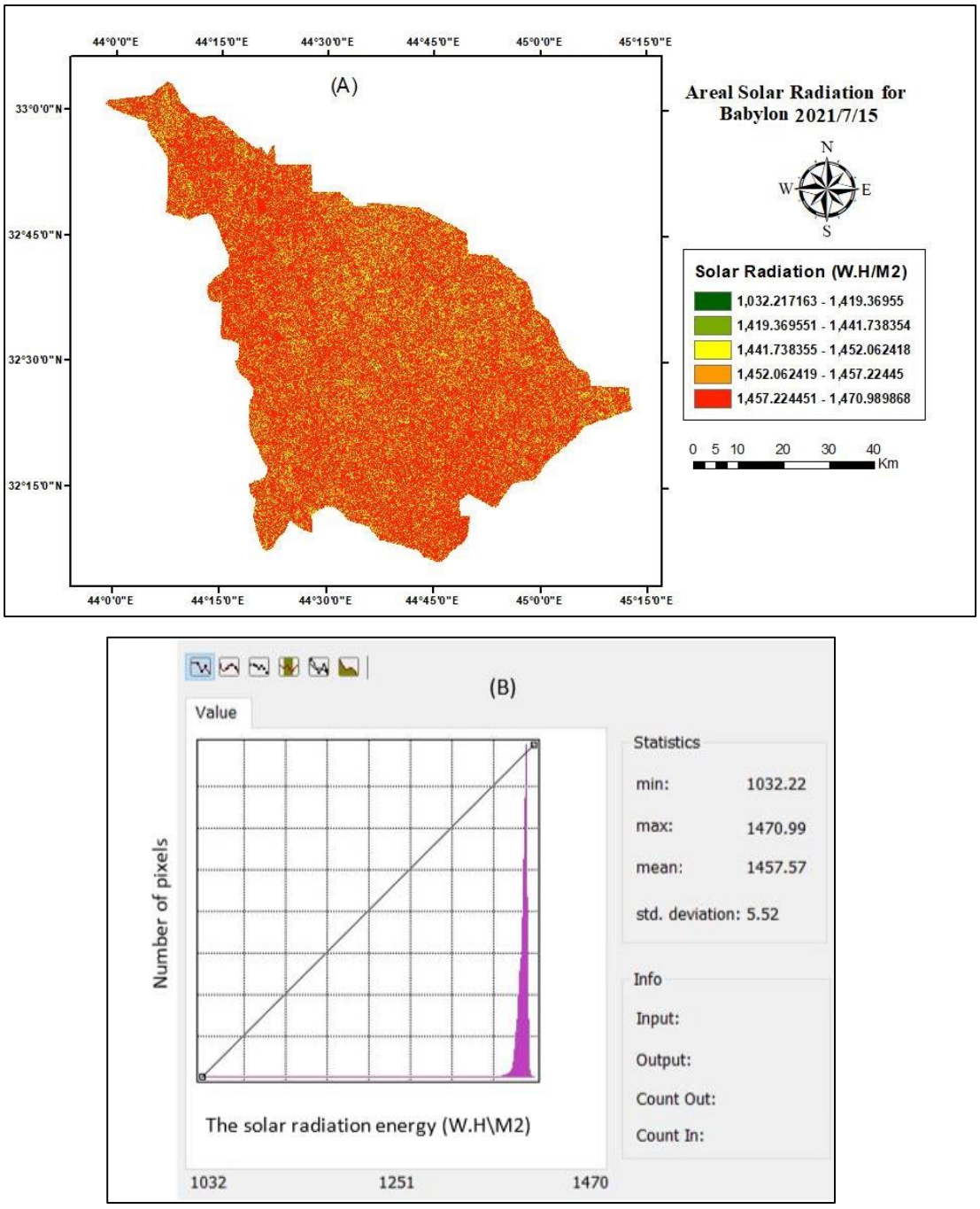

Figure (4-19): (A): The average distribution of the solar radiation energy for Babylon province during (15-7-2021). (B): The histogram for the numbers of the pixels and the values of the solar radiation energy that belong to it.

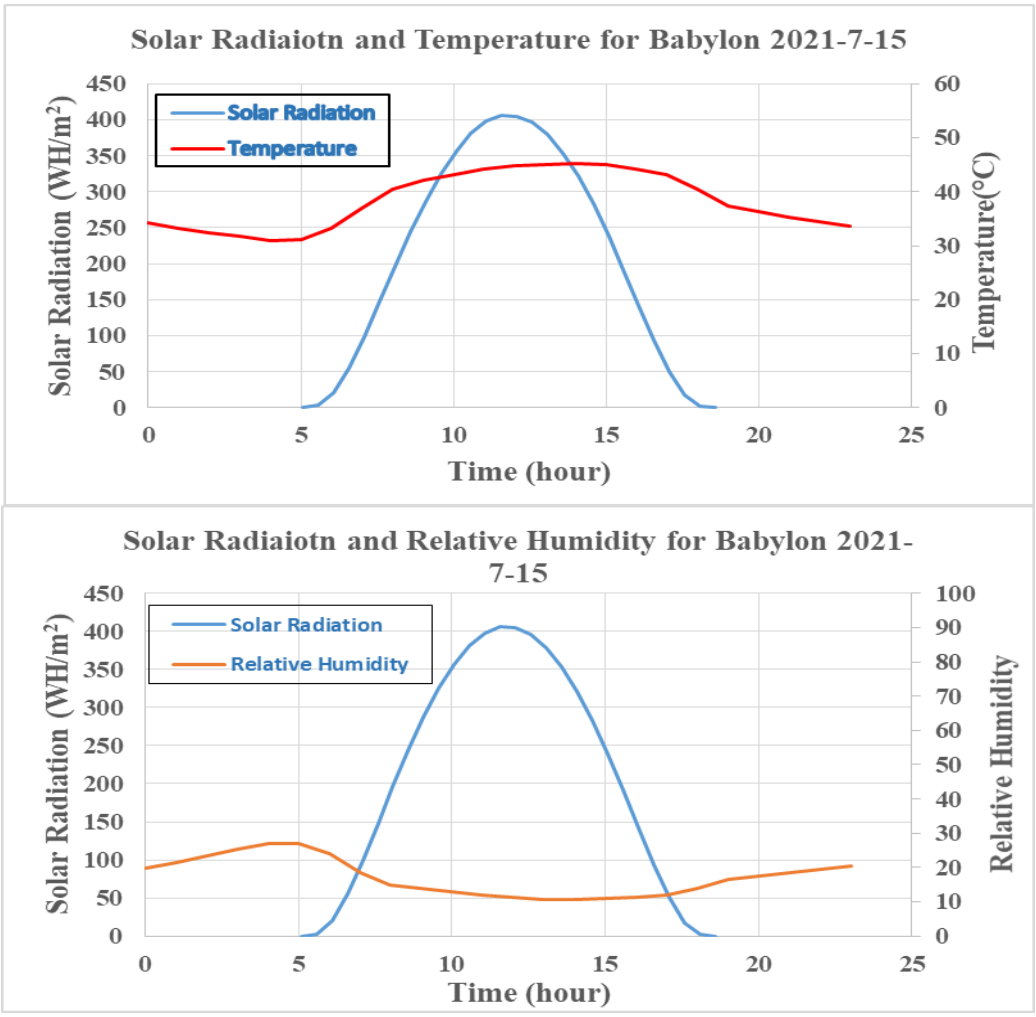

Figure (4-20): The relation between the Solar Radiation with temperature and relative humidity for Babylon during the day (15-7-2021).

Table (4-6): The solar radiation energy with sun duration day length for 15-7-2021 is (14.14 H) for one point in Babylon province.

Solar Radiation W.h.m^{-2}	Sun duration h	Solar Radiation	Sun duration
0.002783	5.083	405.1735	12.083
2.955169	5.583	396.1881	12.583
20.65949	6.083	378.9017	13.083
55.06618	6.583	353.7464	13.583
99.13304	7.083	321.3758	14.083
147.5396	7.583	282.6835	14.583
196.6261	8.083	238.8382	15.083
243.8045	8.583	191.3502	15.583
287.1567	9.083	142.1973	16.083
325.2139	9.583	94.06043	16.583
356.8399	10.083	50.74969	17.083
381.1685	10.583	17.79269	17.583
397.5709	11.083	2.094435	18.083
405.6382	11.583	0.000875	18.583

4.7 The Land Surface Temperature (LST)

There are many steps that must be calculated so that we can calculate the Earth's surface temperature, which is shown in Figure (3-6). The Earth's surface temperature was calculated for five months of the year 2021 for the study area.

4.7.1 The Results of the LST in July

Figure (4-21) shows the maps of the TOA, NDVI, PV, Emissivity and BT in panels (A), (B), (C), (D), and (E) respectively and calculate from equation (3-1),(3-3),(3-5),(3-6),(3-2) respectively.

Figure (4-22) shows the special distribution of the Land Surface Temperature values of Babylon province the highest temperature reach to 58.3C^{o}and lowest values reach to 26.7C^{o} in 15-7-2021.

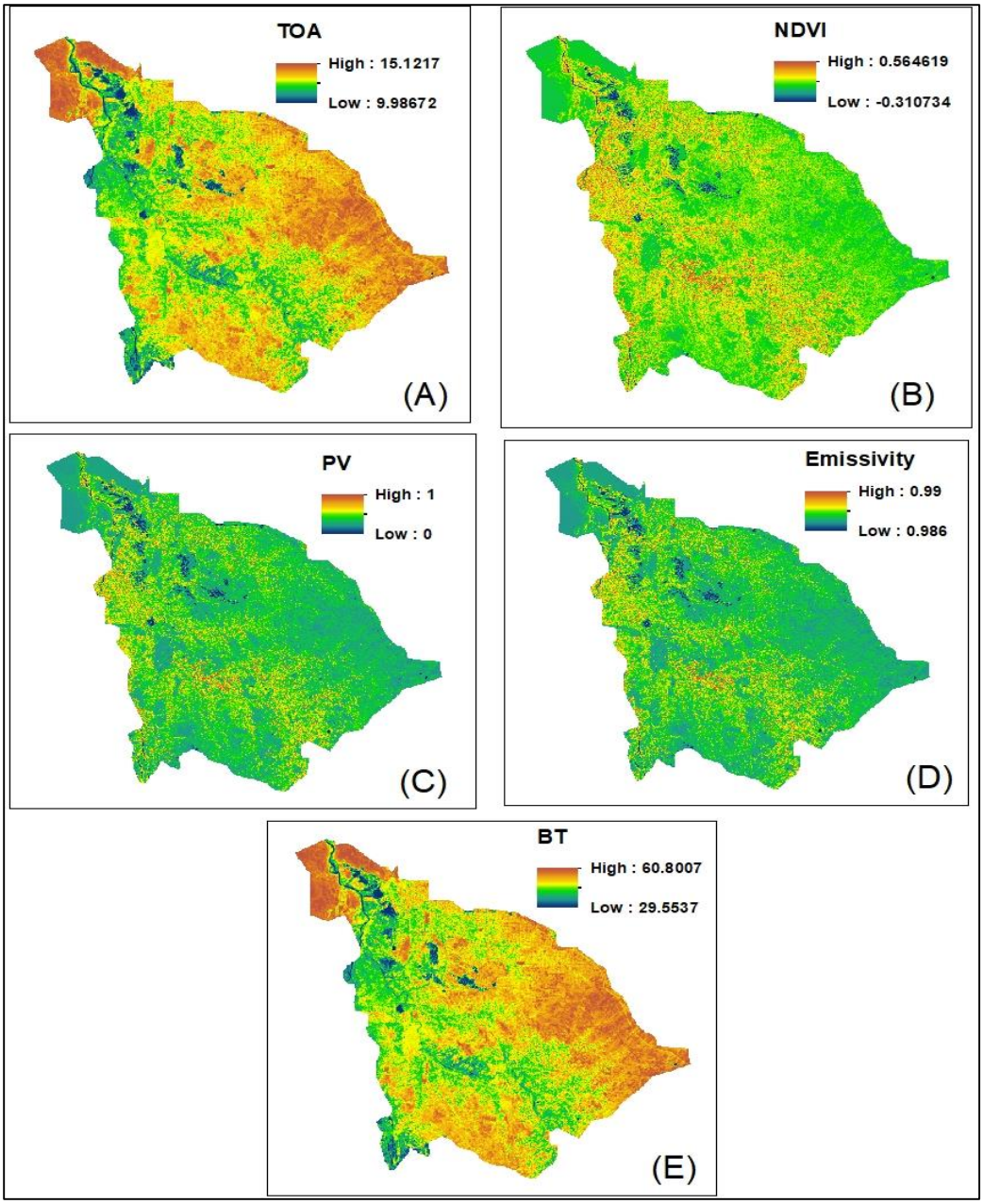

Figure (4-21): The maps of the TOA, NDVI, PV, Emissivity and BT are shown in panels (A), (B), (C), (D) and (E) respectively of Babylon province 2021-7-15.

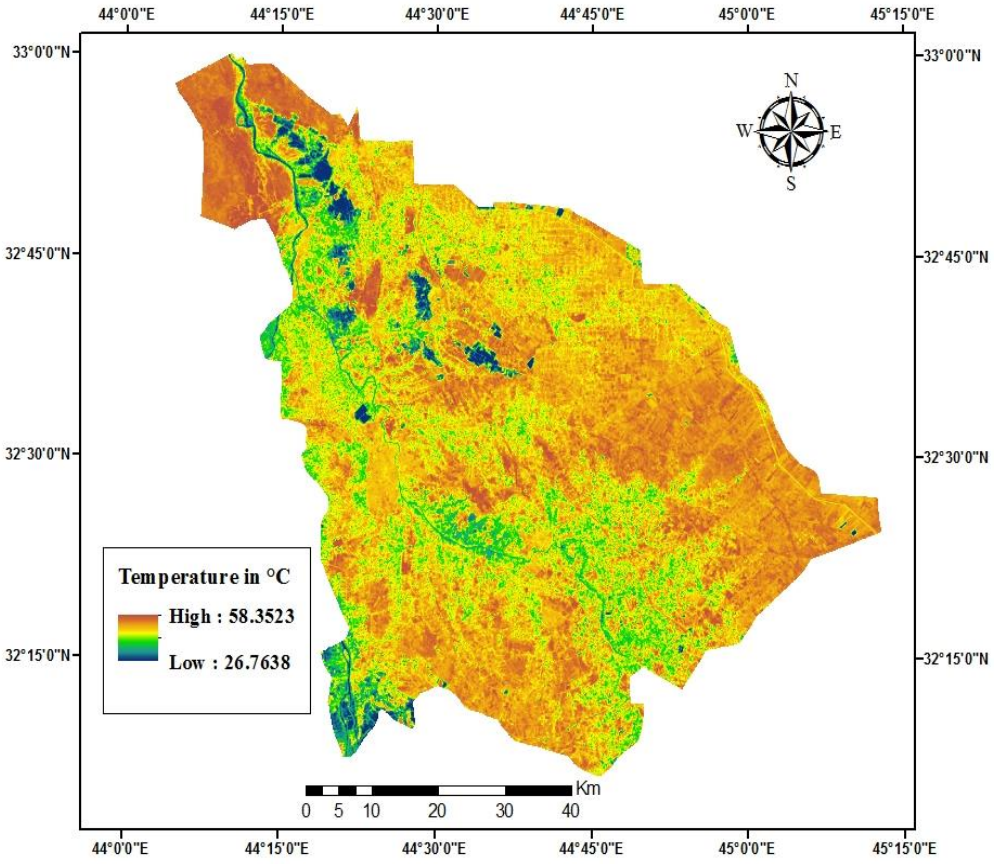

Figure (4-22): The special distribution of the Land Surface Temperature values of Babylon province the highest temperature reach to 58.3Cºand lowest values reach to 26.7Cº in 15-7-2021.

4.8 The Solar Radiation in August

All information about the climate for the day of observation is shown in Table (4-7). Also in this month, the day was divided into four periods, given that the daylight hours in this month are 14 hours, and each of these periods is four hours, except for the last period, which is two hours, as was determined. Areal solar radiation using the USGS digital elevation model for the study area and for the specified time period Table (4-8). Figure (4-23) A, represents the first period, which shows the spatial distribution of solar radiation. Figure (4-23) B, shows the distribution of solar radiation in the form of a histogram for the current statistical process, and the graph shows the number of pixels with specific values for solar radiation. Figures (4-24), (4-25) and (4-26) show maps and charts for different periods. Figure (4-27) show the average distribution of solar radiation through the observation day in all (4-28). The upper part shows the average solar radiation and the temperature calculated during the observation day. As for the lower part of the same figure, it was between the average values of solar radiation and relative humidity.

Table (4-7): The climate state was taken from ECMWF for the time of observation.

The observing day	The Day time length hour	Temperature C^{o}	Relative humidity	Precipitation mm/day
15/8/2021	14	38.65	15.56 %	0

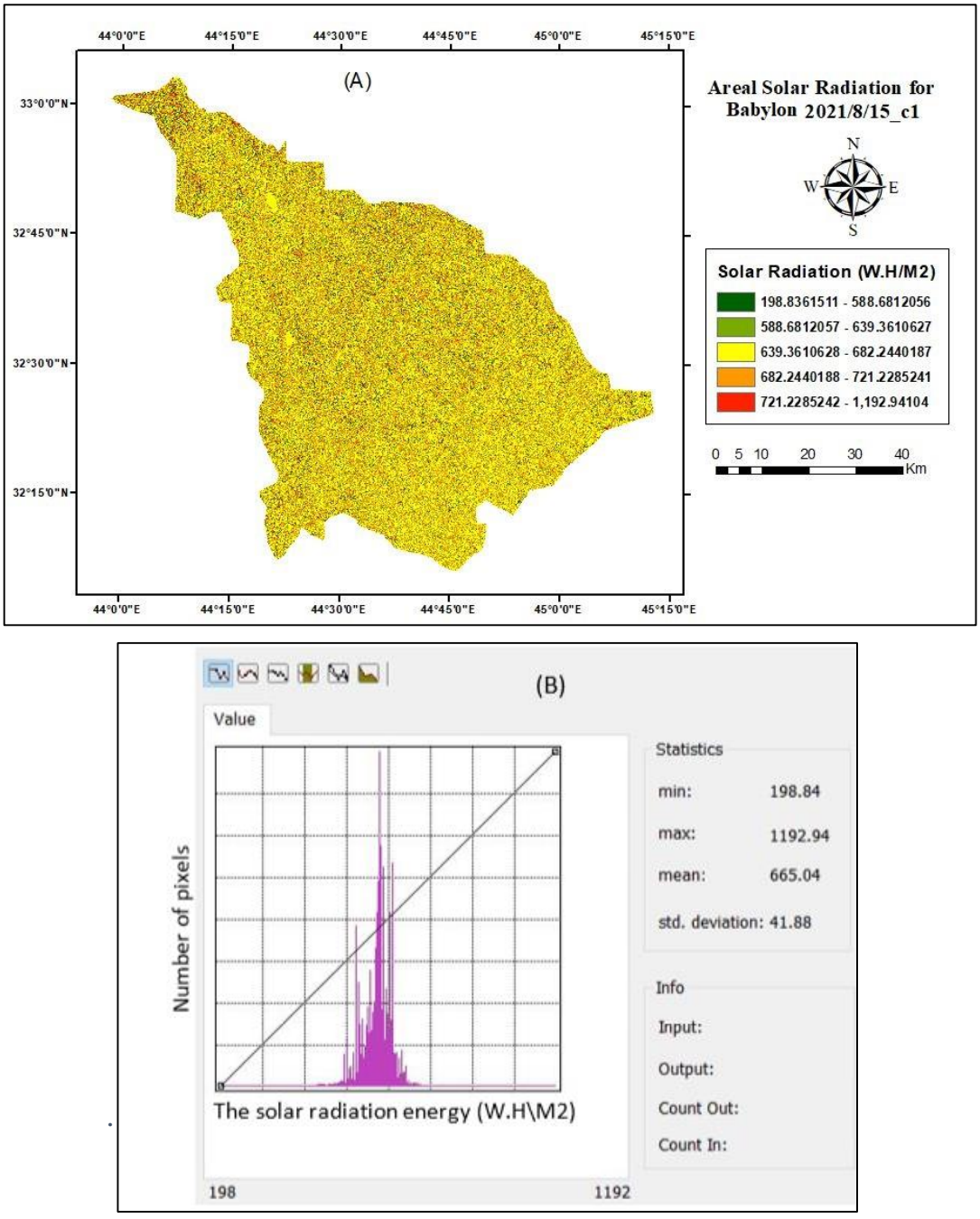

Figure (4-23): (A): The distribution of the solar radiation energy for Babylon province in the first period in (15-8-2021). (B): The histogram for the numbers of the pixels and the values of the solar radiation energy that belong to it.

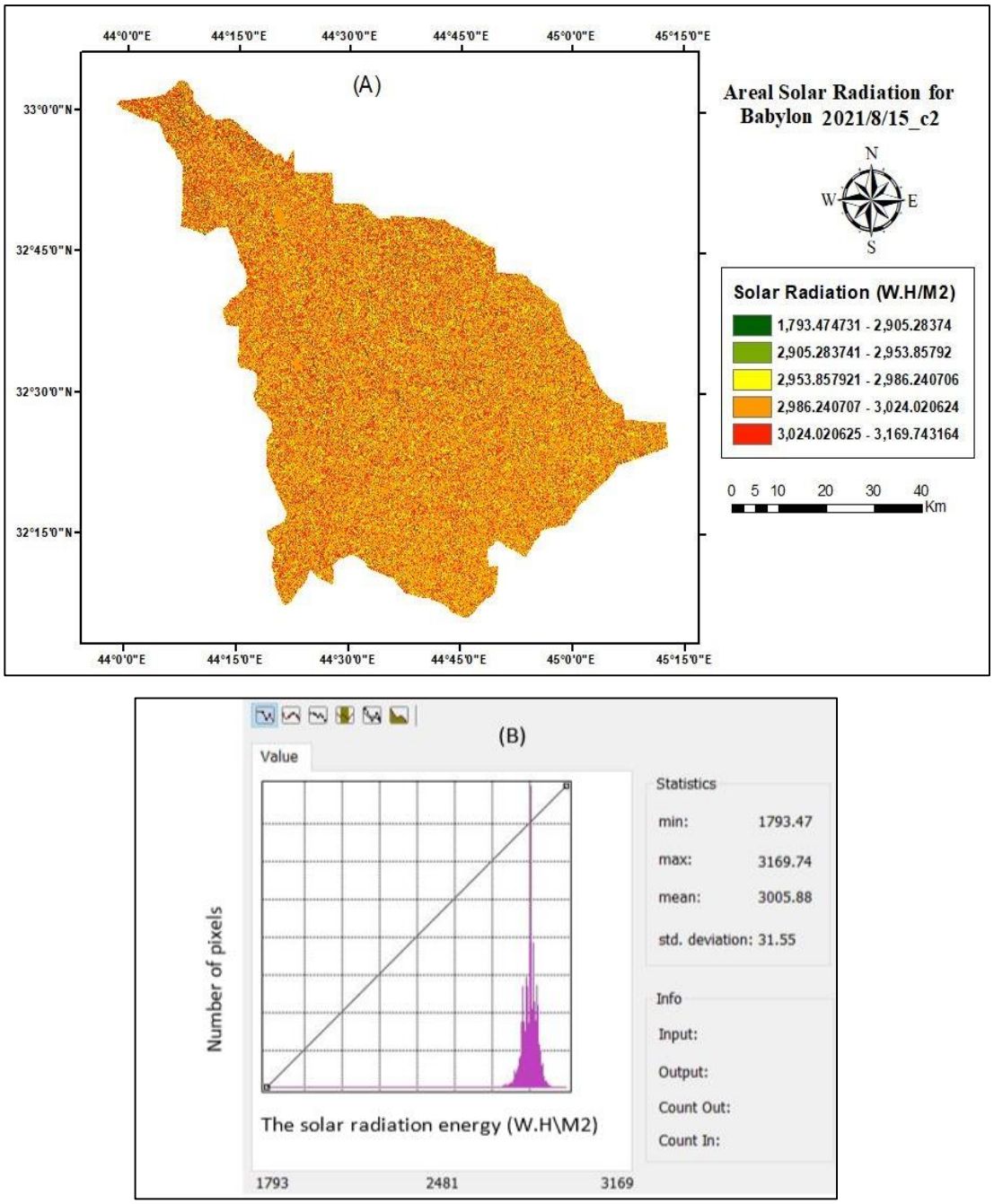

Figure (4-24): (A): The distribution of the solar radiation energy for Babylon province in the second period in (15-8-2021). (B): The histogram for the numbers of the pixels and the values of the solar radiation energy that belong to it.

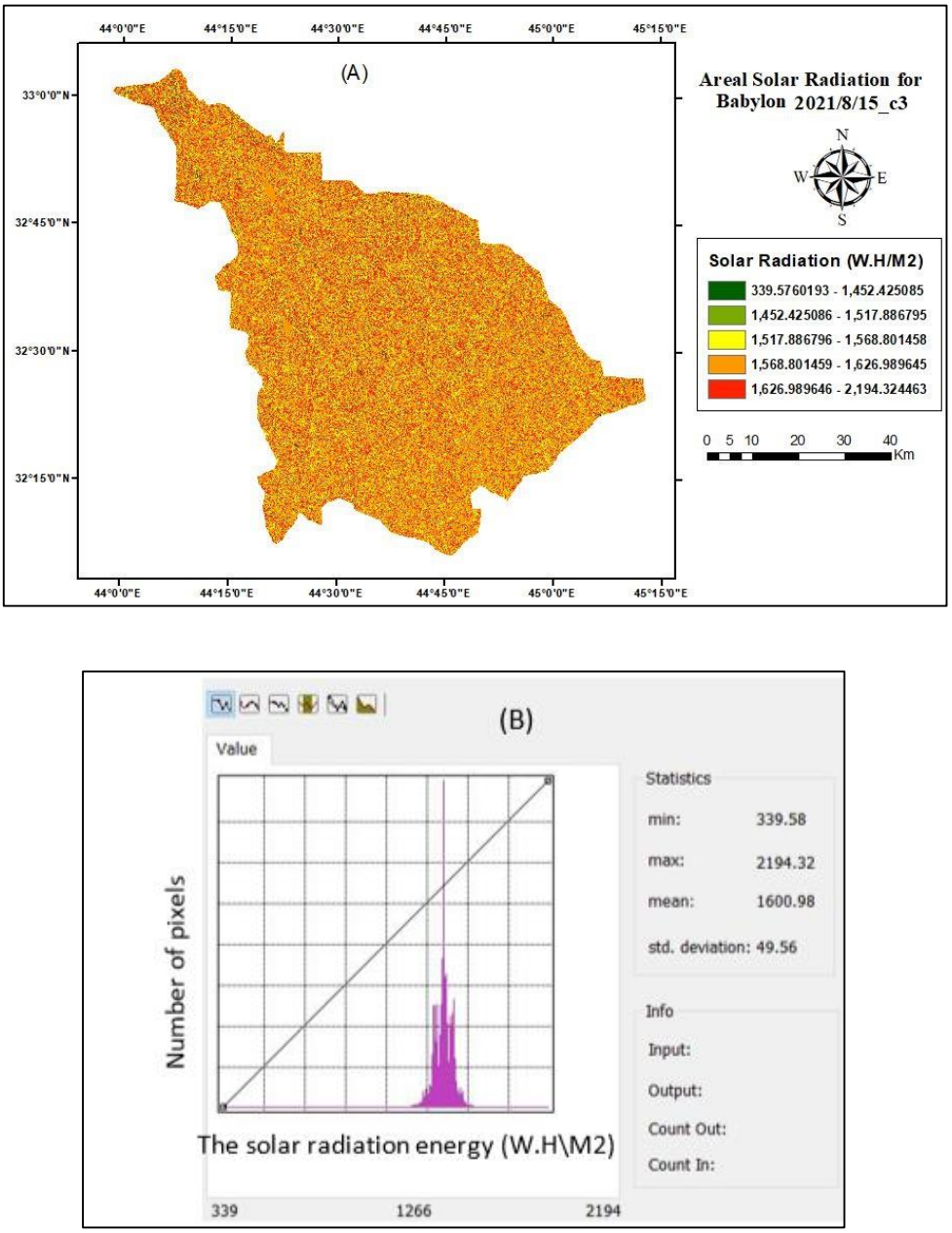

Figure (4-25): (A): The distribution of the solar radiation energy for Babylon province in the third period in (15-8-2021). (B): The histogram for the numbers of the pixels and the values of the solar radiation energy that belong to it.

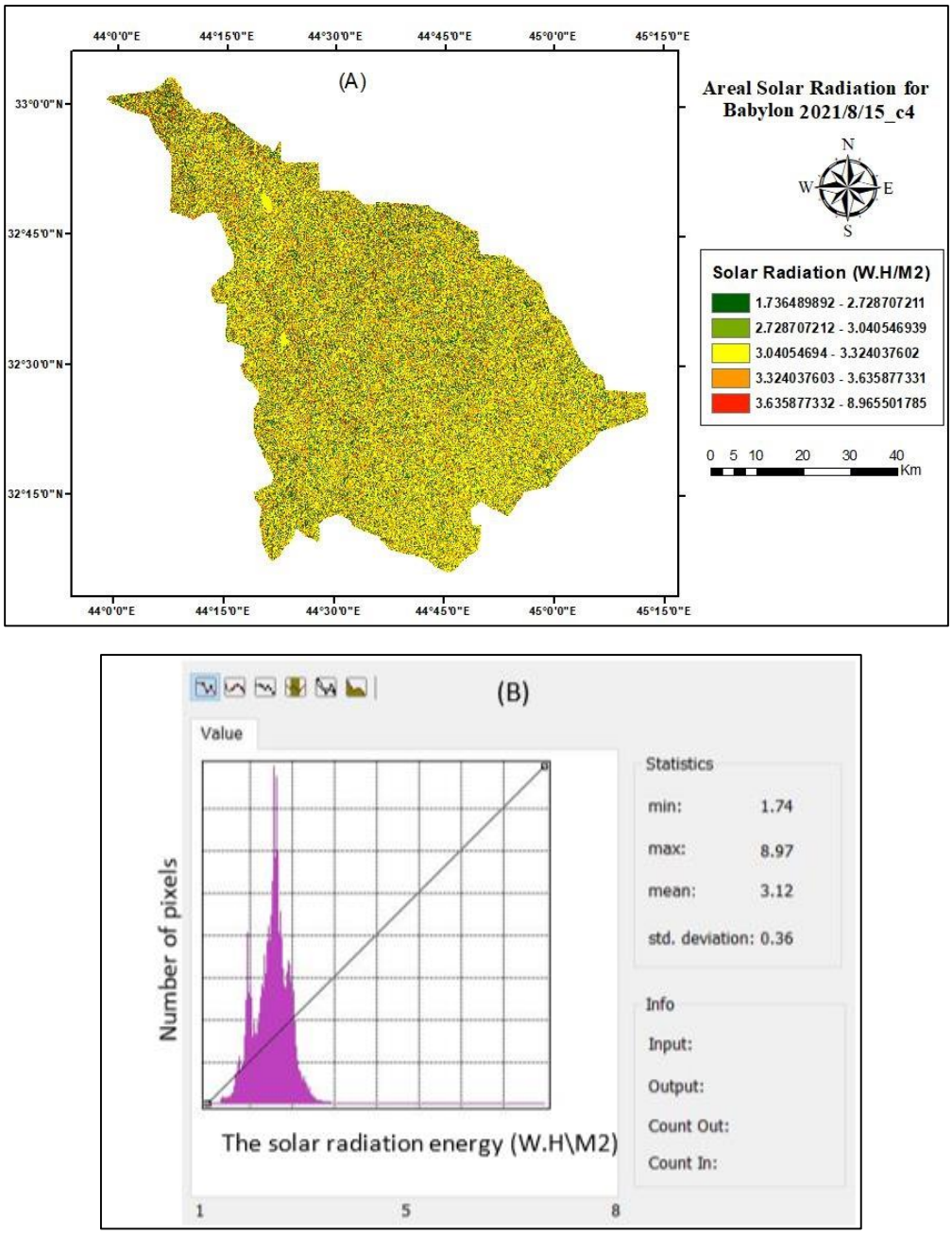

Figure (4-26): (A): The distribution of the solar radiation energy for Babylon province in the Fourth period in (15-8-2021). (B): The histogram for the numbers of the pixels and the values of the solar radiation energy that belong to it.

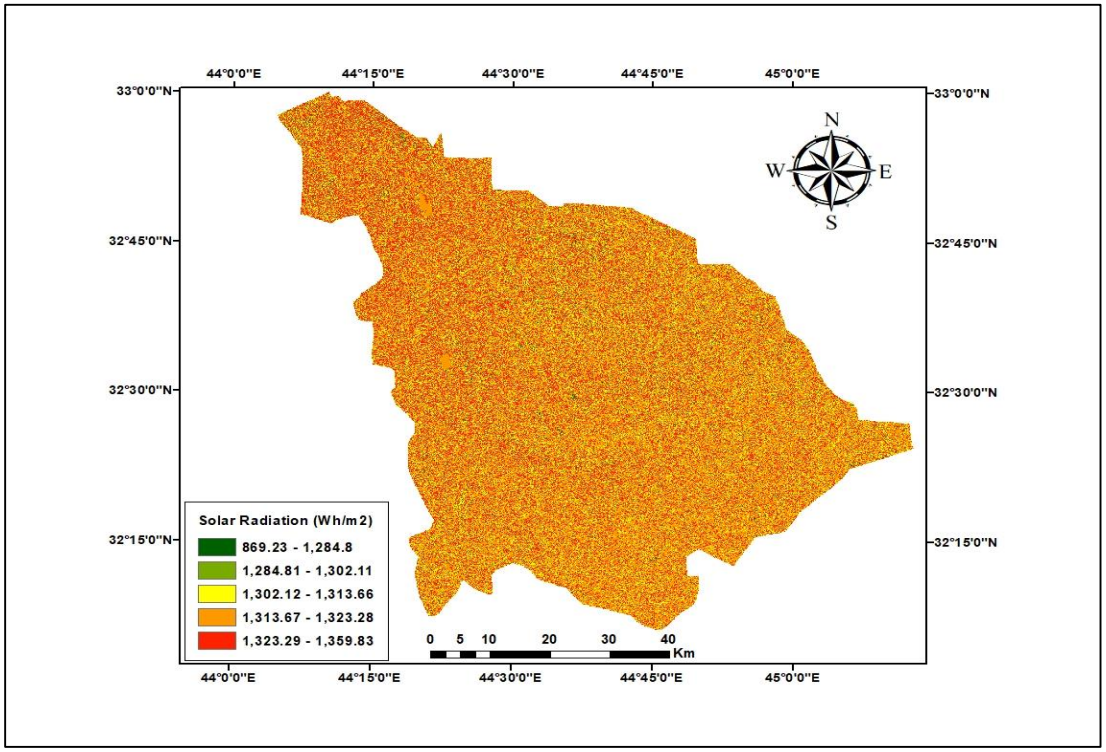

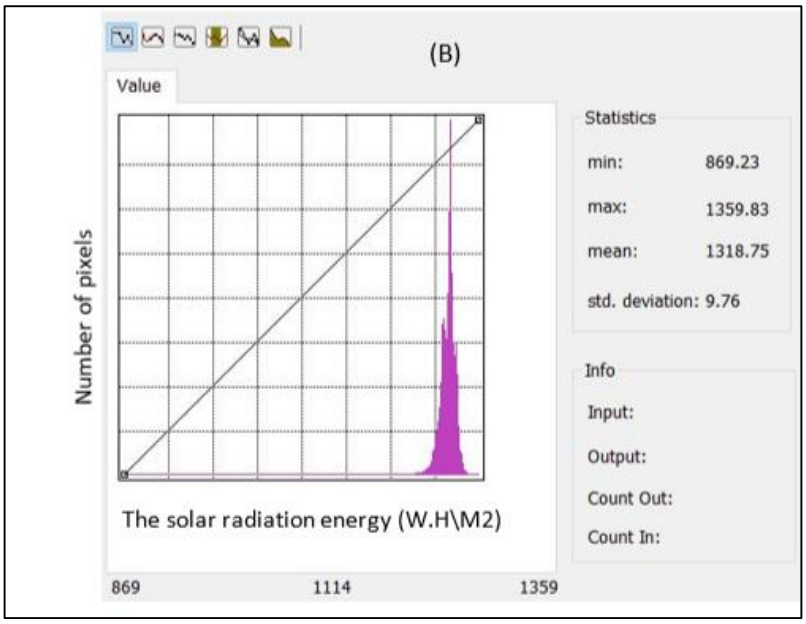

Figure (4-27): (A): The average distribution of the solar radiation energy for Babylon province during (15-8-2021). (B): The histogram for the numbers of the pixels and the values of the solar radiation energy that belong to it.

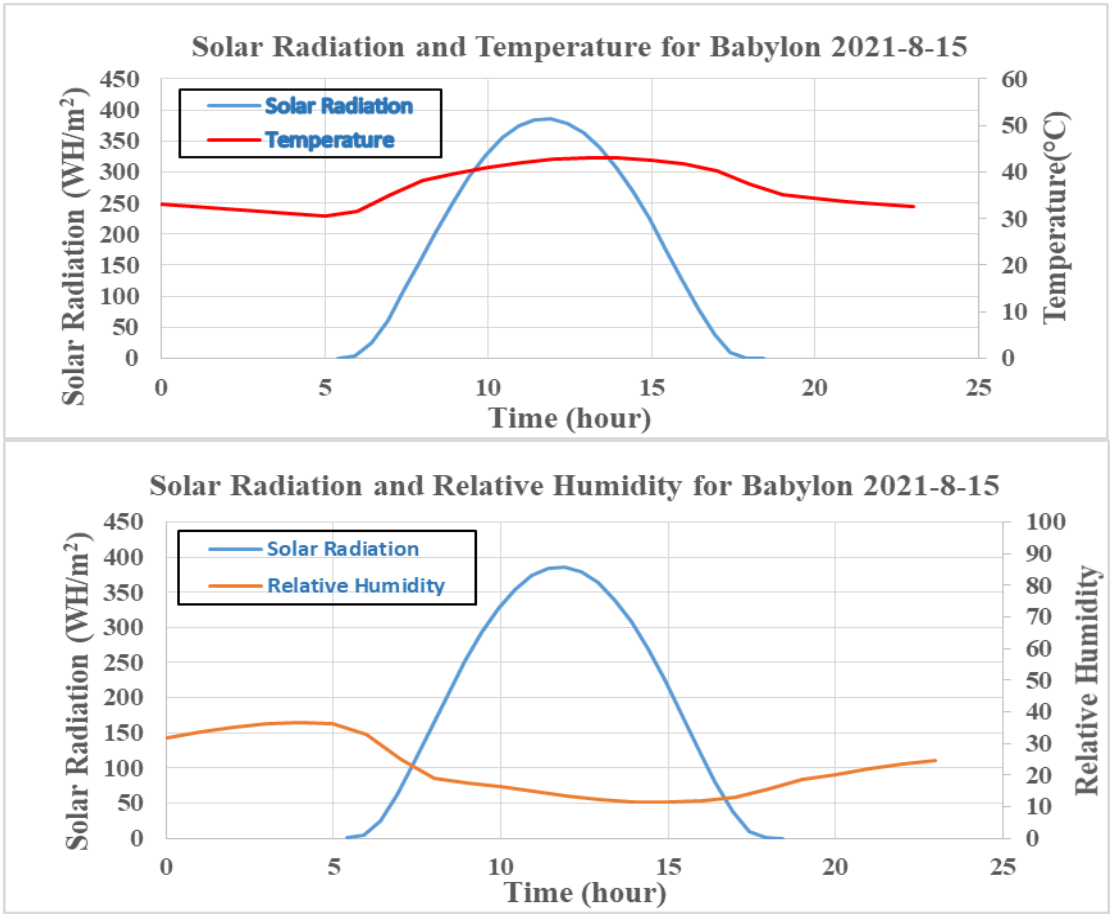

Figure (4-28): The relation between the Solar Radiation with temperature and relative humidity for Babylon during the day (15-8-2021).

Table (4-8): The solar radiation energy with sun duration day length for 15-8-2021 is (13.48 H) for one point in Babylon province.

Solar Radiation W.h.m^{-2}	Sun duration h	Solar Radiation	Sun duration
0.004742	5.416	378.9227	12.416
3.822083	5.916	363.1402	12.916
24.36974	6.416	339.0638	13.416
61.7634	6.916	307.3442	13.916
107.8843	7.416	268.8985	14.416
157.1693	7.916	224.9574	14.916
205.9448	8.416	177.1567	15.416
251.6744	8.916	127.7131	15.916
292.5152	9.416	79.76665	16.416
327.087	9.916	38.00943	16.916
354.353	10.416	9.418421	17.416
373.5587	10.916	0.272455	17.916
384.199	11.416	1.52E-06	18.416
386.0022	11.916		

4.9 The Land Surface Temperature (LST)

The flow chart shown in Figure (3-6). shows the steps that must be calculated to determine the distribution of the LST, where samples were taken for five months of the year 2021 as a model to cover all seasons of the year for the study area.

4.9.1 The Results of the LST in August

Figure (4-29) shows the maps of the TOA, NDVI, PV, Emissivity and BT in panels (A), (B), (C), (D) and (E) respectively and calculate from equation (3-1), (3-3),(3-5),(3-5),(3-2) respectively in August 15/8/2021.

As for Figure (4-30), it shows the distribution of the temperature values of the earth's surface in the province of Babylon, where the upper temperature was 58.3 Cº and the lower was 26.7 Cº on the day of observation.

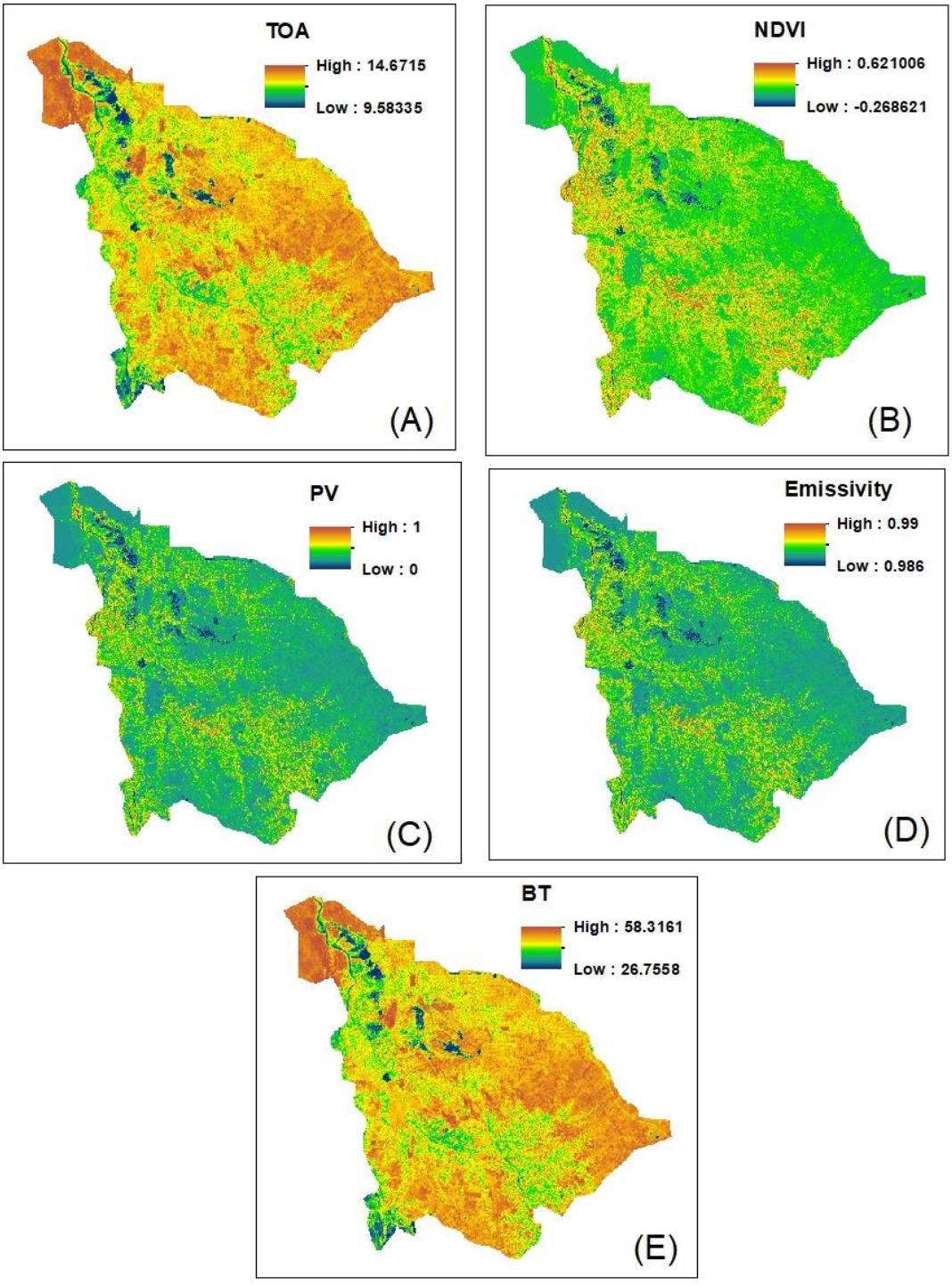

Figure (4-29): The maps of the TOA, NDVI, PV, Emissivity and BT are shown in panels (A), (B), (C), (D) and (E) respectively of Babylon province 2021-8-15.

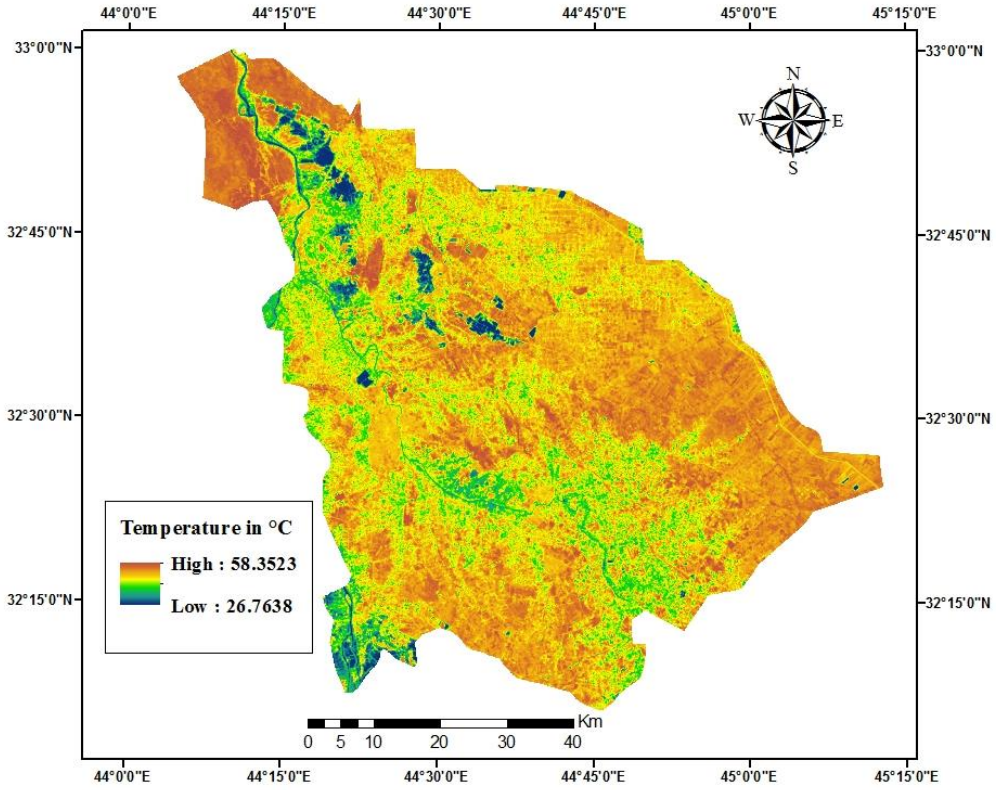

Figure (4-30): The special distribution of the Land Surface Temperature values of Babylon province the highest temperature reach to 58.3 Cº and lowest values reach to 26.7 Cº in 15-8-2021.

4.10 The Solar Radiation in October

Table (4-9) All climate information for the day of observation. The day of observation in the month of October was divided into three periods, given that the daylight hours on this day are 12 hours, each period of four hours. The digital elevation model from USGS was used. The spatial solar radiation was determined for the periods specified for the day of observation Table (4-10). Figure (4-31) A, that is, shows the first period of the spatial distribution of solar radiation, and Figure B shows the graph of the pixel numbers and radiation energy values to which specific values of solar radiation belong. All maps and graphs for the rest of the periods for the day of observation have been show in Figures (4 -32) and (4-33), while Figure (4-34) shows the average distribution of solar radiation for the day of observation. The upper part of Figure (4-35) show the rate amount of solar radiation and the calculated temperature, and the lower part of the same Figure has been displays the rate amount of solar radiation and relative humidity during the observation day.

Table (4-9): The climate state was taken from ECMWF for the time of observation.

The observing day	The Day time length hour	Temperature Cº	Relative humidity	Precipitation mm/day
15/10/2021	12	27.56	23.12 %	0.29

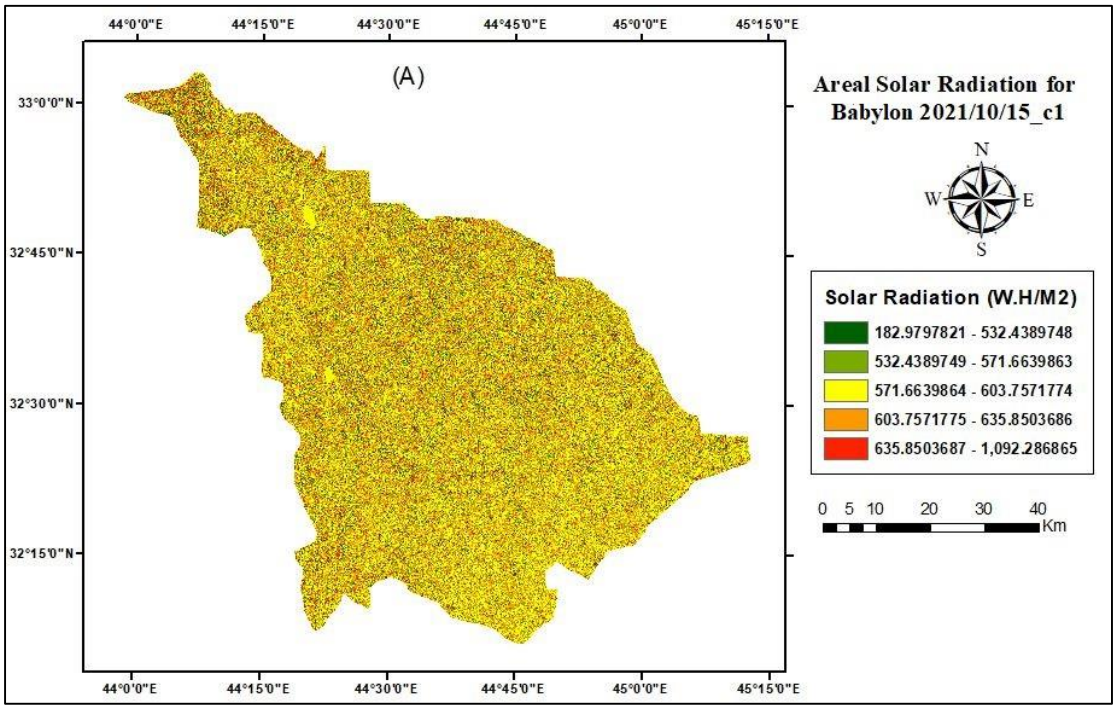

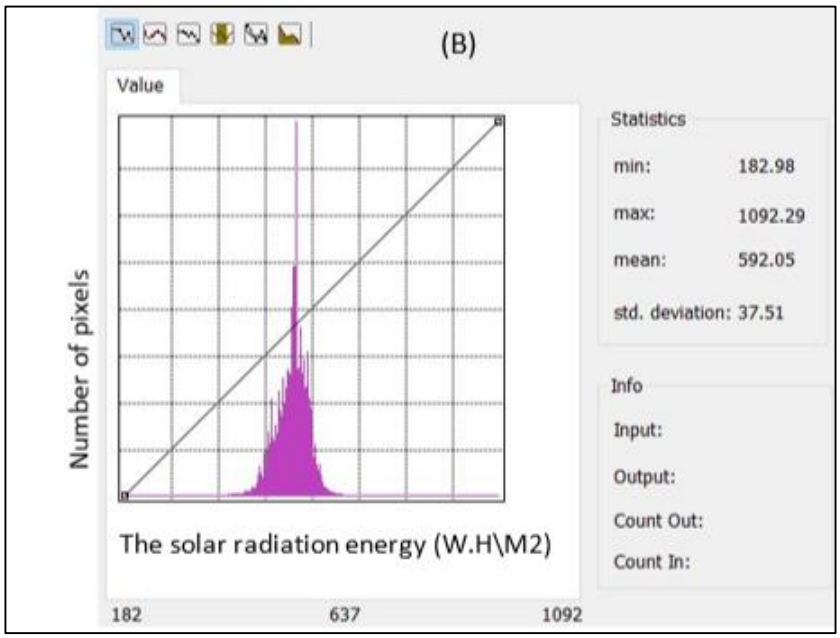

Figure (4-31): (A): The distribution of the solar radiation energy for Babylon province in the first period in (15-10-2021). (B): The histogram for the numbers of the pixels and the values of the solar radiation energy that belong to it.

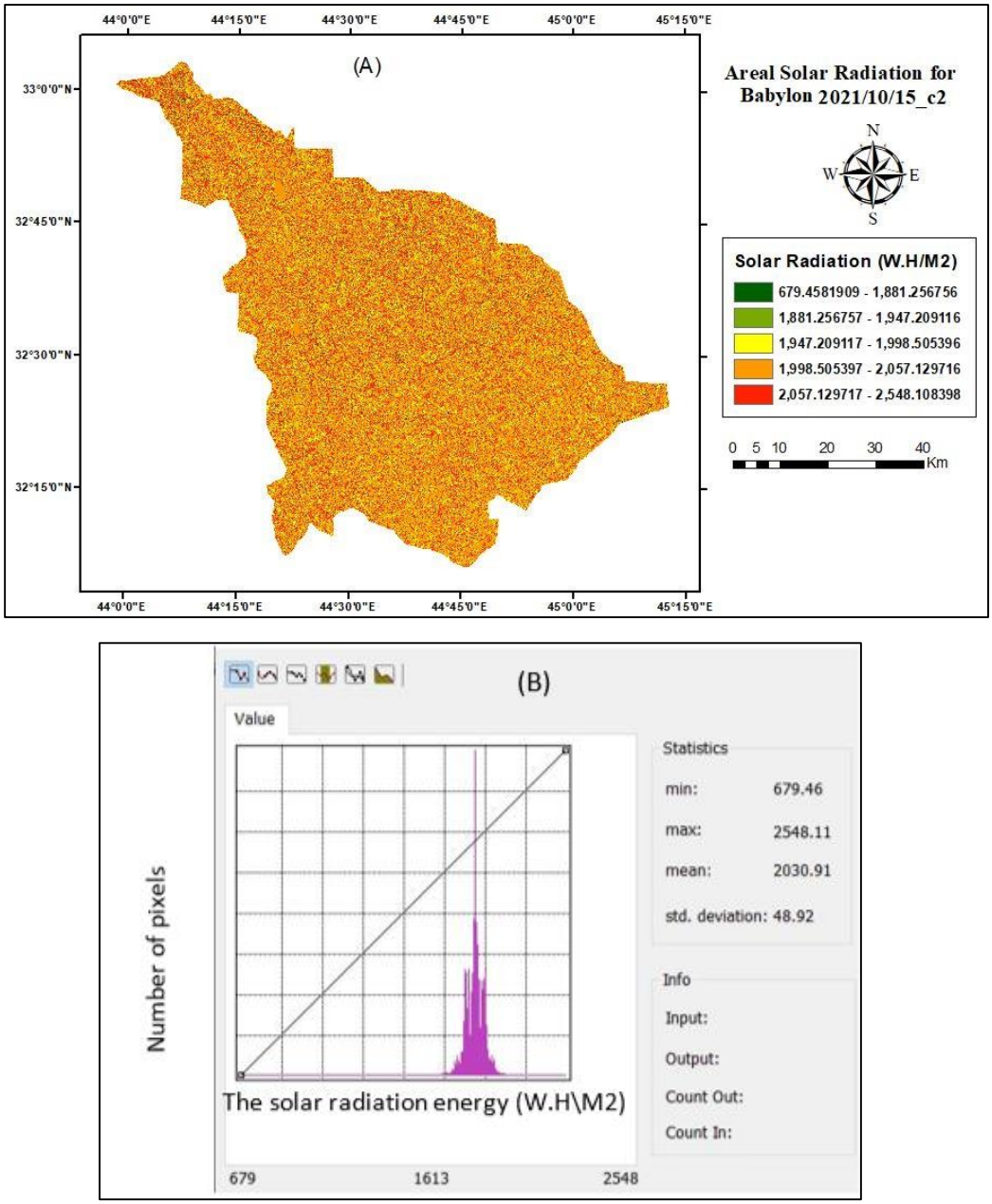

Figure (4-32): (A): The distribution of the solar radiation energy for Babylon province in the second period in (15-10-2021). (B): The histogram for the numbers of the pixels and the values of the solar radiation energy that belong to it.

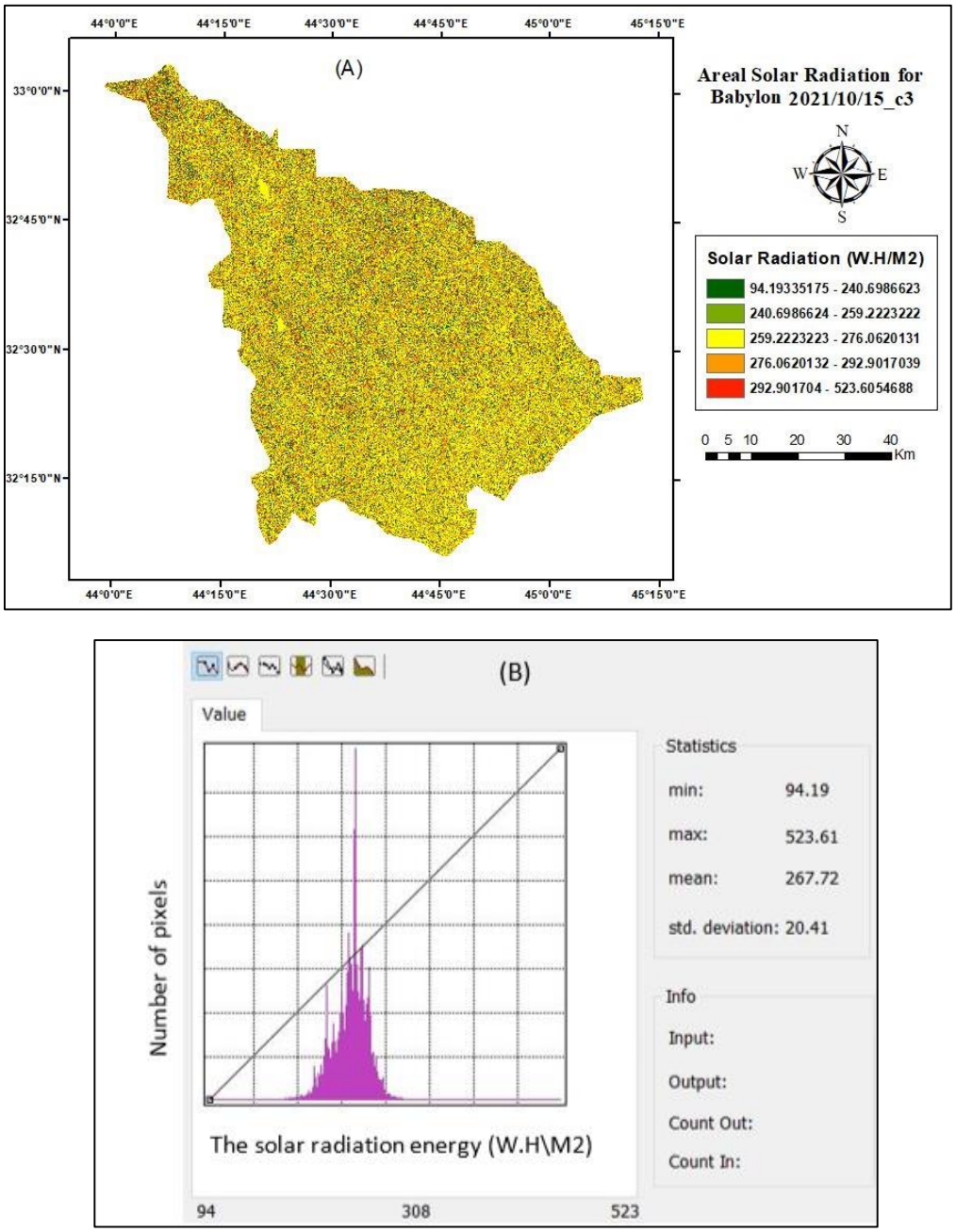

Figure (4-33): (A): The distribution of the solar radiation energy for Babylon province in the third period in (15-10-2021). (B): The histogram for the numbers of the pixels and the values of the solar radiation energy that belong to it.

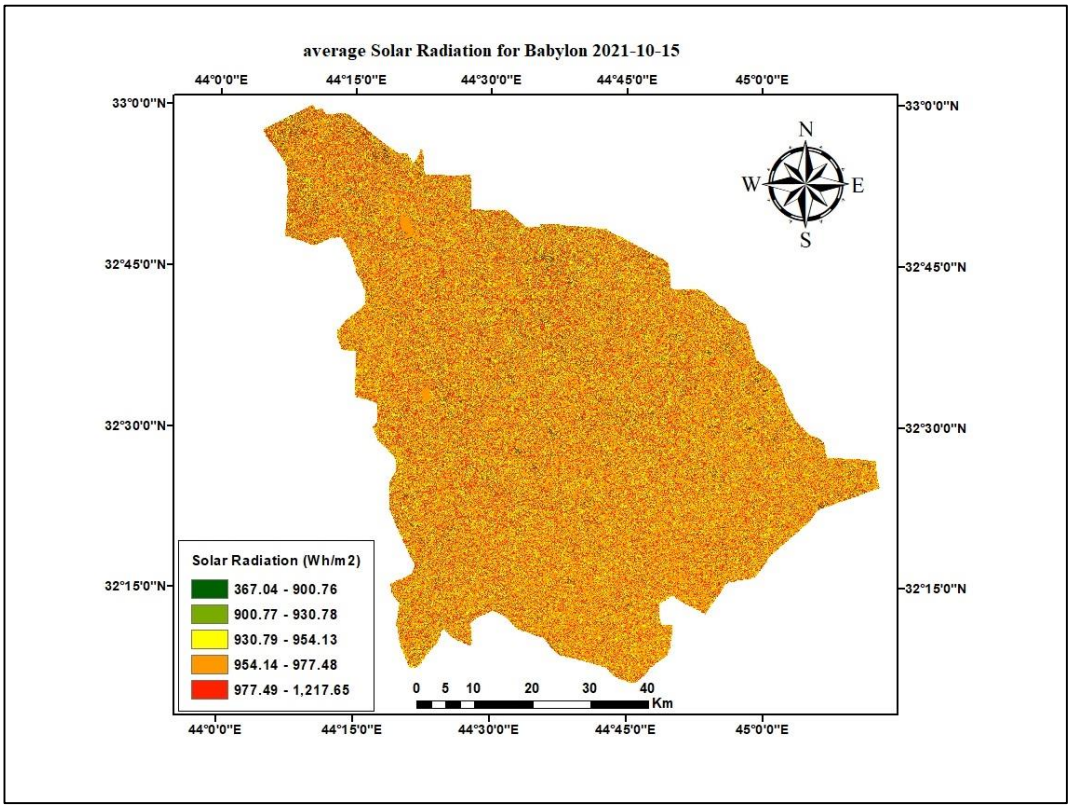

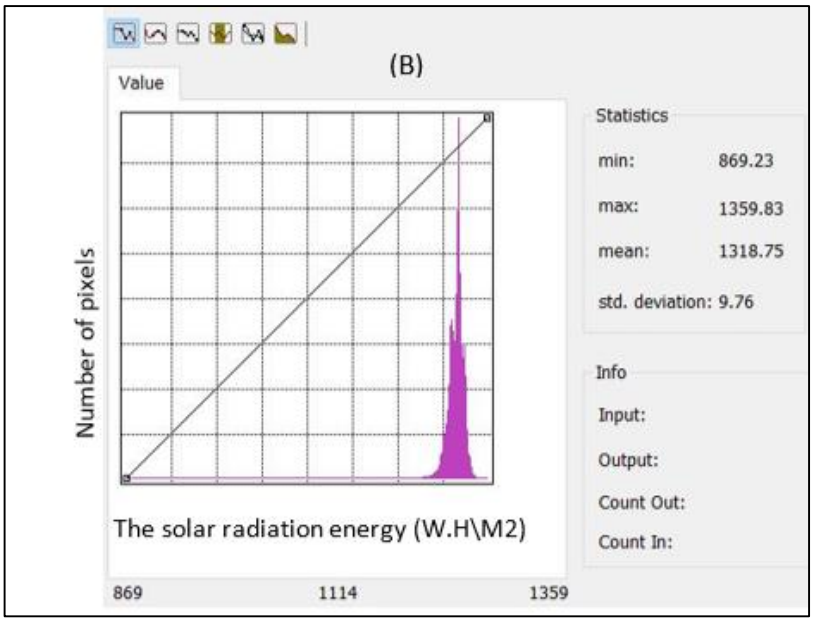

Figure (4-34): (A): The average distribution of the solar radiation energy for Babylon province during (15-10-2021). (B): The histogram for the numbers of the pixels and the values of the solar radiation energy that belong to it.

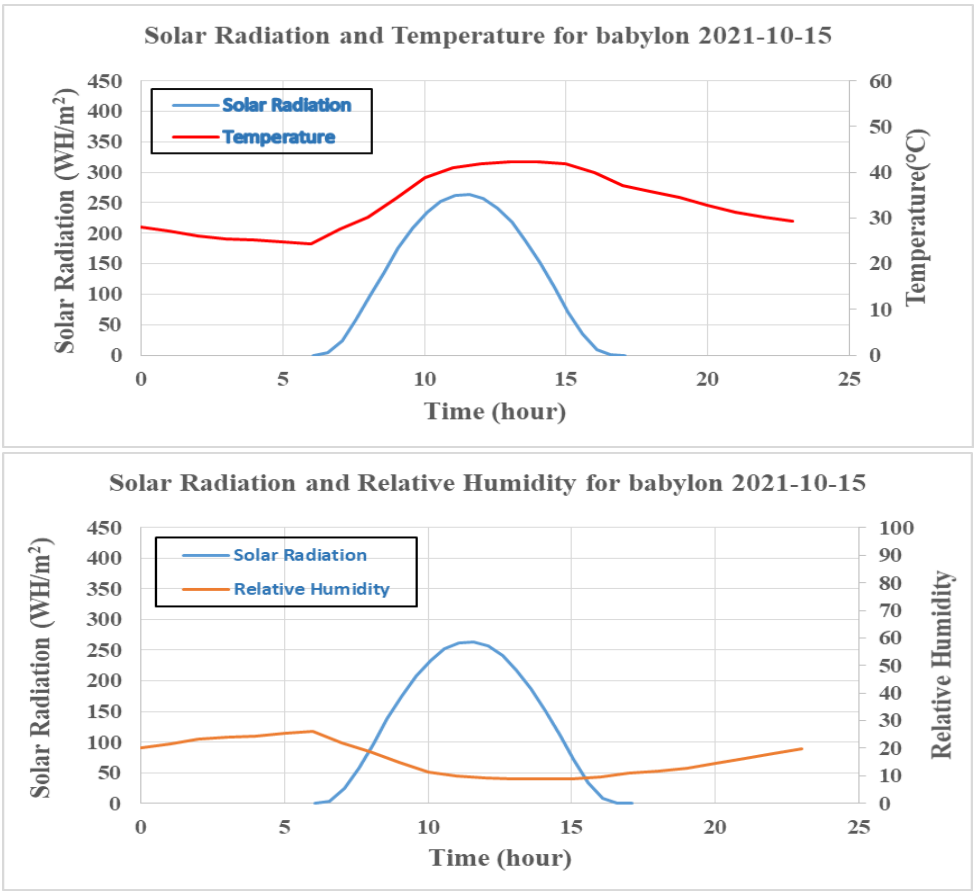

Figure (4-35): The relation between the Solar Radiation with temperature and relative humidity for Babylon during the day (15-10-2021).

Table (4-10): The solar radiation energy with sun duration day length for 15-10-2021 is (11.25 H) for one point in Babylon province.

Solar Radiation W.h.m^{-2}	Sun duration h	Solar Radiation	Sun duration
0.005438	6.083	256.4476	12.083
3.946359	6.583	240.9426	12.583
23.6231	7.083	217.5907	13.083
57.61384	7.583	187.2698	13.583
97.48894	8.083	151.2924	14.083
137.876	8.583	111.5853	14.583
175.399	9.083	71.04922	15.083
207.8484	9.583	34.24968	15.583
233.7265	10.083	8.334544	16.083
252.0186	10.583	0.20206	16.583
262.0785	11.083	5.91E-07	17.083
263.571	11.583		

4.11 The Land Surface Temperature (LST)

To determine the distribution of the LST, there are several steps that need to be calculated, that were presented in the flow chart Figure (3-6).The LST of the study area was calculated in five months (January, march, July, August and October) of the year 2021 to cover the different seasons of the year for Babylon province.

4.11.1 The Results of the LST in October

Figure (4-26) shows the maps of the TOA, NDVI, PV, Emissivity and BT in panels (A), (B), (C), (D) and (E) respectively and calculate from equation (3-1),(3-3),(3-5),(3-6),(3-2) respectively in October 15/10/2021.

As for Figure (4-37), it shows the special distribution of the surface temperature values for Babylon Province, where the highest surface temperature was 39.9 Cº and the lowest temperature was 19.9 Cº for the monitoring day 10-15-2021.

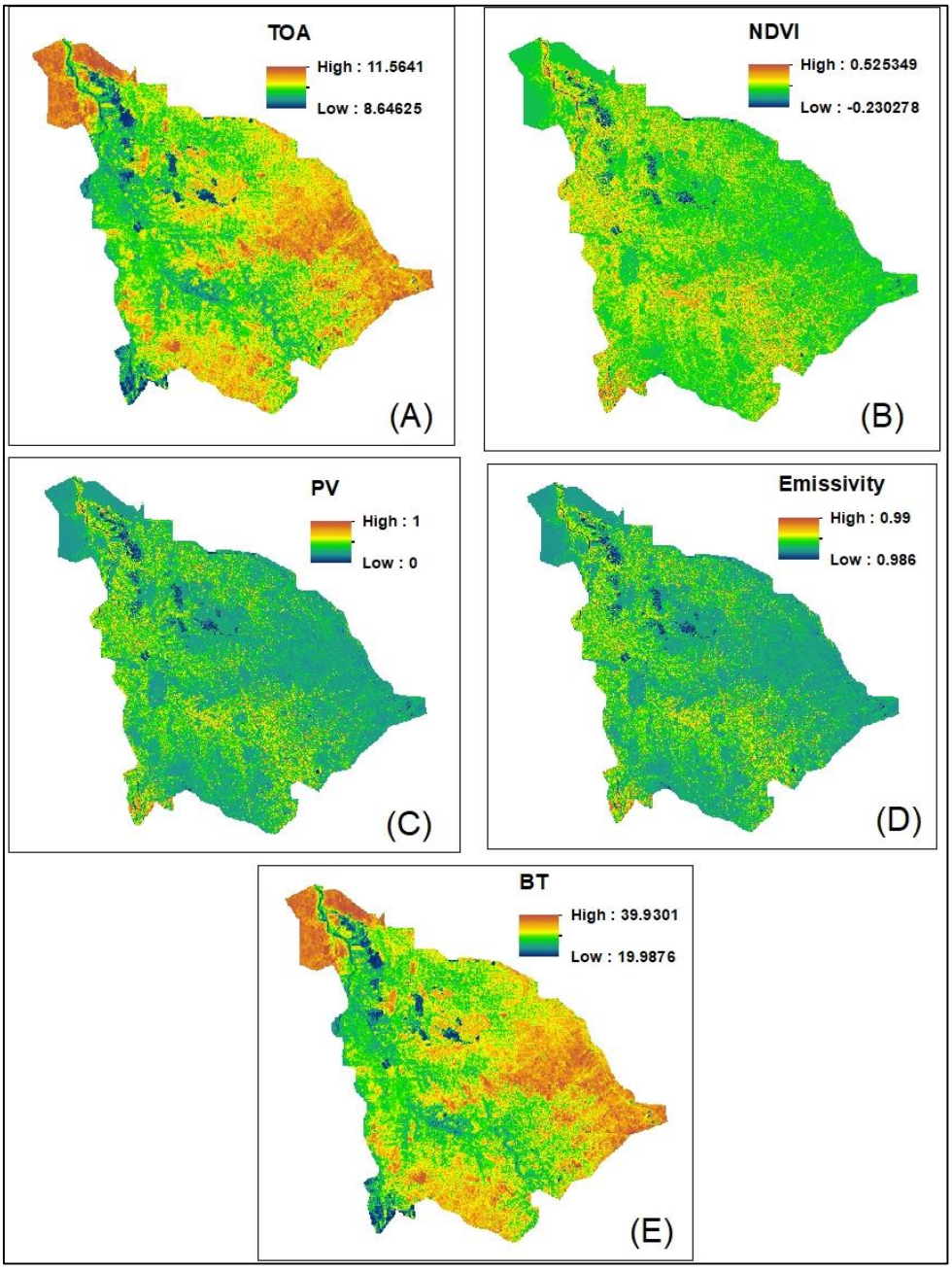

Figure (4-36): The maps of the TOA, NDVI, PV, Emissivity and BT are shown in panels (A), (B), (C), (D) and (E) respectively of Babylon province 2021-10-15.

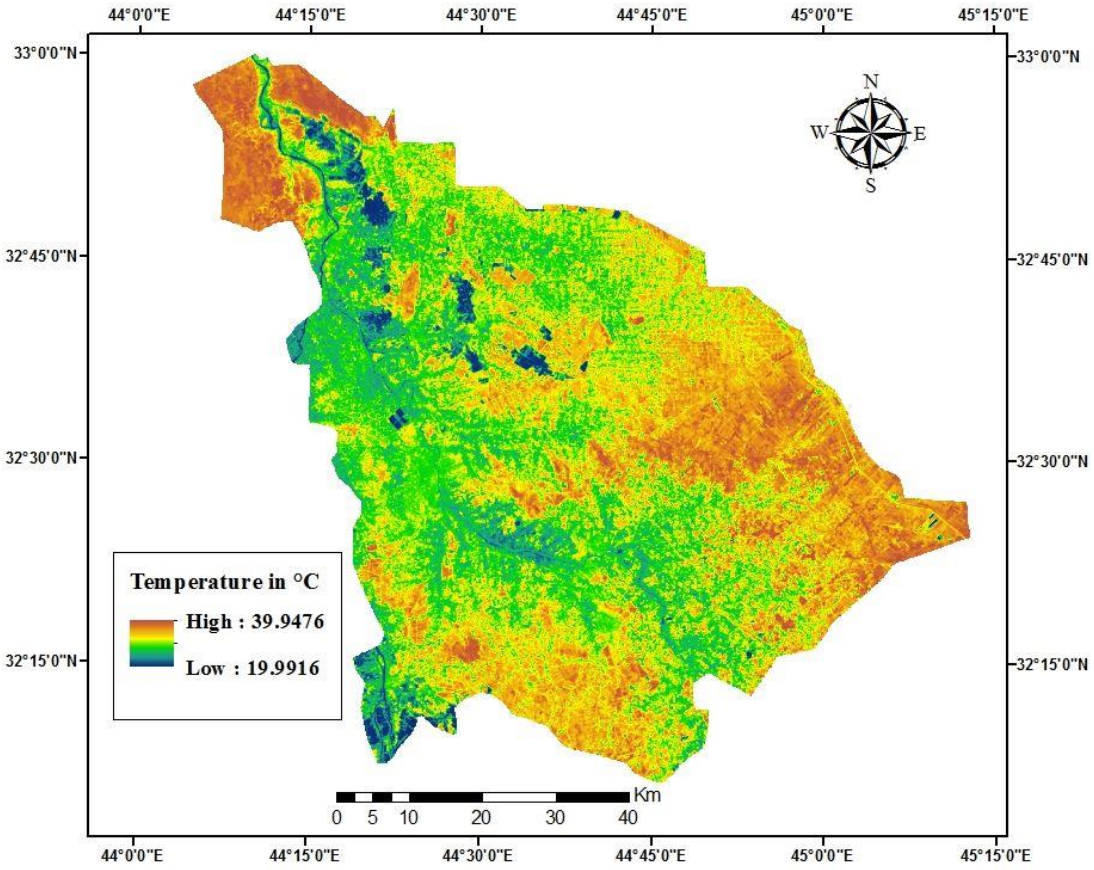

Figure (4-37): The special distribution of the Land Surface Temperature values of Babylon province the highest temperature reach to 39.94 Cº and lowest values reach to 19.99 Cº in 15-10-2021.

4.12 Injuries Statistics

Skin cancer incidence statistics for the study area were obtained from the Oncology Center at Marjan Hospital in Babil Province, as well as the National Cancer Hospital in Najaf Province, which are shown in Table (4-11).

The chart (4-38) indicates the percentages of the numbers of injuries for the study area, while the chart (4-39) indicates the distribution of the numbers of injuries by numbers in the study area. The results indicate that the city of Hilla (the center of Babylon Province) had the highest injuries,

It is possible that the population density in this region, in addition to direct exposure to sunlight, being the center of the province and containing industrial areas and construction sites, is also a major reason for the high number of injuries, as exposure to sunlight is more and more severe compared to the rest of the districts and districts of the province, which are characterized by an agricultural nature and few numbers of population.

Table(4-11): Statistics of skin cancer cases, Morgan Hospital in Babylon and National Cancer Hospital in Najaf.

NO	Area	NO. of case
1	Hilla	12
2	Musayyib	4
3	Abi gharak	6
4	Al Mahaweel	4
5	Kotha	1
6	Al Kifl	3
7	Western Hamza	2
8	Hashemite	2

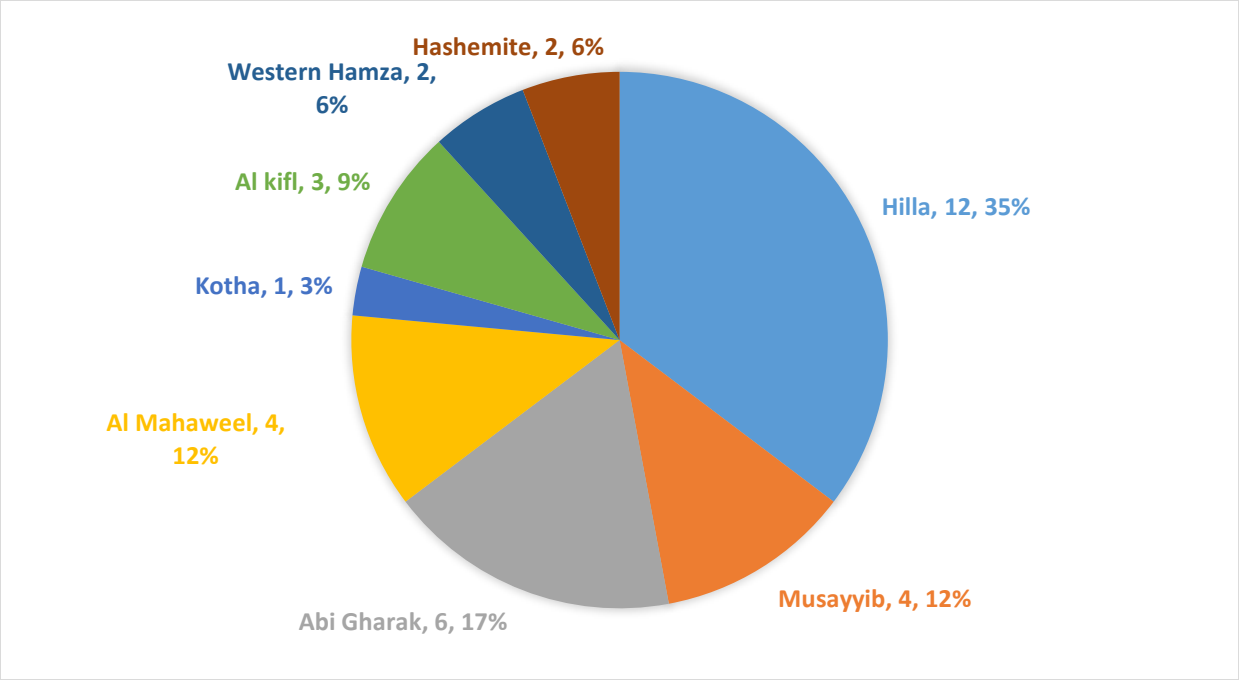

Figure (4-38): The chart shows the percentage of the numbers of infections distributed over the regions of Babylon.

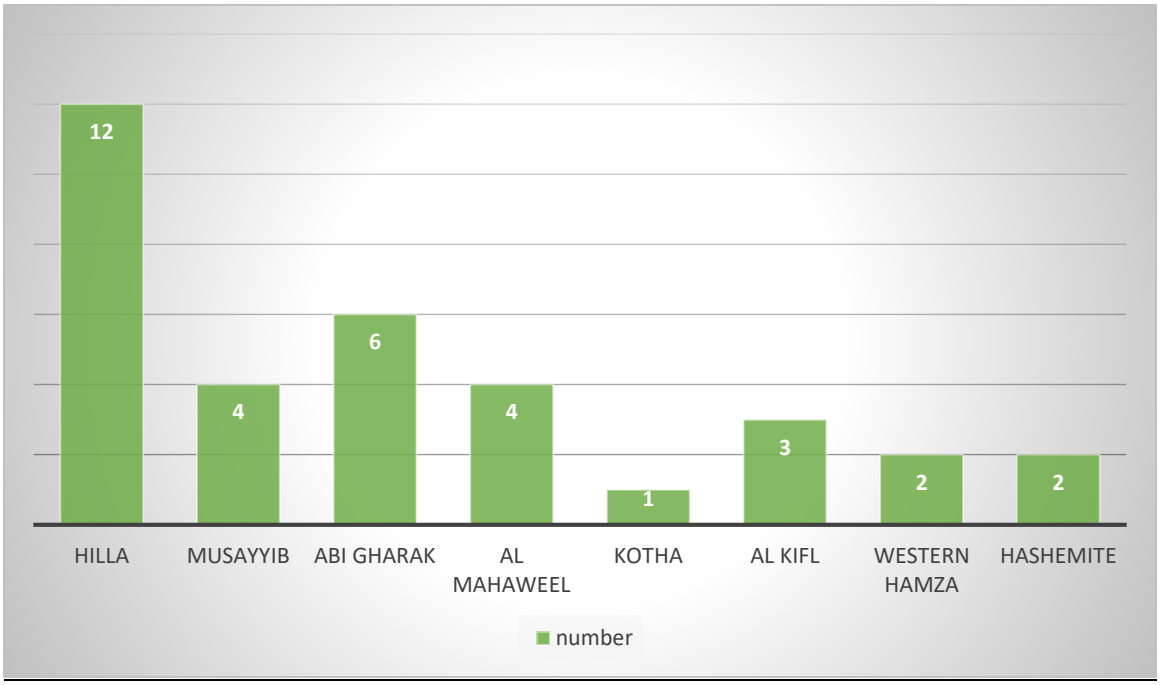

Figure (4-39): Graphic representation of the number of injuries distributed over the regions of Babylon.

CHAPTER FIVE

Discussions, Conclusions and Recommendations

5.1 Results and Discussions

In this chapter, the researcher will discuss the results that are obtained in this thesis, as the topic of the thesis deals with three research projects, due to the complexity of the subject that is studied and the urgent need for such topics, especially in recent times after the researcher witnessed the remarkable and unprecedented rise in temperatures, specifically in the summer season.

1- The distribution of solar radiation for five months of the year 2021 for Babylon province, which are shown in Figures (4-4), (4-11), (4-19), (4-27), (4-34). These Figures show the distribution of solar radiation is high in July and August, as the amount of radiation reached its highest value in July (405,6382) W. H/m^2, and it reached its lowest value in January, reaching (175.8) W. H/m^2, this is during the peak period of sunrise, and this discrepancy is due to several reasons, including the length of daylight hours, the angle of the sun's fall, and the topography of the region, where the researcher notice that the value of solar radiation is close and high in the summer, while the rest of the seasons are relatively low and do not pose a danger, and through the graphs it is shown in the same figures above that the distribution of solar radiation for the five months also increases clearly in the months of July and August, as it represents the summer season, and begins to gradually decrease in the autumn, winter and spring seasons. It is observed that the spatial distribution of the solar radiation of the province during the four seasons do not show a distinct area with a sharp solar radiation intensity, this may be due to the absence of areas distinguished by elevation

characteristic above the sea level, as well as the location of the province within a narrow area of latitude between (32˚6` N to 33˚8` N). Thus, most of the region is exposed to the same intensity of solar radiation as well as the same climatic factors, of course, during a certain period of the year.

2- The Figures (4-5), (4-12), (4-20), (4-28), and (4-35), represent the relationship between solar radiation with temperature and relative humidity. Figure (4-5) shows data for the month of January, which represents the winter season, where the highest value of temperature and relative humidity reaches 20 Cº, while the relative humidity reaches more than 90%. Figure (4-12) represents the data for the month of March, the spring season. The highest level of relative humidity reached 60%, while the temperature may reach the limits of 29 Cº. When observing Figure (4-20), the data for the month of July, the summer season, and there are a clear rise in temperatures, which reach 47 Cº and the obvious decrease in relative humidity, reaching its highest value of 22%. When looking at Figure (4-28), which represents data for the month of August, we also notice a clear increase in temperatures and a decrease in relative humidity, as it reaches 46 Cº and the humidity reaches 30%. Figure (4-35) for the month of October, which represents the autumn season. The temperatures reach a peak of approximately 40 Cº, while the relative humidity reaches its highest value to 26%. Through the foregoing, we notice that the relationship is inverse between temperatures and relative humidity, when temperatures rise, relative humidity decreases, and vice versa, and this is evident through the data proven in the forms that have been discussed.

3- The statistical information about the cancer cases in particular skin cancer, which were presented in Table (4-11) and translated in Figures (4-38) and (4-

39), shows there is a difference in the distribution of cases of skin cancer across the districts of the province, although there are no distinct areas that are exposed to solar radiation. The province center showed the highest rate of injuries, followed by the Abu Gharq district, and in third place were the districts of Mahmoudiya and Musayyib, which shows an equal rate of cases. The lowest number of cases appeared in the district of Al-Kotha. The reason for the difference in the number of infections in the districts of the province may be due to the difference in the population density in the districts, and therefore the cases are concentrated in the center of the province, Hilla addition to the genetic factors for the possibility of cancer.

4- Through Figure (4-7), which shows the LST for the month of January, we note that the highest surface temperature of the Earth was 15.9 Cº, while the lowest temperature was -2.3 and this represents the winter season. As for Figure (4-14), which represents the LST for the month of March in the spring season, the highest temperature of the Earth's surface reached 31.5 Cº and the lowest temperature was 13.7 Cº. As for Figure (4-22), it represents the LST data for the month of July, the summer season, there are a clear rise in the temperature of the Earth's surface, as it reached the highest degree of 58.3 Cº and the lowest is 26.7 Cº, and this is a clear indication of the clear rise in the LST, and Figure (4-30) which represents LST data for the month of August in the summer season. The temperature reached 25.7 Cº, Figure (37-4), which shows the data for the month of October, the autumn season. The special data indicates that the highest temperature of the LST reaches 39.94 Cº and the lowest temperature reaches 19.9 Cº. From the foregoing, I note that the LST increases in arid areas and urban areas, in which there are many buildings and

an increase in population density, and decreases in areas of an agricultural nature and areas of water bodies. Therefore, urban areas and arid areas have higher degrees and lower humidity.

5.2 Conclusions

Through the maps and the results of the research, it is possible to summarize the most important findings of this thesis:

1- Through maps of the spatial distribution of solar radiation, distinct areas are not shown to be exposed to solar radiation at certain time periods of the year. It turns out that the measured and arriving rays vary in intensity with time the afternoon period is one of the most severe periods in the daily measurement readings, and therefore must be careful when exposed to the sun in these periods.

2- The province of Babylon Province is divided into eight administrative regions, and the numbers of skin cancer infections are clarified in numbers for these regions, where the highest value is in the center and then Abu Gharq, then Mahmoudia and Musayyib according to the statistics obtained from the Health Department of Babylon and the Department of Health of Najaf.

3- Through the aforementioned results, maps and research, the researcher note that the distribution of solar radiation in does not show distinct areas with the presence of very high solar radiation, despite the discrepancy that we witnessed in the radiation values between the seasons, due to the geographical nature of the city of Babylon, as it does not contain high areas (mountains and hills) and does not contain either on low areas (plains and valleys), but their lands are almost flat. Therefore, a qualitative study was

directed to the effect of solar radiation on human health and the damage it causes to the skin, especially (skin cancer). It is noted that the height of the land of the city of Babylon is similar to the extent Great for the city of Baghdad, and this means that the intensity of ultraviolet radiation that was received for the city of Babylon is almost equal to the city of Baghdad. A decrease in the incoming radiation and an increase in the percentage of humidity in the rest of the seasons, and that the danger in exposure to radiation lies in the duration of exposure to high radiation.

5.3 Future Works

The future work can be summarized in several points that emerged in our perception during the current research:

1- Focusing on large areas of Iraq, especially that its land includes a variety of terrain, such as the southern and eastern regions of Iraq.
2- Calculation of the UV Index in the province of Babylon during one year by using TOVS method (TIROS Operational Vertical Sounder), which is applied and measured within ultraviolet radiation measuring devices carried on satellites NOAA (National Oceanic Atmospheric Administration).
3- Expanding with statistics that include cases of skin cancer, as well as some skin diseases that are affected by increased ultraviolet radiation, after consulting dermatologists.

5.4 Recommendations

It is clear in recent times the rise in temperatures and increase in an abnormal way, especially in the summer, and this is due to several reasons, including the lack of rain, the increase in desertification areas, and the increase in the hole of the ozone layer. Therefore, we recommend the following points

1- Increasing the follow-up and in-depth research on this subject, using the updated versions of the Landsat 9 program.
2- Doing a broader study to include all regions of Iraq with regard to the rise in air temperatures and the LST.
3- Doing a detailed study on ultraviolet radiation and its impact on human health, and it should be comprehensive in all regions of Iraq.
4- Not to be exposed to sunlight directly and for long periods, especially at noon in the summer season, due to the high percentage of ultraviolet radiation during these times, and thus it has a negative effect on the skin.
5- Wearing hats and sunglasses or using sunscreen before going out at noon in the summer. It is preferable not to go out unless necessary.
6- Staying away from sun loungers and tanning beds, since their working principle depends on ultraviolet radiation, and this in itself is a danger to human health.

References

[1] Theo Koupelis ” The Solar System “Edison State College, 4th Edition, pp(307-333), (2011).

[2] D. Müller, O. C. St. Cyr, I. Zouganelis,"The Solar Orbiter mission" Astronomy & Astrophysics (A&A), 642, A1 (2020).

[3] John D. Fix “Astronomy” Journey to The Cosmic Fronter, 6th Edition, pp(470-490), (2012).

[4] Cain, Fraser, "How long does it take sunlight to reach the Earth?", phys.org, (2022).

[5] Christopher T. Russell. "The Solar Wind and Magnetospheric Dynamics", Institute of Geophysics and Planetary Physics University of California, Los Angeles, (2018).

[6] Antiochos, S. K.; Mikić, Z.; Titov, V. S.; Lionello, R.; Linker, J. A., "A Model for the Sources of the Slow Solar Wind". The Astrophysical Journal. 731 (2): 112, (2011).

[7] Solar Radiation Theory, Uppsala University, Translation to Arabic by Dr. Khalafallah Omar Kassem 2021.Copyright © Joakim Widén, Joakim Munkhammar, Khalafallah Omar p.p 21-25 (2021).

[8] Rose Roberts "Radical Human Ecology: Intercultural and Indigenous Approaches Routledge". p. 350. ISBN, (2016).

[9] "Earth's Seasons ". Astronomical Applications Department. The United States Naval Observatory (USNO). September 21, (2015).

[10] Petersen, J.; Sack, D.; Gabler, R.E. "Fundamentals of Physical Geography" Cengage Learning. p. 18. ISBN, (2014).

[11] Deguara, Brittney "When does winter officially start in New Zealand ", Stuff, (2019).

[12] Rohli, R.V.; Vega, A.J. "Climatology "Jones & Bartlett Learning, LLC. p. 30. ISBN, (2011).

[13] Williams, David R. "Earth Fact Sheet". NASA/Goddard Space Flight Center, (2018).

[14] "Atmospheres and Planetary Temperatures". American Chemical Society ,(2023).

[15] Hall, Shannon "Earth's Tectonic Activity May Be Crucial for Life—and Rare in Our Galaxy". Scientific American,(2022) .

[16] Obu, J. "How Much of the Earth's Surface is Underlain by Permafrost?". Journal of Geophysical Research: Earth Surface. American Geophysical Union (AGU). 126 (5),(2021).

[17] Glynn C. Hulley , Darren Ghent, "TAKING THE TEMPERATURE OF THE EARTHSteps towards Integrated Understanding of Variability and Change" Elsevier Inc, this book is available from the British Library ISBN: 978-0-12-814458-9, pp 60-64 ,(2019).

[18] Abdulla - Al Kafy a,b, Abdullah-Al- Faisal a,c, Abdullah Al Rakib a, Sumita Roy a ,Jannatul Ferdousi d, Vinay Raikwar e, Marium Akter Kona f , S.M. Abdullah Al Fatin,"Predicting changes in land use/land cover and seasonal land surface temperature using multi-temporal landsat images in the northwest region of Bangladesh",Heliyon journal7 (2021) e07623,(2021).

[19] C. Huang, Z. Zhao, L. Wang, Z. Zhang, X. Luo, "Point and interval forecasting of solar irradiance with an active Gaussian process", IET Renew Power Gener, 14 (6) pp. 1020-1030, (2020).

[20] A.E. Gürel, Ü. Ağbulut, Y. Biçen, "Assessment of machine learning, time series, response surface methodology and empirical models in prediction of global solar radiation", J Clean Prod, pp. 122-353, (2021).

[21] Vieira, S. K. Solanki, N. A. Krivova and Usoskin, "Evolution of the solar irradiance during the Holocene". Astronomy & Astrophysics. 531: A6, (2011).

[22] Y. Liu, Y. Zhou, Y. Chen, D. Wang, Y. Wang, Y. Zhu, "Comparison of support vector machine and copula-based nonlinear quantile regression for estimating the daily diffuse solar radiation: a case study in China", Renew Energy, 146, pp. 1101-1112, (2020).

[23] Zell, Holly, "Earth's Upper Atmosphere". NASA. Retrieved (2017).

[24] Joe Buchdahl. "Atmosphere, Climate & Environment Information Programme". Ace.mmu.ac.uk, (2012).

[25] Williams, Matt "What is the Atmosphere Like on Other Planets?", Universe Today, (2019).

[26] Gunell, H.; Maggiolo, R.; Nilsson, H.; Stenberg Wieser, G.; Slapak, R.; Lindkvist, J.; Hamrin, M.; De Keyser, J. "Why an intrinsic magnetic field does not protect a planet against atmospheric escape". Astronomy and Astrophysics. 614: L3,(2018).

[27] Zahnle, K.; Schaefer, L.; Fegley, B. "Earth's Earliest Atmospheres". Cold Spring Harbor Perspectives in Biology. 2 (10): a004895, (2010).

[28] "Atmospheric Temperature Trends, 1979–2005". NASA/Earth Observatory. 6 July 2007. (2015).

[29] "The Stratosphere - overview". scied.ucar.edu. University Corporation for Atmospheric Research, (2018).

[30] "CHAPTER 10. STRATOSPHERIC OZONE". acmg.seas.harvard.edu, (2020).

[31] N.Butchart, A.A. Scaife, J. Austin, S.H.E. Hare, J.R. Knight. "Quasi-biennial oscillation in ozone in a coupled chemistry-climate model" the Wayback Machine, Journal of Geophysical Research, (2014).

[32] Society, National Geographic, "ozone layer". National Geographic Society, (2021).

[33] Maverakis E., Miyamura Y., Bowen MP, Correa G., Ono Y. and Goodarzi H., "Light, including ultraviolet". Journal of Autoimmunity. 34 (3): J247-57. (2010).

[34] Solomon, Susan, "Emergence of healing in the Antarctic ozone layer". Science. 353 (6296): 269–74, (2016).

[35] Narayanan DL., Saladi RN. and Fox JL., "Ultraviolet radiation and skin cancer". International Journal of Dermatology. 49 (9): 978–86(2010).

[36] Mata, Douglas A.; Williams, Erik A.; Sokol, Ethan; Oxnard, Geoffrey R.; Fleischmann, Zoe; Tse, Julie Y.; Decker and Brennan . "Prevalence of UV Mutational Signatures Among Cutaneous Primary Tumors". JAMA Network Open. **5** (3): e223833(2022).

[37] R. Almuqati, A. S. Alamri, and N. R. Almuqati, “Knowledge, attitude, and practices toward sun exposure and use of sun protection among non-medical, female, university students in Saudi Arabia: a cross-sectional study”, International Journal of Women’s Dermatology, vol. 5, no. 2, pp. 105–109,(2019).

[38] Gunell, H.; Maggiolo, R.; Nilsson, H.; Stenberg Wieser, G.; Slapak, R.; Lindkvist, J.; Hamrin, M.; De Keyser, J., "Why an intrinsic magnetic field does not protect a planet against atmospheric escape ". Astronomy and Astrophysics. 614: L3, (2018).

[39] Williams, Matt , "What is the Atmosphere Like on Other Planets". Universe Today,(2016).

[40] Choudhury, Asim Kumar Roy , "Unusual visual phenomena and colour blindness", Principles of Colour and Appearance Measurement, Elsevier, pp. 185–220, (2014).

[41] Bingfang Wu, Shufu Liu, Weiwei Zhu, Mingzhao Yu, Nana Yan and Qiang Xing, "A Method to Estimate Sunshine Duration Using Cloud Classification

Data from a Geostationary Meteorological Satellite (FY-2D) over the Heihe River Basin", Sensors — Open Access Journal, (2016).

[42] WMO, " Measurement of Sunshine Duration " , Guide to Meteorological Instruments and Methods of Observation, (2008).

[43] Gerhard Holtkamp,"The Sunniest and Darkest Places on Earth" ,Scilogs 22:22 15. June, (2009).

[44] Ji-Long Chen a b c d, Guo-Sheng Li c d, Sheng-Jun Wu a b Show more, "Assessing the potential of support vector machine for estimating daily solar radiation using sunshine duration",Energy Conversion and Management, Volume 75, November , Pages 311-318(2013).

[45] "Key statistics for basal and squamous cell skin cancers". www.cancer.org. American Cancer Society. Archived from the original on 10 January 2017. Retrieved 9 January (2017).

[46] Mata, Douglas A.; Williams, Erik A.; Sokol, Ethan; Oxnard, Geoffrey R.; Fleischmann, Zoe; Tse, Julie Y.; Decker, Brennan "Prevalence of UV Mutational Signatures Among Cutaneous Primary Tumors" ,jama network open 5, 388-396, (2022).

[47] Naraya namurthy V, Padma priya P, Noora safrin A, Pooja B, Hema K, Nithya kalyani K, Samsuri F "Skin cancer detection using non-invasive techniques". RSC Advances. 8 (49): 28095–28130, (2018).

[48] Maverakis E, Cornelius LA, Bowen GM, Phan T, Patel FB, Fitzmaurice S, et al, "Metastatic melanoma - a review of current and future treatment options". Acta Dermato-Venereologica. 95 (5): 516–524(2015).

[49] Lin JS, Eder M, Weinmann S, "Behavioral counseling to prevent skin cancer: a systematic review for the U.S. Preventive Services Task Force". Annals of Internal Medicine. 154 (3): 190–201(2011).

[50] Bibbins-Domingo K, Grossman DC, Curry SJ, Davidson KW, Ebell M, Epling JW, "Screening for Skin Cancer: US Preventive Services Task Force Recommendation Statement". JAMA. 316 (4): 429–435(2016).

[51] Ferrante di Ruffano L, Dinnes J, Deeks JJ, Chuchu N, Bayliss SE, Davenport C, "Optical coherence tomography for diagnosing skin cancer in adults". The Cochrane Database of Systematic Reviews. 12: CD013189 (2018).

[52] Wang H, Naghavi M, Allen C, Barber RM, Bhutta ZA, Carter A, "Global, regional, and national life expectancy, all-cause mortality, and cause-specific mortality for 249 causes of death, 1980-2015: a systematic analysis for the Global Burden of Disease Study 2015". Lancet. 388 (10053): 1459–1544(2016).

[53] Dinnes J, Deeks JJ, Chuchu N, Matin RN, Wong KY, Aldridge RB, "Visual inspection and dermoscopy, alone or in combination, for diagnosing keratinocyte skin cancers in adults". The Cochrane Database of Systematic Reviews (12): CD011901(2018).

[54] K.Spradlin, M. Bass, W. Hyman, and R. Keathley, “Skin cancer: knowledge, behaviors, and attitudes of college students,” Southern Medical Journal, vol. 103, no. 10, pp. 999–1003(2010).

[55] S. Cheng, S. Lian, Y. Hao et al., “Sun-exposure knowledge and protection behavior in a north chinese population: a questionnaire-based study”, Photodermatology, Photoimmunology & Photomedicine, vol. 26, no. 4, pp. 177–181, (2010).

[56] N. Al-Ansari and A. chabuk, "Soil Characteristics in Selected Landfill Sites in the Babylon Province, lraq", (2017).

[57] Zahraa A.N.Hamza, “Assessment the Land Vegetation Cover for Babylon Government by Using Remote Sensing and GIS Techniques” University of Babylon, College of Science,pp9-10 (2021).

[58] Al-Rijabo, "Study of Spatial Variation of Total Solar Radiation Falling on Horizontal surface in Iraq", Renewable Energy, 35, pp 2228-2234, (2011).

[59] Abdul Qayoom Jakhrani, "Selection of models for calculation of incident solar radiation on tilted surfaces", Polish Polar Research, 31(1), pp 17-32, (2013).

[60] E. J. Knight and G. Kvaran, "Landsat-8 Operational Land Imager Design, Characterization and Performance", (2014).

[61] Taehong Sung, Sang Youl Yoon and Kyung Chun Kim, "A Dual Loop Organis Rankink Cycle Utilizing Boil-Off GAS IN LNG Tanks and Exhaust of Marine Enging", 3rd International Seminar on ORC Power Systems, pp144-184, (2015).

[62] Bibbins-Domingo K, Grossman DC, Curry SJ, Davidson KW, Ebell M, Epling JW, "Screening for Skin Cancer: US Preventive Services Task Force Recommendation Statement". JAMA. **316** (4): 429–435, (2016).

[63] Ahmed A. Hameed, Neamah Mohsen AL-Fatlawy & Ali M. AL-Salihi, " Estimation of hourly global solar radiation incident of inclined surface in Iraq at different sky condition", International Journal of Research in Applied,Natural and Social Sciences, pp 13-28, (2017).

[64] Hilmi Cenk Bayrakçı, Cihan Demircan, Ali Keçebaş "The development of empirical models for estimating global solar radiation on horizontal surface: A case study" Renewable and Sustainable Energy Reviews 81, 2771-2782, (2018).

[65] Alberto Modenese, Leena Korpinen and Fabriziomaria Gobba, "Solar Radiation Exposure and Outdoor Work: An Underestimated Occupational Risk", Int. J. Environ. Res. Public Health, 15(10), 2063,(2018).

[66] Melina Arnold, Esther de Vries, David C Whiteman, Ahmedin Jemal, Freddie Bray, Donald Maxwell Parkin, Isabelle Soerjomataram, "Global burden of cutaneous melanoma attributable to ultraviolet radiation in 2012", International journal of cancer 143 (6), 1305-1314, (2018).

[67]Ayatf , Abed and Ebtesam F.Khanjer,"Guess Solar Radiation Energy on Iraq by using DEMS and ArcGIS Techniques", Indian Journal of Natural Sciences,Vol.9 /Issue 52,pp 16523-16528 (2019).

[68] Junliang Fan, Lifeng Wu, Fucang Zhang, Huanji Cai ,Xin Ma and Hua Bai, "Evaluation and development of empirical models for estimating daily and monthly mean daily diffuse horizontal solar radiation for different climatic regions of China",Renewable and Sustainable Energy Reviews ,Vol 105 , P 168-186,(2019).

[69] E. F. Khanjer, W. A. Hassan, B. S. Ismael and N. K. Gazal, "Radon Distribution in Baghdad Province by Using Remote sensing techniques", J. Phys. Conf. Ser., No.1, vol. 1530, (2020).

[70] Sajjad Hussain, Muhammad Mubeen, Ashfaq Ahmad, Waseem Akram, Hafiz Mohkum Hammad, Mazhar Ali, Nasir Masood, Asad Amin, Hafiz Umar Farid, Syeda Refat Sultana, Shah Fahad, Depeng Wang, Wajid Nasim, "Using GIS tools to detect the land use/land cover changes during forty years in Lodhran district of Pakistan" Environmental Science and Pollution Research 27 (32), 39676-39692, (2020).

[71] Miguel Rivas, Gloria M.Calaf, David Laroze, Elisa Rojas, Joaquín Mendez, Juan Honeyman and María C.Arayaf,"Solar ultraviolet A radiation and nonmelanoma skin cancer in Arica, Chile"Journal of Photochemistry and Photobiology B: Biology, Vol 212, 112047,(2020).

[72] A f Abed, E F Khanjer and S A Abdullah,"Evolution and set up the maps for solar radiation of Iraq using Data observation and Angstrom model during monthly July2017", IOP Conf. Ser.: Mater. Sci. Eng. 757 012038(2020).

[73] H Ebru Colak, Tugba Memisoglu, Yasin Gercek"Optimal site selection for solar photovoltaic (PV) power plants using GIS and AHP: A case study of Malatya Province, Turkey" Renewable energy 149, 565-576, (2020).

[74] Tao Hai, Ahmad Sharafati , Achite Mohammed Sinan Q. Salih, " Global Solar Radiation Estimation and Climatic Variability Analysis Using Extreme Learning

Machine Based Predictive Model", Digital Object Identifier 10.1109/ACCESS.2020.2965303, pp 120-142, (2020).

[75] Mawloud Guermoui, Farid Melgani, Kacem Gairaa and Mohamed

Lamine Mekhalfi,"A comprehensive review of hybrid models for solar radiation forecasting", Journal of Cleaner Production Vol 258, 120357 (2020).

[76] Laura Hudson, Eyman Rashdan, Catherine A. Bonn, Bhaven Chavan, David Rawlings and Mark A. Birch-Machin, "Individual and combined effects of the infrared, visible, and ultraviolet light components of solar radiation on damage biomarkers in human skin cells", the FASEB Journal, Vol 34, Iss3, Pages 3874-3883 (2020).

[77] Ümit Ağbulut, Ali Etem Gürel and Yunus Biçenc, " Prediction of daily global solar radiation using different machine learning algorithms pp: 50-55, (2020).

[78] L. Karthikeyan, I. Chawla and A. K. Mishra, "A review of remote sensing applications in agriculture for food security: Crop growth and yield, irrigation, and crop losses", J. Hydrol., vol. 586, p. 124905, (2020).

[79] H. S. Abbas and A. S. Mahdi, "Study of Desertification using Remote Sensing Imagery in South Iraq", Iraqi Journal of Science, No. 4, vol. 60, p. 904, (2019).

[80] Wang S, Koch B. “Determining profits for solar energy with remote sensing data”. 2010;35(7):2934-8 (2010).

[81] Angelis-Dimarkis A, Biberacher M, Dominguez J, Fiorese G, Gadocha S, Gnansounou E, et al. Methods and tools to evaluate the availability of renewable energy sources. Renew Sustain Energy Rev 2011;15(2):1182-200 (2012).

[82] Sozen A, Arcaklioglu E, Ozalp M. Estimation of solar potential in Turkey by artificial neural networks using meteorological and geographical data. Energy Convers Manage 2004;45(18-19):3033-52 (2004).

[83] ATLAS. Wasteland atlas of Iraq. Hyderabad: National Remote Sensing Centre (NRSC);(2010).

[84] D. Culinovic, " Remote sensing data & Data Analysis in Tableau", (2021).

[85] C. Shyam S and A. Rajeev K, "Estimation of hourly solar radiation on horizontal and inclined surfaces in Western Himalayas," *Smart grid Renew. energy*, vol. (2011).

[86] K.-D. Jäger, O. Isabella, A. H. M. Smets, R. A. van Swaaij, and M. Zeman, *Solar energy: fundamentals, technology and systems*. UIT Cambridge, (2016.

[87] Jawad, L.A. The Climatic Quality Index Determination for Iraq Using Meteorological Stations Data, Iraqi Journal of Science, 57 (4C): 3005-3016(2016).

[88] Waheed, R. B. Bonnell, S.O. Prasher and E. Paulet, " Measuring performance in precision agriculture: CART-A decision tree approach", Agric. Water Mgmt, (2006).

[89] L. Karthikeyan, I. Chawla, and A. K. Mishra, "A review of remote sensing applications in agriculture for food security: Crop growth and yield, irrigation, and crop losses", vol. 586, p. 124905, (2020).

[90] James W. Merchant ,Sunil Narumalani,"Integrating Remote Sensing and Geographic Information Systems ", University of Nebraska - Lincoln ,pp 17-19,(2009).

[91] U. Martensson, "Introduction to Remote Sensing and Geographical Information Systems," Department of Physical Geography and Ecosystems Sciences, p. 55, (2011).

[92] Grassi S, Ndaona C, Abhari RS. Large scale technical and economical assessment of wind energy potential with a GIS tool: case study Iowa. Energy Policy 2012;45:73-85(2012).

[93] Inas Riyadh Wdaah,"Using Multispectral Satellite Images for the Sustainable Development of Karbala Province", University of Kufa, Faculty of Science p.9, (2022).

[94] Siraki, A.G. and Pillary, P, " Study of optimum tilt angles for solar panels in different latitudes for urban applications". Solar Energy, 86, pp 920-928., (2012).

[95] Hossain J, Sinha V, Kishore VVN. A GIS based assessment of potential for wind farms in India. Renew Energy 2011;36(12):3257-67(2011).

[96] Ramachandra TV, Shruthi BV. Wind energy potential mapping in Karnataka, India, using GIS. Energy Convers Manage 2005;46(9-10):1561-78(2005).

[97] Rumbayan M, Abudureyimu A, Nagasaka K. Mapping of solar energy potential in Indonesia using artificial neural network and geographical information system. Renew Sustain Energy Rev 2012;16(3):1437-49(2012).

[98] Gastli A, Charabi Y. Solar electricity prospects in Oman using GIS-based solar radiation maps. Renew Sustain Energy Rev 2010;14(2):790-7.R. Mahtta. / Renewable Energy 71 255-262 261(2014).

[99] O. M. Chua and K. Yunus, "Metals Pollution in Tropical Wetlands", (2019).

[100] M. F. Goodchild, "Twenty years of progress: GIS science in 2010", Journal of Spatial Information Science (1). doi: 10. 5311/JOSIS.2010.1, (2010).

[101] Ahmed Jassim Mohammed, Application of GIS technologies in estimating the amount of solar energy in Basra province and the potential for use in desalination of seawater, Basra Studies Journal, Basra University, Issue 35, (2020).

[102] Dawood. Juma'a Muhammad, "Principles of Geographical Information Systems", King Saud University, Makkah Al-Mukarramah, Kingdom of Saudi Arabia, p. 215,(2014).

[103] Mahdi, E. J., "Assessment of Solar Energy Potential for Photovoltaic (PV) Systems Applications in Iraq" , Ph.D. Thesis, College of Science, University of Baghdad, Baghdad, Iraq, 159 pp.(2018).

[104] Balasubramanian A., "FOUR DATA MODELS IN GIS ",University of Mysore,Mysore,DOS in Earth Science -MYSOREOrdinal,(2017).

[105] Jensen, John R.; Jensen, Ryan R., "5: Spatial Data Models and Databases". Introductory Geographic Information Systems. Pearson. pp. 125–127 (2013).

[106] Bolstad, Paul , "GIS Fundamentals: A First Text on Geographic Information Systems" (6th ed.). XanEdu. pp. 39–71(2019).

[107] M. Arr, "Kerala Environment Congress 2012 Focal Theme at RGCB Auditorium, Thiruvananthapuram Organised by Centre for Environment and Development", (2012).

[108] Okan E, "Application of Geographic Information System (GIS) in Education", Journal of Technical Science and Technologies, 1(2):53-58, ISSN:2298-0032, (2012).

[109] Gheidaa S. Hadi, “IRAQI Solar Energy Assessment Using GIS and RS Techniques”, University of Baghdad College of Science, p 69, (2015).

[110] Israa J. Muhsin “High resolution digital elevation model (DEM) for university of Baghdad campus” Ph.D. thesis, university of Baghdad, college of science, (2010).

[111] Ramachandra T. V. Bharath H. Aithal, Durgappa Sanna D., "Land Surface Temperature Analysis in an Urbanising Landscape through MultiResolution Data", Journal of Space Science & Technology , Volume 1, pp 1-10, (2012).

[112] Bilu Susan Babu, "Comparative Study on the Spatial Interpolation Techniques in GIS",International Journal of Scientific & Engineering Research, Volume 7, Issue 2, ISSN 2229-5518,(2016).

[113] Munday, Jeremy, "Tackling Climate Change through Radiative Cooling". Joule. 3 (9): 2057–2060. doi S2CID, (2019).

[114] Stickler, Greg, "Educational Brief - Solar Radiation and the Earth System ". National Aeronautics and Space Administration, (2016).

[115] Fu, P. " A Geometric Solar Radiation Model with Applications in Landscape Ecology". Ph.D. Thesis, Department of Geography, University of Kansas, Lawrence, Kansas, USA (2000).

[116] Fu, P., and P. M. Rich. " The Solar Analyst 1.0 Manual. Helios Environmental Modeling Institute" (HEMI), USA (2000).

[117] Fu, P., and P. M. Rich. "A Geometric Solar Radiation Model with Applications in Agriculture and Forestry." Computers and Electronics in Agriculture 37:25–35 (2002).

[118] Rich, P. M., and P. Fu. "Topoclimatic Habitat Models." Proceedings of the Fourth International Conference on Integrating GIS and Environmental Modeling (2000).

[119] Kang-tsung Chang,"INTRODUCTION TO GEOGRAPHIC INFORMATION SYSTEMS",Ninth Edition,University of Idaho, NY 10121, p 6, (2019).

[120] H. S. Abbas and A. S. Mahdi, "Study of Desertification using Remote Sensing Imagery in South Iraq", Iraqi Journal of Science, No. 4, vol. 60, p. 904, (2019).

[121] O. Rozenstein, Z. Qin, Y. Derimian and A. Karnieli, "Derivation of Land Surface Temperature for Landsat-8 TIRS Using a Split Window Algorithm" p. 5768, (2014).

[122] E. J. Knight and G. Kvaran, "Landsat-8 operational land imager design, characterization and performance" *Remote Sens.*, No. 11, vol. 6, p. 10286, (2014).

[123] M. Montanaro, A. Lunsford, Z. Tesfaye, B. Wenny and D. Reuter, "Radiometric Calibration Methodology of the Landsat 8 Thermal Infrared Sensor", (2014).

[124] M. Moraca and A. Pepe, "Studio comparativo tra lo stato dei luoghi prima e dopo l'incendio del Vesuvio tramite analisi satellitare", (2017).

[125] C. Loyd, "Putting Landsat 8's Bands to Work ", Map Box, June 14, (2013).

[126] C. Parente and R. Santamaria, "Synthetic Sensor of Landsat 7 ETM+ Imagery to Compare and Evaluate Pan-sharpening Methods", (2014).

[127] E. O. Makinde and A. D. Obigha, "Comparison between Landsat 7 Enhanced Thematic Mapper Plus (ETM+) and Landsat 8 Operational Land Imager (OLI) Assessment of Vegetation Indices", Niger. J. Environ. Sci. Technol., No. 2, vol. 1, pp. 355-356, (2017).

[128] Daniel Clewley ,Jane Whitcomb ,Mahta Moghaddam ,Kyle McDonald ,Bruce Chapman,"Evaluation of ALOS PALSAR Data for High-Resolution Mapping of Vegetated Wetlands in Alaska" ,Viterbi School of Engineering, University of Southern California, Los Angeles, CA 90089, USA,(2015).

[129] Walawender, J. P., Hajto, M. J., Iwaniuk, P. A new ArcGIS toolset for automated mapping of Land Surface Temperature with the use of LANDSAT satellite data. Proc. IEEE IGARSS, 22– 27 July 2012, Munich, Germany, pp. 4371–4374.temperature: Current status and perspectives. Remote Sensing of Environment, Vol.131, pp.14-37(2012).

[130] Kumar, D., Shekhar, S. Statistical analysis of Land Surface Temperature–vegetation indexes relationship through thermal remote sensing. Ecotoxicology and Environmental Safety, Vol.121, pp.39-44(2015).

[131] Richards, J. A., Jia, X., Remote sensing Digital Image Analysis. P. 439, 4th Edition, springer (2006).

[132] Lillesand, T. M. Remote sensing and image interpretation. Edition, John Wiley and Sons, Inc., USA. (2008).

[133] Campbell, J. B. Introduction to remote sensing, Fourth Edition, Guilford publication, Inc (2007).

الخلاصة

تضمنت الاطروحة دراسة توزيع شدة الإشعاع الشمسي في محافظة بابل لخمسة اشهر مختلفة (كانون الثاني ،آذار ، تموز، آب ، تشرين الأول) لتغطية الفصول الأربعة لسنة2021 حيث تم اختيار شهري تموز و آب لفصل الصيف لما يشهده من ارتفاع كبير بدرجات الحرارة وتميزه بشدة اشعاع شمسي عالي، تم ذلك باعتماد القمر الصناعي ALOSPALSAR حيث ان له قابلية تصوير واسعة النطاق وعالية الدقة ومتعدد الاطياف ويوفر صور ذات دقة 10م، تم التقاط خمسة صور من صور الارتفاع الرقمي DEM لتغطية محافظة بابل التي تبلغ مساحتها (5119كم^2) كل شهر قيد الدراسة من موقع المسح الجغرافي الأمريكي.

المرحلة الثانية كانت اجراء دمج للصور باستخدام برنامج الموزائيك وبعدها تمت التصحيحات الهندسية والمكانية وتم استقطاع محافظة بابل وذلك باعتماد تقنية نظم المعلومات الجغرافية Arc GIS رسمت خمسة خرائط لمحافظة بابل تضمنت التوزيع المكاني للإشعاع الشمسي، حيث تم حساب الاشعاع الشمسي لكل يوم على ثلاث او اربع فترات اعتماداً على طول فترة النهار حيث تم حساب الاشعاع الشمسي كل 30 دقيقة، وبينت النتائج ان اعلى معدلات الاشعاع الشمسي كانت في تموز وآب والتي تمثل فصل الصيف لتصل الى معدلات عالية ما بين (382.0022- 405.6382) W. H. m^{-2} , حيث كانت كمية الاشعاع تحسب لأربع فترات اعتماداً على عدد ساعات النهار اما لبقية الأشهر فكانت كمية الاشعاع بمستويات طبيعية تتراوح ما بين (176.4067- 263.5710-307.6873)W. H .m^{-2}. بالنسبة لبقية الفصول وللأشهر كانون الثاني وآذار وتشرين الأول وكانت كمية الاشعاع تحسب لثلاث فترات وتركزت مناطق الاشعاع العالي في المناطق الجرداء وتقل في المناطق الحضرية والزراعية، تم حساب معدل الاشعاع خلال النهار لكل يوم رصد، ودراسة علاقته مع كل من درجة حرارة الهواء والرطوبة النسبية حيث لوحظ ان معدل الاشعاع يقترن بعلاقة طردية مع درجة حرارة الهواء وعكسية مع الرطوبة النسبية فالزيادة الحاصلة في كمية الاشعاع الشمسي ترافقها زيادة في درجة حرارة الهواء ونقصان في الرطوبة النسبية والزيادة في الرطوبة النسبية يرافقها انخفاض في كمية الاشعاع.

تمت دراسة درجة حرارة سطح الأرض بالاعتماد على كل من تقنية التحسس عن بعد ونظم المعلومات الجغرافية وتم اعتماد الحزم الحرارية والحمراء القريبة للقمر الصناعي لاندسات 8 تم رسم التوزيع المكاني

لدرجة حرارة سطح محافظة بابل لخمسة اشهر لسنة 2021 لتغطية الفصول الأربعة لسنة الدراسة حيث أظهرت النتائج التفاوت الواضح في درجات حرارة سطح الأرض للفصول الأربعة وكانت اعلى قيم لها في شهر تموز و آب (فصل الصيف) لتصل الى مستويات عالية جداً لامست 60 درجة مئوية وهذه تشكل خطراً على حياة الانسان اما في بقية الفصول فقد كانت درجة حرارة سطح الأرض متدنية ومتفاوتة ايضاً فقد لامست 25 درجة مئوية في فصل الشتاء في يوم مشمس وبلغت 40 درجة مئوية في فصلي الربيع والخريف. كما تناولت الاطروحة دراسة شدة الاشعاع الشمسي وتأثيره على صحة الانسان من خلال ظهور حالات إصابة بسرطان الجلد في المدينة، وبالاعتماد على بيانات اعداد الإصابات التي تم الحصول عليها من دائرة صحة بابل ودائرة صحة النجف لمنطقة الدراسة، حيث كانت النتائج موزعة على جميع مناطق واقضية محافظة بابل، اعلى تركيز للإصابات في مدينة الحلة مركز محافظة بابل مقارنة مع بقية المناطق وتليها منطقة ابي غرق وبعدها منطقتي المسيب والمحاويل ثم بقية المناطق ومن المرجح ان تكون أسباب توزيع الإصابات ليست فقط الشدة العالية للاشعاع الشمسي وارتفاع درجات الحرارة انما الكثافة السكانية والتلوث البيئي والمباني والمعامل وغيرها من الأسباب .

وزارة التعليم العالي والبحث العلمي

جامعة بابل - كلية العلوم

قسم الفيزياء

تقييم الإشعاع الشمسي والإصابة بسرطان الجلد في محافظة بابل باستخدام تقنيات الاستشعار عن بعد

اطروحة

مقدمة الى قسم الفيزياء - كلية العلوم - جامعة بابل كجزء من متطلبات نيل شهادة الدكتوراه في فلسفة الفيزياء

من قبل

غزوان عبد الاله دهش عزيز

بكالوريوس في علوم الفيزياء / ٢٠٠٥

ماجستير في علوم الفيزياء / ٢٠١٧

بإشراف

أ.د. أميرة ابو السود حمادي مهجج

أ.د. ابتسام فاضل خنجر ادريس

٢٠٢٣ م

١٤٤٥ هـ